TECHNISCHE UNIVERSITÄT MÜNCHEN

Fakultät für Chemie

Lehrstuhl für Technische Chemie II

Dimerization of 1-Butene

on

Ni Based Solid Catalysts

Andreas Ehrmaier

Vollständiger Abdruck der von der Fakultät für Chemie der Technischen Universität München zur Erlangung des akademischen Grades eines

Doktors der Naturwissenschaften (Dr. rer. nat.)

genehmigten Dissertation.

Vorsitzender:		Hon.-Prof. Dr. Richard W. Fischer
Prüfer der Dissertation:	1.	Prof. Dr. Johannes A. Lercher
	2.	Prof. Dr. Klaus Köhler

Die Dissertation wurde am 29. Mai 2019 bei der Technischen Universität München eingereicht und durch die Fakultät für Chemie am 8. Juli 2019 angenommen.

Das Geheimnis aller Erfinder ist, nichts für unmöglich anzusehen.

Justus Freiherr von Liebig

Für meine Frau Lena

und meine Familie

Abstract

Selective dimerization of 1-butene on Ni exchanged zeolite LTA to n-octene and methyl heptene occurs via Cossee-Arlman mechanism. With increasing conversion, isomerization to 2-butene led also to dimethylhexene and catalyst deactivation. Dimerization of 1-butene was an order of magnitude faster than dimerization of 2-butene. The presence of alkali and alkali earth cations increased the isomerization rates, but did not affect the dimerization activity of Ni sites, allowing to reach higher selectivities to n-octene and methylheptenes.

Kurzzusammenfassung

Die selektive Dimerisierung von 1-Buten an Ni-ausgetauschtem Zeolith LTA zu n-Octen und Methylhepten erfolgt über den Cossee-Arlman-Mechanismus. Mit zunehmendem Umsatz führte die Isomerisierung zu 2-Buten auch zu Bildung von Dimethylhexen und zur Deaktivierung der Katalysatoren. Die Dimerisierung von 1-Buten war um eine Größenordnung schneller als die Dimerisierung von 2-Buten. Das Vorhandensein von Alkali- und Erdalkalikationen erhöhte die Isomerisierungsraten, beeinflusste aber nicht die Dimerisierungsaktivität von Ni-Zentren, wodurch höhere Selektivitäten an n-Octen und Methylheptenen erreicht werden konnten.

Acknowledgement

It is impossible to write a PhD thesis or successfully pass the studies without the generous help of many people. I would like to take the chance and say “thank you” to all, who supported on my way. I wouldn’t be, where I am now, if you all hadn’t been there.

First, I want to thank Prof. Johannes Lercher for giving me the opportunity to prepare my PhD thesis in his group. Johannes, thank you for confidence and all your support during the past years. You have given me the chance to work on a challenging and exciting topic. Doing my studies in your international group gave me the opportunity to learn a lot, may it be from the scientific point of view, as well as on intercultural differences and traditions. I enjoyed every single day in your group and it was a pleasure for me to work with you.

I warmly thank Ricardo Bermejo de Val for being my supervisor and helping me with the preparation of all the reports, presentations, the manuscripts, and finally this thesis. Ricardo, you always had an open ear for my issues and helped with useful comments and suggestions. Thank you for your pleasant and relaxed nature, for the trust you gave me, for the fruitful scientific discussions and all your advice.

In the earlier stage of by work at TC2, Maricruz Sanchez-Sanchez and Yue Liu were supervising me. Thank you, Maricruz, for your help with the first reports and presentations and for getting the project started. I could always come to you with my questions. Yue, thank you for all your unconventional ideas and your innovative way to access the issues of the topic from a different angle. In the same way, I want to thank Andy Jentys. Whenever I had a question, you had an answer. Thank you for all the funny stories in the lab!

Further, I want to thank EVONIK Performance Materials GmbH for funding this project. Special thanks go to Stephan Peitz, who supervised the project from EVONIK site and always contributed to the project issues. Thank you for the useful discussions.

Without our great technician, Xaver Hecht, not a single setup would work in TC2. Xaver, you are the heart and soul of the whole group. I can’t imagine, how life will be, once you are taking your well-deserved retirement. Thank you very much for all your BET measurements and your

help with the reactor, GC, IR, … and all the fun in the lab. Only because of your help and your skills, we were able to have quite a relaxed life in the lab.

Grateful thanks go to Martin Neukamm, for doing the AAS measurements and Andreas Marx for your help in all electronic issues.

Special thanks go to our assistants, Uli, Steffi, Katja and Bettina, who took care of all the bureaucratic hindrances. Thank you for keeping administrative issues out of our business and for your help with them, if they were inevitable for us. Bettina, I'm sorry for all the incomplete or wrongly filled forms…

During the last years, there were many students helping me in the lab. A special thank goes to my Master students, Michaela Dumberger, Jakob Faustmann, and Robert Kick, you really supported me a lot. I also want to thank my Bachelor and practical course students, Alexander Schmitt, Andrea Klenner, Carolin Gleißner, Daniel Reisinger, Daniel Weber, Hussayn Ahmed, Jan Paetzold, Lara Milakovic, Laura Roemer, Leon Schuchmann, Lukas Graser, Matthias Singer, Max Hiller, Max Steck, Niklas Pfirem, Patrick Walke, and Tanja Rieß. It was a pleasure and fun to work with you. I am quite happy, that Lara and Niklas decided to do their PhD here as well, and I am proud to have the two of you as colleagues now.

With this, I am happy now to thank all my nice colleagues. Yes, I made it – finally. But it definitely would not have been possible without all of you around. Thank you for your help, your advice, the support and the fun we had in the lab and in the bunker, the wonderful group events (Weimar, BBQ, playing soccer, …), all the scientific and semi-scientific discussions. Especially I want to mention Daniel Melzer, Matthias Steib, Felix Kirchberger, Lara Milakovic, Teresa Schachtl, Laura Löbbert, Ferdinand Vogelgsang, Niklas Pfriem, Verena Höpfl, Manuel Weber, Martin Baumgärtl, Manuel Wagenhofer, Roland Weindl, Martina Braun, Peter Hintermeier, and Sebastian Eckstein, Takaaki Ikuno, Wanqiu Liu, Insu Lee, Edith Berger, Christoph Denk, Martina Aigner, Alexander Wellmann, Ilka Vincon, Mirjam Wenig. You all have not only been very kind and friendly colleagues, which made every single day at work a good day. You have also become very good friends! Therefore, I say thank you!

I also want to mention some former colleagues, Eva Willnecker, Sebastian Foraita, Stefan Schallmoser, Kai Sanwald, Sebastian Grundner, and Jenny Hein. Thank you for introducing me to the group and helped me getting started.

Further, my sincerely thanks go to all my friends at home, and those, who I met at university. Thank you that I always can count on you and for the great times we had.

The greatest thanks I want to contribute to my family. My parents, Hemma and Andreas, who supported me all my life. You gave me the chance to do, whatever I wanted to. I know, I always can rely on you, you are always there. Thank you for believing in me all the time and that you enabled me my studies, my Master's thesis abroad and finally this PhD. In the same way I want to thank my two brothers, Johannes and Sebastian, together with Nina and Sophie. I know, you are always there for me, whatever I need. I am so glad to have you all around.

Last but not least, I want to thank my wife, Lena. You made it with me through the hardest times, but you never stopped believing in me. Thank you for your trust. You are my home. Thank you for your love!

List of Abbreviations

°C	Degrees on a Celsius scale
AAS	Atom absorption spectroscopy
Al	Aluminum
Al-Py	Pyridine adsorbed to Al LAS
Å	Angstrøm
bar	bar
BAS	Brønsted acid site
BEA	Zeolite Beta
BET	Brunauer-Emmett-Teller
BJH	Barrett-Joyner-Halenda
B-Py	Pyridine adsorbed to BAS
C	Carbon
C_{12}	Molecules containing 12 carbon atoms
C_{16}	Molecules containing 16 carbon atoms
C_4	Molecules containing 4 carbon atoms
C_8	Molecules containing 8 carbon atoms
Ca	Calcium
Ca-LTA or Ca-LTA-5A or LTA-5A	Zeolite calcium-LTA
cat	Catalyst
CBU	Composition building unit
C-C (bond)	Carbon carbon bond
cm^{-1}	Reciprocal centimeter
Co	Cobalt

Cu	Copper
DMH	Dimethylhexene
E_a	Activation energy
eq	Equilibrium
EtOH	Ethanol
eV	Electron volts
FAU	Zeolite Faujasite
g	Grams
GC	Gas chromatography
H	Hydrogen
h	hour
HF	Hydroflouric acid
H-Py	H-bonded pyridine
IFP	Institute Francais du Petrole
IR	Infrared
K	Potassium
k_{di}	Rate constant for dimerization
keV	Kilo electron volts
kJ	Kilojoule
k_{tri}	Rate constant for trimerization
LAS	Lewis acid site
Li	Lithium
LTA	Zeolite Linde Type A
M	Metal
mA	Milliampere
mbar	Millibar

Mg	Magnesium
MHSV	Molar hourly space velocity
min	Minute
ml	Milliliter
mmol	Millimol
mol_C	Mol carbon
M-Py	Pyridine adsorbed to co-cation LAS
MR	Membered ring
N2	Nitrogen
Na	Sodium
Ni	Nickel
Ni(NO3)2	Nickel nitrate
NiO	Nickel oxide
Ni-Py	Pyridine adsorbed to NI LAS
O	Oxygen
p	pressure
PBU	primary building unit
PFR	Plug flow reactor
pH	pH value
Pt/Al_2O_3	Platinum supportet on alumina
PVC	Polyvinyl chloride
S	Selectivity
s	Second
SBU	Secondary building unit
SEM	Scanning electron microscopy
Si	Silicon

SiC	Silicon carbide
SiO2	Silica
SiO2-Al2O3 or AiO2/Al2O3 or SiAl	Silica alumina
SOD	Sodalite
Sr	Strontium
T	Temperature
TGA	Thermogravimetric analysis
Ti	Titan
TOF	Turnover frequency
UOP	Universal Oil Products
WHSV	Weight hourly space velocity
Wt.%	Weight percent
X	Conversion
XANES	X-ray absorption near edge spectroscopy
XAS	X-ray absorption spectroscopy
XRD	X-ray diffraction spectroscopy
Y	Yield
Zr	Zirconia
ν_{as}	Antisymmetric stretching

Table of contents

Introduction

Valorization of butenes

Light weight olefins of the C_4 fraction are formed as by-products from several cracking processes.[1-2] This mixture consisting of 1-butene, *cis*- and *trans*-2-butene, butadiene, as well as *iso*-butane and *iso*-butene is called C_4 raffinate, whereas the specific amount of the components varies as function of cracking method and conditions.[2]

Simple blending of the C_4 raffinate to gasoline fuel is limited due to the low vapor pressure and the high olefin content. To avoid unprofitable burning, diverse valorization methods are performed. One of the most common valorization methods are the oligomerization and alkylation over Brønsted acid catalysts.[3] Especially the alkylation of isobutane and linear C_4-olefins leads to highly branched isooctanes, which are blended to gasoline fuels to increase the octane number.[4-5]

Besides the production of fuel additives, the selective dimerization towards linear products over metal based catalysts has gained interest in the formation of linear and monobranched octenes, applied as feedstock for in the production of plasticizers, e.g. for PVC, or as co-monomers in linear low density polyethylene.[2, 6]

The production of polymer additives gains higher value to the C_4 fraction as the production of fuel additives – with the only additional expense of another catalyst, containing Ni as a relative cheap metal.

The industrial research interest resulted in two predominant dimerization processes that are currently applied in large scale dimerization processes.

In the 1970s, the *Institute Francais du Petrole* (IFP) developed the DIMERSOL X and later the DIFASOL process. In both cases, a homogeneous Ni complex is applied as catalyst for the dimerization of light olefins. While the catalyst could not be recycled in the DIMERSOL process[6], the usage of ionic liquids in the further evolved DIVERSOL allowed catalyst recovery.[6-7]

Avoiding these problems, Hüls and UOP applied a heterogeneous catalyst system in their OCTOL process.[8] Among both processes, OCTOL and DIFASOL, the main fraction among the dimers is methylheptenes (50 %) with approx. 20 % linear octenes.[9] It should be mentioned that both industrial processes can be operated with different catalyst system. On the one hand, there is a metal based catalyst applied for the formation of linear dimers. A simple exchange of the catalyst to a Brønsted acid containing catalyst adapts the process for the production of branched dimers.[8-9]

Dimerization mechanisms

Brønsted acid catalyzed mechanism

The dimerization of olefins over Brønsted acid catalysts was one of the earliest methods for valorization of the light olefin range.[7] For the dimerization of olefins (Scheme 0-1)[10-11], the initial step involves the formation of a carbenium ion through the H^+ - addition to the double bond (Scheme 0-1, I). According to this, the mechanism is often called carbenium ion mechanism. According to Markovnikov's rule,[12] the proton attacks the primary C-atom of an α-olefin, which leads to the more stable secondary carbenium ion. Due to this higher stability, the nucleophilic attack of the second alkene molecule (Scheme 0-1, II) always happens at an internal C-atom, leading exclusively to branched dimers. The formation of a di- or monobranched product is distinguished, whether the second α-olefin attacks with the first or the second C-atom. Upon deprotonation the olefin dimers are generated and the H^+ catalyst is recovered (Scheme 0-1, III).

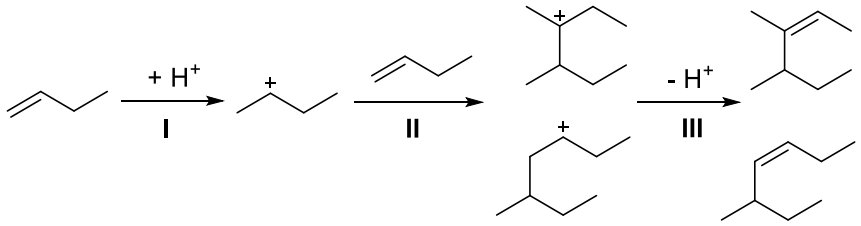

Scheme 0-1. Brønsted acid catalyzed carbenium-ion pathway (adapted from[10-11]).

Metallacycle mechanism

Dimerization over a metal based catalyst involves a cyclic metal-carbon intermediate as one possible mechanism. This so called metallacycle mechanism is discussed in literature and is proven to be the predominant mechanism from Cr catalyzed oligomerization reactions.[13-16] The mechanism involves the π-coordination of 2 olefin molecules to the metal center (Scheme 0-2). Subsequently, the metallacycle is formed through the concerted formation of two M-C bonds and the C-C bond (Scheme 0-2, I). With the coordination of another olefin molecule, the cycle is released, and a complex with a π-bond monomer and dimer is formed (Scheme 0-2, II). In the last step, the dimer is substituted by a fresh monomer, which releases the dimer molecule and recovers the initial complex (Scheme 0-2, III).

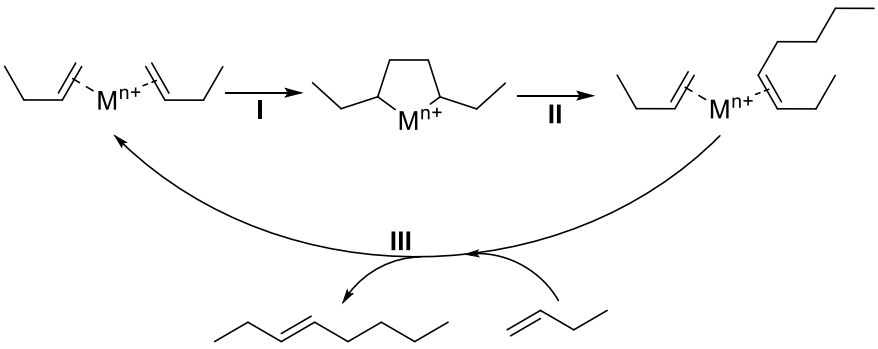

Scheme 0-2. Dimerization of α-olefins via a metallacylce intermediate (adapted from [13-16]).

Thereby, the dimer selectivity is determined by the orientation of the monomers in the π-complex, before the cycle is formed. Despite of massive stereochemical hindrances, a statistical ratio of single, double or unbranched dimers is expected.

Coordinative route via Ni based catalysts

Homogeneous catalysis over metal complexes – especially over Ni and Co based complexes - allowed the suggestion of a coordinative route without a cyclic transition state starting from a metal hydride (Scheme 0-3).[6, 17-23] This mechanism is discussed and applied for both, homogeneous as well as heterogeneous systems and was first described by Cossee[20] and Arlman[23], for which it is called Cossee-Arlman mechanism. After the coordination of the first butene molecule (Scheme 0-3, I), a Ni alkyl complex is formed upon insertion of the olefinic C=C into the Ni-H bond (Scheme 0-3, II). Subsequently another butene molecule is coordinated to the complex (Scheme 0-3, III) and inserted into the Ni-C bond (Scheme 0-3, IV). The Ni-H catalyst is recovered through β-H-elimination of the olefin dimer (Scheme 0-3, V).

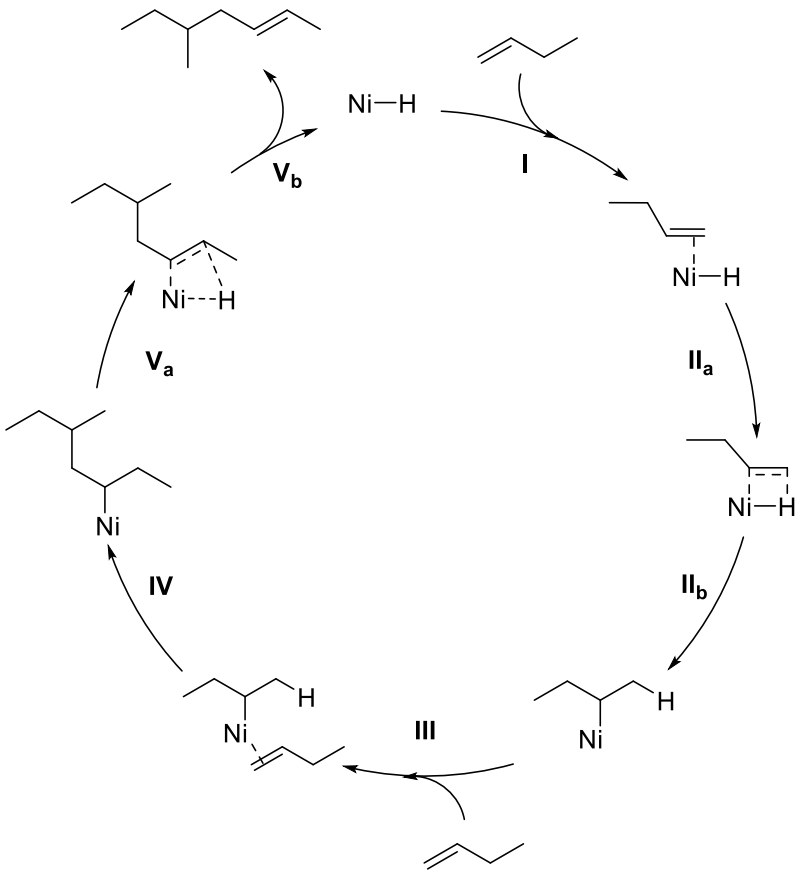

Scheme 0-3. Coordinative dimerization pathway (adapted from [6, 17-23]).

In contrast to the carbenium ion mechanism, the metal based pathways allow the formation of all isomers (including linear dimers). The selectivity is determined by two steps: by the

orientation of the first butene molecule before the alkyl formation, and by the orientation of the second butene molecule before it is inserted into the Ni-C bond.

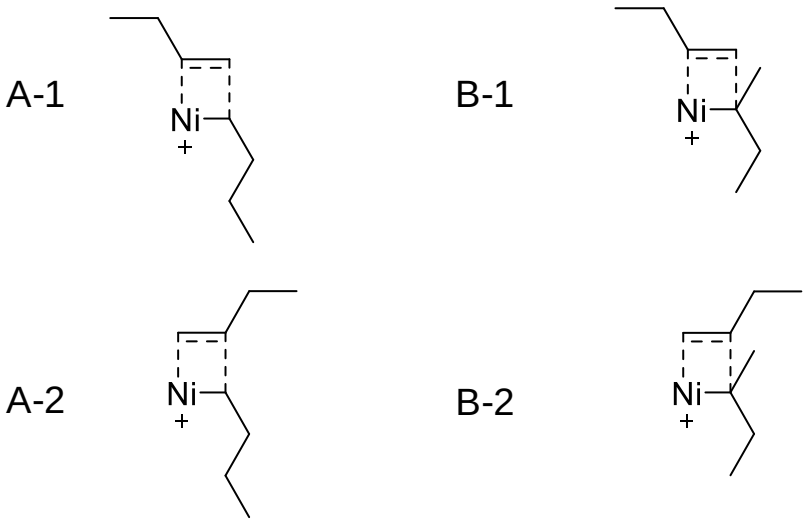

Scheme 0-4. Determination of the dimer selectivity among coordinative dimerization mechanism.

Scheme 0-4 demonstrates the different possibilities for the two steps of the dimerization reaction. Thereby, it must be distinguished between an initial 1- or 2-adsorption (Scheme 0-4 A and B, respectively). The orientation of the second butene molecule upon insertion determines, whether the dimer is linear (Scheme 0-4 A-1), mono- (Scheme 0-4 A-2 and B-1) or di-branched (Scheme 0-4 B-2).

The complete dimerization routes to the different possible dimers of 1-butene are demonstrated in Scheme 0-5. As already mentioned above, the initial adsorption can either be at the C_1 atom (1'-adsorption) or at the C_2 atom (2'-adsorption). The subsequent insertion of the second butene can also happen at two different positions: at the C_1-atom of the fresh butene (1'- insertion) or at the C_2 (2'-insertion). By this, the selectivity to the three possible stereoisomers, linear octene, 3-methylheptene or 3,4-dimethylhexene, is defined.

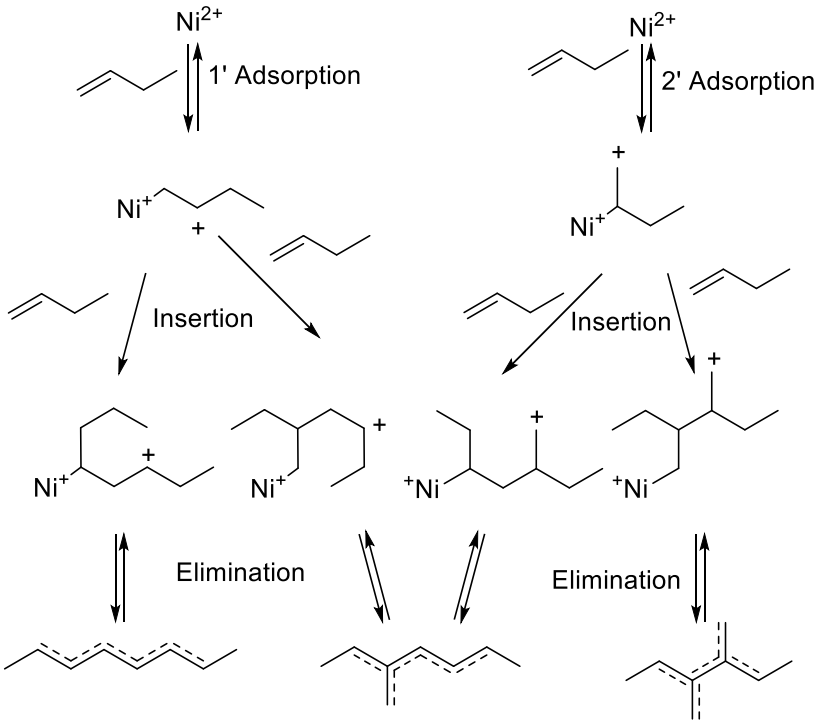

Scheme 0-5. Overview over pathways in coordinative dimerization mechanism (adapted from [24]).

After each C-C coupling in all mechanisms, there are two options to proceed. Either another olefin attacks, which leads to trimers, and subsequently to oligomers, or, the polymerization reaction is stopped by an elimination. Differences in the activation barriers for C-C-coupling and product desorption result in different rate constants for chain propagation and chain termination. This defines, whether predominantly oligomers or dimers are formed (Scheme 0-6).[25-26] The oligomerization is terminated. Karl Ziegler found this effect in 1955, and could explain the predominance of dimers over metal catalyzed polymerization reactions by the so-called “Nickel-effect”.[27-28]

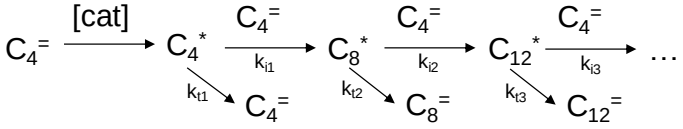

Scheme 0-6. Chain propagation (rate constant k_i) and termination (rate constant k_t) for catalyzed oligomerization reactions (adapted from [27-28]).

Besides Ni as most prominent metal also other transition metals, e.g. Ti, Zr or Co, were applied and tested in dimerization.[19, 29-31] However, Ni turned out to be the best suited catalyst for olefin dimerization reaction.

Structure and properties of zeolites

A widely used support material in heterogeneous catalysis is amorphous SiO_2 or SiO_2-Al_2O_3. Besides its high stability and high availability, these mesoporous materials offer large surface areas,[32] which allow high dispersions of the catalytic active species. Among the mesopores, the active sites are randomly distributed, and due to the relatively large pores easily accessible.

In contrast to the amorphous silica alumina, zeolites are highly structured SiO_2-Al_2O_3 materials with well-defined pore size distributions.[32] Zeolites consist of tetrahedrally coordinated Si and Al atoms, which are linked to each other via O-bridges. These TO_4 (T=Si, Al) units are called "primary building units" (PBU), while the name "secondary building unit" (SBU) describes the linked groups containing more than one TO_4 tetrahedrons.[33] This can be a 4-, 5- or a 6-membered ring, for example (Figure 0-1), whereas the number always refers to the number of T-atoms in the structure.

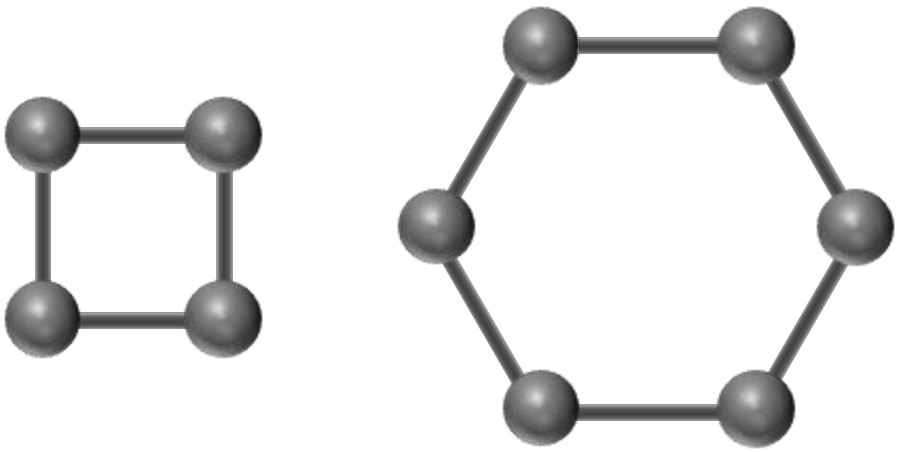

Figure 0-1. Secondary building units containing 4 (left) and 6 (right) T-atoms. [34]

The combination of these SBUs gives more complex structures, which can be found in many zeolites.[34] A typical example for these so called "composition building units" (CBU) is the sodalite cage (Figure 0-2), which has 4- and 6-MR SBUs.

Figure 0-2. Sodalite cage.[34]

Direct connection of multiple sodalite cages at its 4-MR windows in all directions gives the zeolite Sodalite (SOD), which exclusively consists of sodalite cages as the included space Is a sodalite cage as well (Figure 0-3 A). When the 4-MR windows are linked to each other via O-bridges, the zeolite Linde Type A (LTA) is formed (Figure 0-3 B), while the O-bridge linking of the sodalite cages at the 6-MR windows leads to Faujasite (FAU; Figure 0-3 C).

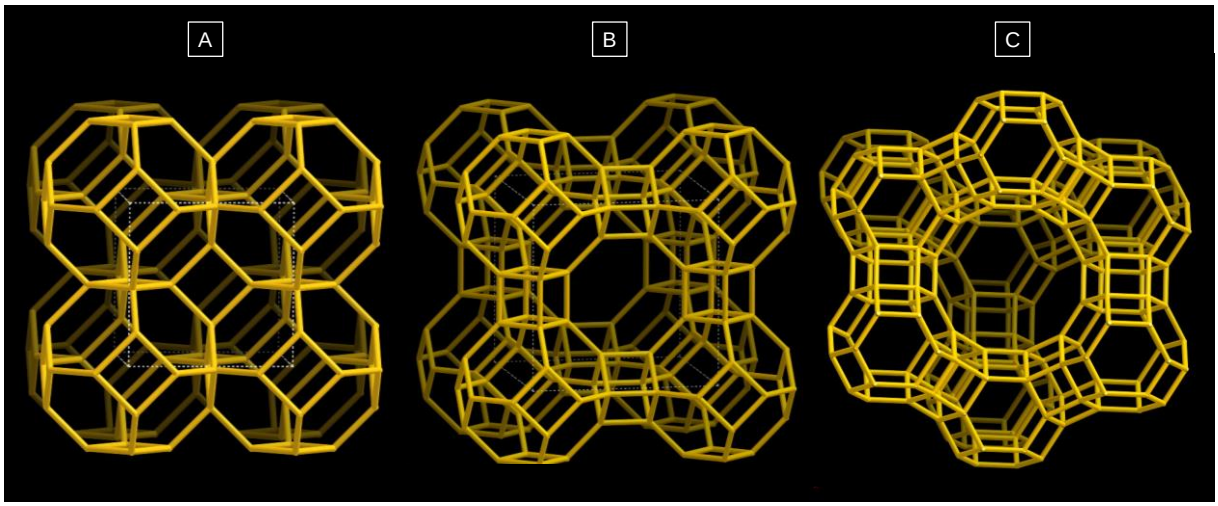

Figure 0-3. Frameworks of zeolites built of sodalite cages. A) Sodalite (SOD), B) Linde Type A (LTA) and C) Faujasite (FAU).[34]

Thereby micropores of different size are formed, which allow selective separation of molecules of a specific size. Therefore, zeolites are often called molecular sieves. By changing the synthesis procedure, these pore sizes and shapes can be well tuned. Depending on their ring size of 8-MR, 10-MR, 12-MR, zeolites are distinguished between small, medium and large pore zeolites, respectively (Table 0-1).[35]

Table 0-1. Classification and size of zeolites. [34]

	Ring size	Pore diameter	Example
Small pore zeolite	8-MR	3.5-4.5 Å	LTA, CHA
Medium pore zeolite	10-MR	4.5-6.0 Å	MFI, FER
Large pore zeolite	12-MR	6.0-8.0 Å	MOR, FAU

Among the primary building units, the SiO_4 tetrahedrons, the SiO_4 tetrahedrons are balanced in charge. Si with the oxidation state of +IV is balanced by four oxygen atoms, which are -II, and donate -I per bond to the Si atom (Scheme 0-7 A). In case of the +III group metal Al, it appears that there is a deficiency in charge, resulting in a negative -1 charge balance for the AlO_4^- tetrahedron (Scheme 0-7 B).

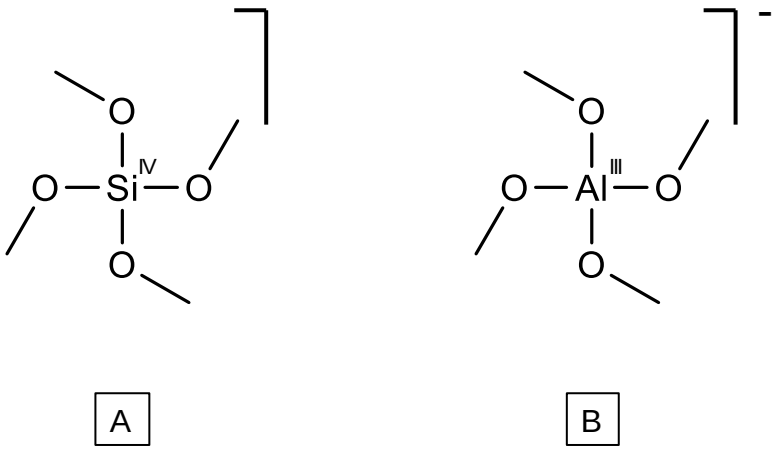

Scheme 0-7. Charge balance of TO_4 tetrahedrons.

To maintain a stable framework, it is inevitable to balance this charge by a positive charge, in the simplest case by a proton. This charge balancing proton is located next to the oxygen atom close to the electron defect site at the Al center (Scheme 0-8).[36-37] Therefore, it can easily be separated as H^+ and the zeolite hence functions as Brønsted acid site. Thereby the amount of acid protons depends on the amount of Al sites, since there is one proton per Al site. As a consequence, it is prohibited that two Al sites are direct neighbors, as two negative charges would lead to the collapse of the framework (Löwenstein's rule).[38]

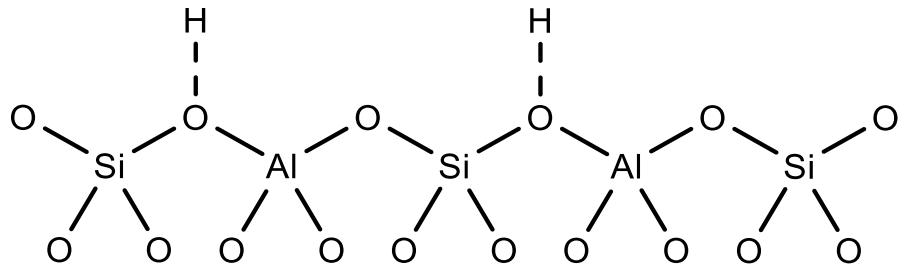

Scheme 0-8. Brønsted acid sites in zeolites.[36-37]

Besides the positively charged protons, metal cations are suitable to balance the charges as well. So, it is possible to exchange the protons by cations with single (eg. Na^+, Li^+, K^+) or double positive charge (e.g. Ca^{2+}, Mg^{2+}, but also Ni^{2+} or Co^{2+}). Thereby, the bivalent cations are able to balance the negative charges of two Al sites, which are in close proximity.

For zeolite LTA, the Si/Al ratio is 1, meaning that it is composed of alternating SiO_4 and AlO_4^- tetrahedrons. Like in most other zeolites, each cation has its defined positions, which was proven by structural analyses.[39-42] There are 3 different positions for cations to be located in LTA (Figure 0-4): At the center of the 6-MR windows (Figure 0-4, I), of the 4-MR windows (Figure 0-4, II) and in the middle of the 8-MR rings (Figure 0-4, III). It must be distinguished, whether monovalent or bivalent cations are present. When there are exclusively M^+ cations are present, they are located at all positions in the center of the rings, with 4 cations being located at the 8-MR windows.[39] This alters the accessible pore size of the LTA. When there are Na^+ cations present, the accessible diameter is at around 4 Å (LTA-4A), while the larger K^+ cation only leaves approx. 3 Å open (LTA-3A). Through the exchange of the monovalent cations by bivalent cations, such as Ca^{2+}, the cations at 8-MR window positions are the first ones which are released. In contrast to the monovalent cations, the bivalent cations do not occupy these positions, but the positions at the 6-MR windows. Thereby this position is split, whereas one of the cations is shifted towards the outside (Figure 0-4, I_a) and one to the inside of the sodalite cage (Figure 0-4, I_b). By this, the accessible pore entrance is increased to ca. 5 Å (LTA-5A).[39]

Ni^{2+} cations as bivalent cations are expected to occupy the altered 6-MR window positions (I_a and I_b).

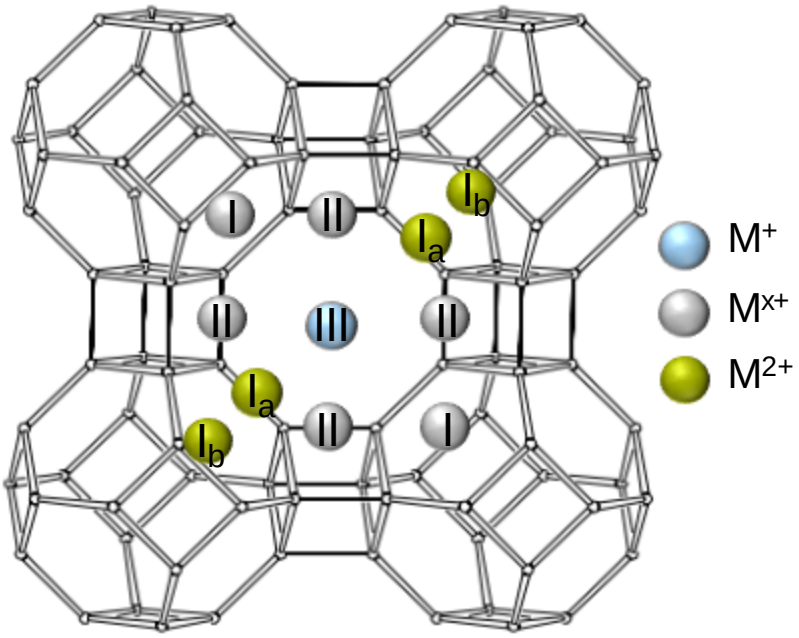

Figure 0-4. Cation positions in zeolite LTA (adapted from [42], LTA from [34]).

Recent achievements in alkene dimerization

Brückner et al. studied the dimerization of butene on amorphous supported Ni catalysts. In-situ EPR studies revealed the necessity of Ni being present in an oxidation state between +1 and +2 to form the active sites.[43] Thereby it is claimed that the active site, a Ni^{+}-H is formed from the Ni precursor and the Brønsted acid sites that are left in the acidic support. As comparison, Ni supported on a non-acidic support, e.g. SiO_2 remained inactive.[44] The second olefin is firstly π-bound and subsequently inserted to start the actual catalytic cycle.[44]

For the dimerization, recent literature[6, 21-22] suggests a Cossee-Arlman type mechanism, starting with a Ni alkyl, which is also supported by theoretical discriminations.

Beyond the amorphous materials, it was shown that highly structured microporous zeolites are well suited as support for the Ni centers. Since Ni functions as charge compensation, which is inevitable in Al containing zeolite material, Ni gets highly dispersed during the ion exchange and is stabilized by the zeolite.[45] Bell and co-workers found that the pore size and the resulting accessibility plays an important role on the activity, i.e. higher conversion rates were observed for larger pores and hence better accessibility.[46] In zeolite materials, the pore size and hence the accessibility can be tuned by different charge compensating cations.[39] Typically alkali and alkali earth metals are applied therefore. It could be shown, that large cations decrease the free volume and with this the catalyst activity.[24]

The support does not influence on the dimerization cycle itself, but seems to affect the Ni precursors and the formation of the active site.

Work on different zeolites were published, but in all cases, the presence of Brønsted acid sites was not excluded.[47-51] Hence, the observed results are all an overlay of metal and proton catalyzed mechanisms.

Scope of the thesis

Many studies focus on the nickel based dimerization or oligomerization of ethylene or propylene,[24, 45-46, 48, 50, 52-55] whereas less work on the dimerization of longer olefins (>C_3) is published.[6, 43-44, 47, 56-57]

While ethylene or propylene are not affected by double bond isomerization, butene can isomerize from 1-butene to *cis*- and *trans*-2-butene and vice versa. This isomerization significantly changes the reaction behavior: The branching of the products depends on the position of the C-C-coupling (see Scheme 0-4 and Scheme 0-5). In case of isomerization of 1- to 2-butene as competitive reaction, less olefinic C_1 atoms are present. Therefore, the pathway of 1-adsorption and 1-insertion is minimized, whereas the selectivity to branched products is increased.

This work focuses on the dimerization of butene over a zeolite supported Ni catalyst. Besides the dimerization there are reactant isomerization or oligomerization as competitive reactions taking place. Since there are protons left in many amorphous and zeolite materials, the Brønsted acid catalyzed dimerization/oligomerization and isomerization are present as well. In this work, a proton free zeolite (Linde Type A, LTA) is used to exclude the reactions of Brønsted acids and allow a clear focus on the Ni based reaction. The usage of 1-butene as reactant allows a deeper insight into the competition of dimerization and isomerization reactions. Upon double bond isomerization 1-butene isomerizes to an internal olefin, which has different possibilities for reaction and therefore changes the product formation. Using this molecule, it is the intention to understand the reaction mechanism and be able to follow the different pathways in the reaction network. Having the deeper insight into the different possibilities of reaction, the role of the co-cations shall be studied. It is to show, whether there are other influences of these cations on the reaction aside of the steric aspects. Also, the role of the spectator cations on the different reactions (isomerization and dimerization) shall be highlighted. This effect shall be studied in both, the zeolite based system, as well as in an amorphous system.

References

(1) Chauvel, A.; Lefebvre, G. G., *Petrochemical Processes: Technical and Economic Characteristics*. Gulf Publishing Company: 1989.
(2) Weissermel, K.; Hans-Jürgen, A., *Industrial Organic Chemistry*. Wiley-VCH: Weinheim, 1997.
(3) Kriván, E.; Marsi, G.; Hancsók, J. Investigation of the Oligomerization of light olefins on ion exchange resin catalyst. *Hungarian Journal of Industry and Chemistry* **2010,** 1.
(4) Nivarthy, G. S.; Feller, A.; Seshan, K.; Lercher, J. A. Alkylation of isobutane with light olefins catalyzed by zeolite beta. *Microporous Mesoporous Mater.* **2000,** 75-87.
(5) Nivarthy, G. S.; He, Y.; Seshan, K.; Lercher, J. A. Elementary Mechanistic Steps and the Influence of Process Variables in Isobutane Alkylation over H-BEA. *J. Catal.* **1998,** 1, 192-203.
(6) Behr, A.; Bayrak, Z.; Peitz, S.; Stochniol, G.; Maschmeyer, D. Oligomerization of 1-Butene with a Homogeneous Catalyst System Based on Allylic Nickel Complexes. *RSC Advances* **2015,** 52, 41372-41376.
(7) Albrecht, S.; Kießling, D.; Wendt, G.; Maschmeyer, D.; Nierlich, F. Oligomerisierung von n-Butenen. *Chem. Ing. Tech.* **2005,** 6, 695-709.
(8) Schulze, J.; Homann, M., *C4-hydrocarbons and derivatives: resources, production, marketing*. Springer Science & Business Media: 2012.
(9) Jones, D. S.; Pujadó, P. P., *Handbook of petroleum processing*. Springer Science & Business Media: 2006.
(10) Sarazen, M. L.; Iglesia, E. Stability of Bound Species During Alkene Reactions on Solid Acids. *Proceedings of the National Academy of Sciences* **2017,** 20, E3900-E3908.
(11) Sarazen, M. L.; Iglesia, E. Experimental and Theoretical Assessment of the Mechanism of Hydrogen Transfer in Alkane-Alkene Coupling on Solid Acids. *J. Catal.* **2017,** 287-298.
(12) Markovnikov, V. Ueber die Abhängigkeit der verschiedenen Vertretbarkeit des Radicalwasserstoffs in den isomeren Buttersäure. *Liebigs Ann. Chem* **1870,** 228-259.
(13) Montgomery, J. Nickel-Catalyzed Reductive Cyclizations and Couplings. *Angew. Chem. Int. Ed.* **2004,** 30, 3890-3908.
(14) Forestière, A.; Olivier-Bourbigou, H.; Saussine, L. Oligomerization of Monoolefins by Homogeneous Catalysts. *Oil & Gas Science and Technology - Rev. IFP* **2009,** 6, 649-667.
(15) Robinson, R.; McGuinness, D. S.; Yates, B. F. The Mechanism of Ethylene Dimerization with the Ti(OR')4/AlR3 Catalytic System: DFT Studies Comparing Metallacycle and Cossee Proposals. *ACS Catalysis* **2013,** 12, 3006-3015.
(16) Tomov, A. K.; Gibson, V. C.; Britovsek, G. J. P.; Long, R. J.; van Meurs, M.; Jones, D. J.; Tellmann, K. P.; Chirinos, J. J. Distinguishing Chain Growth Mechanisms in Metal-catalyzed Olefin Oligomerization and Polymerization Systems: C2H4/C2D4 Co-oligomerization/Polymerization Experiments Using Chromium, Iron, and Cobalt Catalysts. *Organometallics* **2009,** 24, 7033-7040.
(17) Chauvin, Y.; Olivier, H.; Wyrvalski, C. N.; Simon, L. C.; de Souza, R. F. Oligomerization ofn-Butenes Catalyzed by Nickel Complexes Dissolved in Organochloroaluminate Ionic Liquids. *J. Catal.* **1997,** 2, 275-278.
(18) Simon, L. C.; Dupont, J.; de Souza, R. F. Two-phase n-butenes dimerization by nickel complexes in molten salt media. *Appl. Catal. A* **1998,** 1, 215-220.
(19) Skupinska, J. Oligomerization of α-Olefins to Higher Oligomers. *Chem. Rev.* **1991,** 4, 613-648.
(20) Cossee, P. Ziegler-Natta Catalysis I. Mechanism of Polymerization of α-Olefins with Ziegler-Natta Catalysts. *J. Catal.* **1964,** 1, 80-88.
(21) Brogaard, R. Y.; Olsbye, U. Ethene Oligomerization in Ni-Containing Zeolites: Theoretical Discrimination of Reaction Mechanisms. *ACS Catalysis* **2016,** 2, 1205-1214.

(22) Henry, R.; Komurcu, M.; Ganjkhanlou, Y.; Brogaard, R. Y.; Lu, L.; Jens, K.-J.; Berlier, G.; Olsbye, U. Ethene Oligomerization on Nickel Microporous and Mesoporous-Supported Catalysts: Investigation of the Active Sites. *Catal. Today* **2018,** 154-163.
(23) Arlman, E. J. Ziegler-Natta catalysis II. Surface structure of layer-lattice transition metal chlorides. *J. Catal.* **1964,** 1, 89-98.
(24) Mlinar, A. N.; Ho, O. C.; Bong, G. G.; Bell, A. T. The Effect of Noncatalytic Cations on the Activity and Selectivity of Nickel-Exchanged X Zeolites for Propene Oligomerization. *ChemCatChem* **2013,** 10, 3139-3147.
(25) Al-Jarallah, A. M.; Anabtawi, J. A.; Siddiqui, M. A. B.; Aitani, A. M.; Al-Sa'doun, A. W. Ethylene dimerization and oligomerization to butene-1 and linear α-olefins: A review of catalytic systems and processes. *Catal. Today* **1992,** 1, 1-121.
(26) Burger, B. J.; Thompson, M. E.; Cotter, W. D.; Bercaw, J. E. Ethylene insertion and .beta.-hydrogen elimination for permethylscandocene alkyl complexes. A study of the chain propagation and termination steps in Ziegler-Natta polymerization of ethylene. *J. Am. Chem. Soc.* **1990,** 4, 1566-1577.
(27) Fischer, K.; Jonas, K.; Misbach, P.; Stabba, R.; Wilke, G. Zum „Nickel-Effekt". *Angew. Chem.* **1973,** 23, 1001-1012.
(28) Ziegler, K.; Holzkamp, E.; Breil, H.; Martin, H. Das Mülheimer Normaldruck-Polyäthylen-Verfahren. *Angew. Chem.* **1955,** 19-20, 541-547.
(29) Wells, P. B.; Wilson, G. R. Butene isomerization catalyzed by supported metals in the absence of molecular hydrogen. *J. Catal.* **1967,** 1, 70-75.
(30) Schultz, R. G.; Engelbrecht, R. M.; Moore, R. N.; Wolford, L. T. Olefin Dimerization over Cobalt-Oxide-on-Carbon Catalysts: II. Butene and Hexene Dimerization. *J. Catal.* **1966,** 3, 419-424.
(31) Takeuchi, D.; Osakada, K. In *Organometallic Reactions and Polymerization*, Osakada, K., Ed. Springer Berlin Heidelberg: Berlin, Heidelberg, 2014; pp 169-215.
(32) Ertl, G.; Knözinger, H.; Schueth, F.; Weitkamp, J., *Handbook of Heterogeneous Catalysis*. Wiley-VCH Verlag GmbH & Co. KGaA: Weinheim, 2008; Vol. 1.
(33) Mozgawa, W.; Król, M.; Barczyk, K., *FT-IR studies of zeolites from different structural groups*. 2011; Vol. 65, p 667-674.
(34) Baerlocher, C.; McCusker, L. B. Database of Zeolite Structures. http://www.iza-structure.org/databases/.
(35) Weitkamp, J. Zeolites and catalysis. *Solid State Ionics* **2000,** 1–2, 175-188.
(36) Woolery, G. L.; Kuehl, G. H.; Timken, H. C.; Chester, A. W.; Vartuli, J. C. On the nature of framework Brønsted and Lewis acid sites in ZSM-5. *Zeolites* **1997,** 4, 288-296.
(37) Ward, J. W. The nature of active sites on zeolites: I. The decationated Y zeolite. *J. Catal.* **1967,** 3, 225-236.
(38) Loewenstein, W. The distribution of aluminum in the tetrahedra of silicates and aluminates. *American Mineralogist: Journal of Earth and Planetary Materials* **1954,** 1-2, 92-96.
(39) Szostak, R., *Hanbook of Molecular Sieves*. Van Nostrand Reinhold: New York, 1992.
(40) Firor, R. L.; Seff, K. Near zero coordinate calcium(2+) and strontium(2+) in zeolite A. Crystal structures of dehydrated Ca6-A and Sr6-A. *J. Am. Chem. Soc.* **1978,** 10, 3091-3096.
(41) Pluth, J. J.; Smith, J. V. Crystal Structure of Dehydrated Calcium-Exchanged Zeolite A. Absence of Near-Zero-Coordinate Calcium(2+) Ion. Presence of Aluminum Complex. *J. Am. Chem. Soc.* **1983,** 5, 1192-1195.
(42) García-Sánchez, A.; García-Pérez, E.; Dubbeldam, D.; Krishna, R.; Calero, S. A Simulation Study of Alkanes in Linde Type A. *Adsorption Science & Technology* **2007,** 6, 417-427.
(43) Brückner, A.; Bentrup, U.; Zanthoff, H.; Maschmeyer, D. The Role of Different Ni Sites in Supported Nickel Catalysts for Butene Dimerization under Industry-Like Conditions. *J. Catal.* **2009,** 1, 120-128.

(44) Rabeah, J.; Radnik, J.; Briois, V.; Maschmeyer, D.; Stochniol, G.; Peitz, S.; Reeker, H.; La Fontaine, C.; Brückner, A. Tracing Active Sites in Supported Ni Catalysts during Butene Oligomerization by Operando Spectroscopy under Pressure. *ACS Catalysis* **2016,** 12, 8224-8228.
(45) Mlinar, A. N.; Baur, G. B.; Bong, G. G.; Getsoian, A. B.; Bell, A. T. Propene Oligomerization over Ni-Exchanged Na-X Zeolites. *J. Catal.* **2012,** 0, 156-164.
(46) Mlinar, A. N.; Shylesh, S.; Ho, O. C.; Bell, A. T. Propene Oligomerization Using Alkali Metal- and Nickel-Exchanged Mesoporous Aluminosilicate Catalysts. *ACS Catalysis* **2013,** 1, 337-343.
(47) Beltrame, P.; Forni, L.; Talamini, A.; Zuretti, G. Dimerization of 1-Butene over Nickel Zeolitic Catalysts: A Search for Linear Dimers. *Appl. Catal. A* **1994,** 39-48.
(48) Ng, F. T. T.; Creaser, D. C. Ethylene Dimerization over Modified Nickel Exchanged Y-Zeolite. *Appl. Catal. A* **1994,** 327-339.
(49) Podrebarac, G. G.; Ng, F. T. T.; Rempel, G. L. The effect of butadiene and reaction conditions on the dimerization of 1-butene over NiY zeolite. *Appl. Catal. A* **1996,** 1, 159-173.
(50) Sohn, J. R. Catalytic activities of nickel-containing catalysts for ethylene dimerization and butene isomerization and their relationship to acidic properties. *Catal. Today* **2002,** 1–2, 197-209.
(51) Yaocíhuatl, M.; Martín, H.; Jorge, A. Dimerization of isobutene over nickel modified zeolites to obtain isooctene. *Catal. Lett.* **2006,** 1-2, 107-113.
(52) Agirrezabal-Telleria, I.; Iglesia, E. Stabilization of Active, Selective, and Regenerable Ni-Based Dimerization Catalysts by Condensation of Ethene within Ordered Mesopores. *J. Catal.* **2017,** 505-514.
(53) Madrahimov, S. T.; Gallagher, J. R.; Zhang, G.; Meinhart, Z.; Garibay, S. J.; Delferro, M.; Miller, J. T.; Farha, O. K.; Hupp, J. T.; Nguyen, S. T. Gas-Phase Dimerization of Ethylene under Mild Conditions Catalyzed by MOF Materials Containing (bpy)NiII Complexes. *ACS Catalysis* **2015,** 11, 6713-6718.
(54) Pillai, S. M.; Ravindranathan, M.; Sivaram, S. Dimerization of Ethylene and Propylene Catalyzed by Transition-Metal Complexes. *Chem. Rev.* **1986,** 2, 353-399.
(55) Roy, D.; Sunoj, R. B. Ni-, Pd-, or Pt-catalyzed ethylene dimerization: a mechanistic description of the catalytic cycle and the active species. *Organic & Biomolecular Chemistry* **2010,** 5, 1040-1051.
(56) Small, B. L.; Schmidt, R. Comparative Dimerization of 1-Butene with a Variety of Metal Catalysts, and the Investigation of a New Catalyst for C□H Bond Activation. *Chemistry – A European Journal* **2004,** 4, 1014-1020.
(57) Nadolny, F.; Hannebauer, B.; Alscher, F.; Peitz, S.; Reschetilowski, W.; Franke, R. Experimental and Theoretical Investigation of Heterogeneous Catalyzed Oligomerization of a Mixed C4 Stream over Modified Amorphous Aluminosilicates. *J. Catal.* **2018,** 81-94.

1. Chapter:

Dimerization of Linear Butenes on Zeolite Supported Ni^{2+}

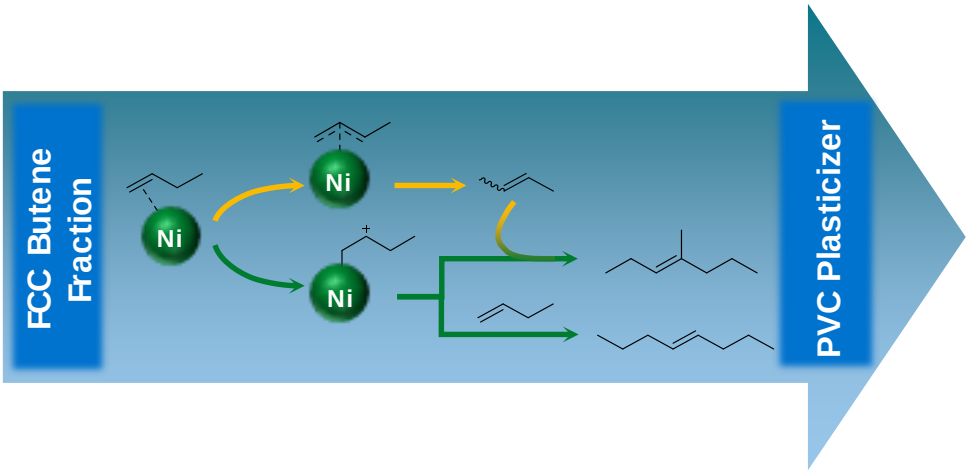

This chapter is based on:

Andreas Ehrmaier, Yue Liu, Stephan Peitz, Andreas Jentys, Ya-Huei (Cathy) Chin, Maricruz Sanchez-Sanchez, Ricardo Bermejo de Val, Johannes Lercher,[1] *"Dimerization of Linear Butenes on Zeolite Supported Ni^{2+}", ACS Catalysis 2019, 1, 315-324*

[1] A.E. prepared and characterized the catalysts, planned, designed and performed the experiments, analyzed and interpreted the data and wrote the manuscript. Y.L., Y.C., M.S., S.P. contributed to the scientific discussion. A.J. helped with the analysis of XAS measurements and contributed to scientific discussion. R.B., J.L. guided the experiments, contributed to the scientific discussion and corrected the manuscript anytime.

ABSTRACT

Nickel and alkali earth modified LTA based zeolites catalyze the dimerization of 1-butene in the absence of Brønsted acid sites. The catalyst reaches over 95% selectivity to n-octenes and methylheptenes. The ratio of these two dimers is markedly influenced by the parallel isomerization of 1-butene to 2-butene, shifting the methylheptene/octene ratio from 0.7 to 1.4 as the conversion increased to 35 %. At this conversion, the thermodynamic equilibrium of 90 % cis- and trans 2-butenes was reached. Conversion of 2-butene results in methylheptene and dimethylhexene with rates that are one order of magnitude lower than with 1-butene. The catalyst is deactivated rapidly by strongly adsorbed products in the presence of 2-butene. The presence of π-allyl bound butene and Ni-alkyl intermediates were observed by IR spectroscopy, suggesting both to be reac-tion intermediates in isomerization and dimerization. Product distribution and apparent activation barriers suggest 1-butene dimerization to occur via a 1'-adsorption of the first butene molecule and a subsequent 1'- or 2'-insertion of the second butene to form octene and methylheptene, respectively. The reaction order of two for 1-butene and its high surface cover-age suggest that the rate determining step involves two weakly adsorbed butene molecules in addition to the more strongly held butene.

INTRODUCTION

Linear and single-branched alkenes and in particular octenes are important intermediates in the synthesis of high value products, such as co-monomers for low density polyethene.[1] The pathway to produce these molecules via dimerization is attractive, because it utilizes abundantly present light olefins. Nickel-based catalysts have been identified as the most promising family of catalytic materials, exhibiting a high activity and selectivity to linear alkenes.[2-7] These catalysts favor the formation of dimers and limit successive C-C bonding formation.

Mechanistically, α-alkene formation has been reported to occur via a Ni-alkyl complex, following the Cossee-Arlman mechanism, a metallacycles route, and proton-transfer mechanisms.[8-10] Catalysts based on Ni dispersed on solid supports, including molecular organic frameworks, were proposed to follow the former mechanism.[6, 11-18 19]

Indeed, ethene oligomerization over Ni exchanged zeolites has been proposed to proceed via formation of a 1' alkyl carbenium ion followed by a migratory insertion, while the products desorb with a ß-hydride elimination (Cossee-Arlman mechanism).[20] It has been suggested that the density of liquid-like ethene is required to aid the desorption of butene, limiting C_4 isomerization and further polymerization via ethene addition.[21]

To achieve high rates and to avoid side reactions, Ni^{2+} cations have to be well separated and the support should be free of other strong acid sites, in particular Brønsted acid sites (BAS). Mesoporous and microporous crystalline aluminosilicates and amorphous aluminosilicates are supports that can potentially achieve such high Ni dispersion,[22-29] provided that two Si-O-Al exchange sites are sufficiently close to stabilize a Ni^{2+} cation. Indeed, zeolites with high framework Al concentrations (Si/Al ~ 1-3) have been shown to be well suited. However, ion exchange with Ni^{2+} still leads frequently to isolated BAS that catalyze alkene dimerization to dimethylhexene, but also lead to isomerization, oligomerization and cracking.[30-33]

The importance to avoid isomerization is best illustrated with the fact that an additional pathway to branched alkenes is available for isomers with internal C=C bonds.[13, 15] In the case of dimerization of butenes, isomerization of 1-butene to 2-butene opens this pathway to undesired products.[34] Therefore, minimizing the relative rate of double bond isomerization is a critical challenge for dimerization of alkenes with more than three carbon atoms. Therefore, it is essential to combine a high concentration of isolated Ni^{2+} with the absence of Brønsted acid sites in order to achieve high selectivity to linear and single-branched alkenes. We have

addressed this by choosing an LTA zeolite to host the Ni^{2+}, adjusting the other exchange cations not only to minimize or eliminate the presence of Brønsted acid sites, but also to adjust the electronic state of Ni^{2+}.

The present manuscript explores, therefore, partially Ni^{2+} exchanged Ca-LTA for butene dimerization. The narrow pores of LTA allow only the conversion at pore mouth or on the outer surface. The rates of dimerization and competing isomerization are studied in the absence of Brønsted acid sites, combining characterization of adsorbed species by IR spectroscopy and kinetic measurements. This study shows a unique chemical environment for Ni^{+2}, weakening its Lewis acidity by coadsorption of a third butene molecule.

RESULTS AND DISCUSSION

1-Butene dimerization on Ni-Ca-LTA catalysts

At the start, a series of Ni-Ca-LTA-based catalysts with different Ni-loadings was prepared and characterized with respect to morphology and crystallinity in order to select an adequate catalyst for mechanistic studies. Details are provided in the Supporting Information. Broadening of the XRD diffraction bands of LTA was observed with increasing Ni loadings (see SI, Figure S1-1), indicating certain loss of crystallinity due to the ion exchange.[35-36] While a hysteresis for the N_2 sorption was not observed for Ca-LTA (Figure S1-2), the sorption volume of the Ni containing catalysts showed important differences during adsorption and desorption, pointing to an increase of mesopore and a decrease of the micropore volume (Table S1-1). To minimize the impact of local lattice destruction, the loading of Ni was limited to 6 wt.% on Ni-Ca-LTA. Changes in the particle size were not observed by SEM (Figure S1-3 and Table S1-2).

Analysis by X-ray absorption spectroscopy (XAS) was used to establish the oxidation state of the Ni in Ni-Ca-LTA in contact with 1-butene. Variations in the Ni-K edge energy (8333 eV) prior and after exposure to 1-butene were not observed in the X-ray absorption near edge structure (XANES). This indicates that Ni is present as Ni^{2+} in the acting catalyst (Figure S1-4 A) and we conclude that Ni^{2+} is the active center for dimerization. [11, 37,38]

The weight based rate of 1-butene dimerization was determined for catalysts containing 2-6 wt.% Ni (Figure S1-5, Table S1-3). The rate of dimerization increased linearly with the Ni concentration. This led us to conclude in turn that all (or a constant fraction) of Ni^{2+} is accessible to the reactants at this level of ion exchange. Therefore, the detailed mechanistic studies were performed on a 6 wt.% Ni exchanged Ni-Ca-LTA catalyst.

The butene conversion rates and product rate distribution upon time on stream for a 6 wt.% Ni exchanged Ca-LTA are shown in Figure 1-1. Rates in butene conversion were the highest within the first five hours ($1.5 \cdot 10^{-4}$ mol_C /g/s). These rates were less than an order of magnitude lower than rates reported for zeolites and mesoporous aluminosilicates with BAS.[11, 25-27] Subsequently, slight deactivation was observed with time on stream. For the mechanistic and kinetic studies in this work, the reported activity data were extrapolated to zero time on stream (TOS). Rates to octene and methylheptene were comparable ($6\text{-}7 \cdot 10^{-5}$ mol_C /g/s), while rates to dimethylhexene were of one order of magnitude lower. To compare the intrinsic dimerization and trimerization activity of Ni-Ca-LTA, we assumed an overall second order reaction for each pathway, i.e., second order in butene for dimerization and first order in both

butene and octene for trimerization. A higher apparent second reaction order constant was observed for trimerization (k_{tri} = 5.67·10^{-9} mol_C/g/s/bar^2) than for dimerization (k_{di} = 1.67·10^{-9} mol_C/g/s/bar^2). Thus, Ni-Ca-LTA has a higher selectivity for trimers than for dimers in the oligomerization of 1-butene. This selectivity is higher than observed for Ni-aluminosilicates in the presence of Brønsted acid sites.[26] Note that the operating temperature below 200°C prevented cracking of 1-butene and products, as was observed with similar catalysts.[25]

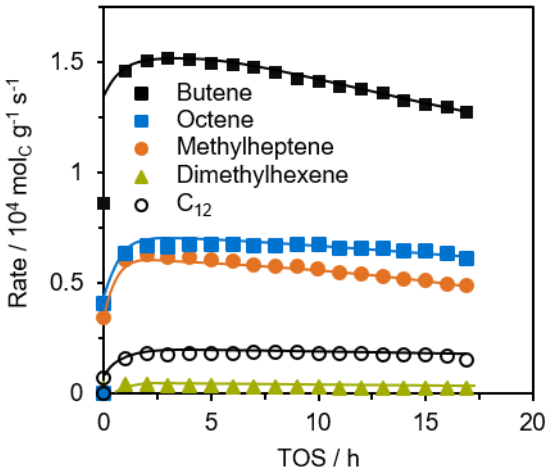

Figure 1-1. Reaction of 1-butene over a 6 wt.% Ni-Ca-LTA. Butene consumption rate (black squares) and formation rates of dimerization products over time on stream with respect to moles of carbon. T = 160 °C, p = 50 bar, WHSV = 38 h^{-1}.

Product distribution with Ni-Ca-LTA catalysts

The oligomerization of 1-butene on a 6 wt.% Ni containing LTA catalyst was conducted at 50 bar, 160 °C and space velocities ranging from 6 to 244 h^{-1} (Figure 1-2). Results show higher than 80 % selectivity towards octenes, with less than 20 % of higher oligomers – mostly trimers (not shown). Within the dimer fraction, the main products were 3-methylheptenes and n-octenes (Figure 1-1 and Figure 1-2 A). Only small amounts (less than 5 % among the dimers) of 3,4-dimethylhexenes were formed. The thermodynamic dimer equilibrium at the given conditions predicts a ratio of dimethylhexene / methylheptene / octene of 34 / 60 / 6 (Figure S1-6), i.e., the products observed are quite distant from equilibrium.

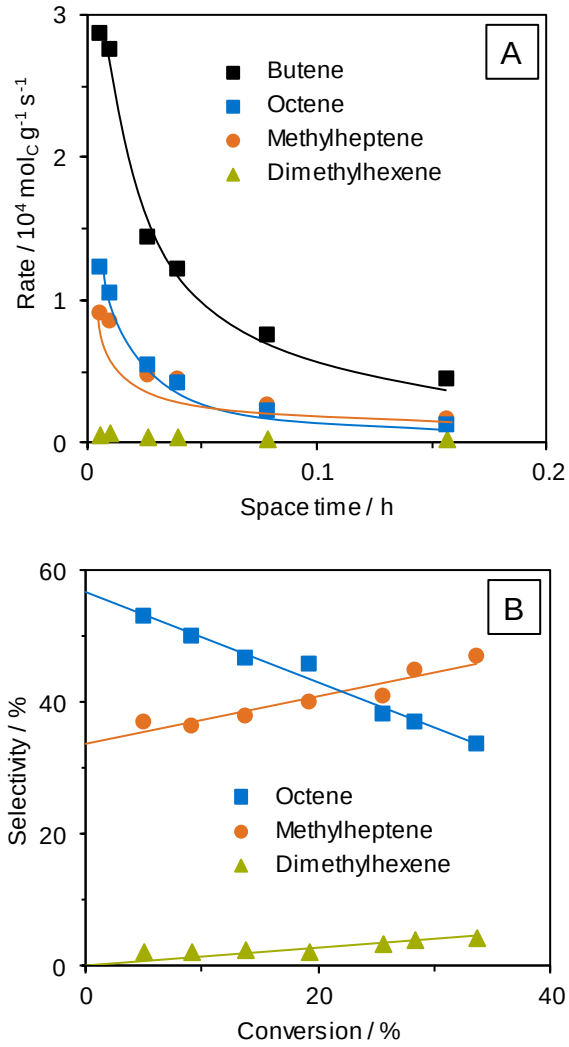

Figure 1-2. A) Effect of space time on catalytic conversion rate of 1-butene (black squares) and dimer distribution, and B) Dimer selectivity as a function of the conversion of 1-butene over a 6 wt.% Ni-Ca-LTA catalyst. T = 160 °C, p = 50 bar, WHSV = 6-245 h^{-1}.

The 1-butene consumption rate with varying space time is shown in Figure 1-2 A. Upon higher space times, 1-butene consumption leveled off at a rate of $5 \cdot 10^{-5}$ mol_C /g/s, corresponding to ca. 35 % conversion. It was not possible to surpass this level of conversion by an increase in space time. However, this value is far from the dimerization thermodynamic equilibrium (close to 100 % 1-butene conversion as shown in Figure S1-6). As the conversion increased, 1-butene was isomerized to 2-butene, reaching the thermodynamic equilibrium (Figure 1-3 A) at the point (Figure 1-2 A) when the 1-butene conversion rate in dimerization leveled off, at approx. $5 \cdot 10^{-5}$ mol_C /g/s (conversion values of ~30-35 %, grey bar in Figure 1-3 A). Figure 1-3 B shows the approach to equilibrium for the two parallel reactions: dimerization and butene double bond isomerization (defined as the ratio of the different isomers, see SI for details).

Isomerization increased rapidly to the value of one with butene conversion, indicating equilibration, while dimerization did not exceed the value of 0.35 (Figure 1-3 B). Therefore, it is suggested that double bond isomerization, i.e., the increasing concentration of 2-butene, limits the conversion level.

The dimer selectivity as a function of 1-butene conversion is shown in Figure 1-2 B. Methylheptene and octene were the predominant products of 1-butene dimerization, while dimethylhexene was formed in significantly lower concentrations. The changes in dimer product selectivity and the double bond isomerization with butene conversion show that octene is formed solely from 1-butene, and that dimethylhexene is solely formed from 2-butene dimerization.

Methylheptene can be formed from both 1- and 2-butene. Scheme 1-1 shows the reaction pathways proposed for the dimerization of 1-butene. The adsorption of the first butene molecule on the Ni active site is hypothesized to take place at the primary (1'-adsorption) or at the secondary carbon atom (2'-adsorption).[20, 39-42] The insertion of the second butene for C-C bond formation, can also take place at the primary (1'-insertion) or secondary (2'-insertion) carbon. The modes of adsorption and insertion and their probability determine the selectivity to the dimer isomers (octene, 3-methylheptene and 3,4-dimethylhexene). The obtained product distribution indicates that the main route in dimerization with Ni-Ca-LTA takes place either by 1'-adsorption of 1-butene and 1'-insertion or 2'-insertion of 1-butene, because n-octene and methylheptene were formed preferentially.

At higher conversions, the increase in selectivity to methylheptene and dimethylhexene is attributed to a higher contribution of the 2'-adsorption and/or 2'-insertion pathway. This is speculated to be also the result of a higher 2-butene concentration from the double bond isomerization of 1-butene (the options for 2-butene are shown in green color in Scheme 1-1). Therefore, octene and methylheptene are concluded to be primary products, dimethylhexene to be a secondary product. It is noted in passing that, the absence of Brønsted acid sites (BAS) is responsible for the low dimethylhexene selectivity. In presence of the latter formation of dimethylhexene (selectivity above 30%) is favored by the formation of secondary carbenium ions. [11, 28, 37, 43]

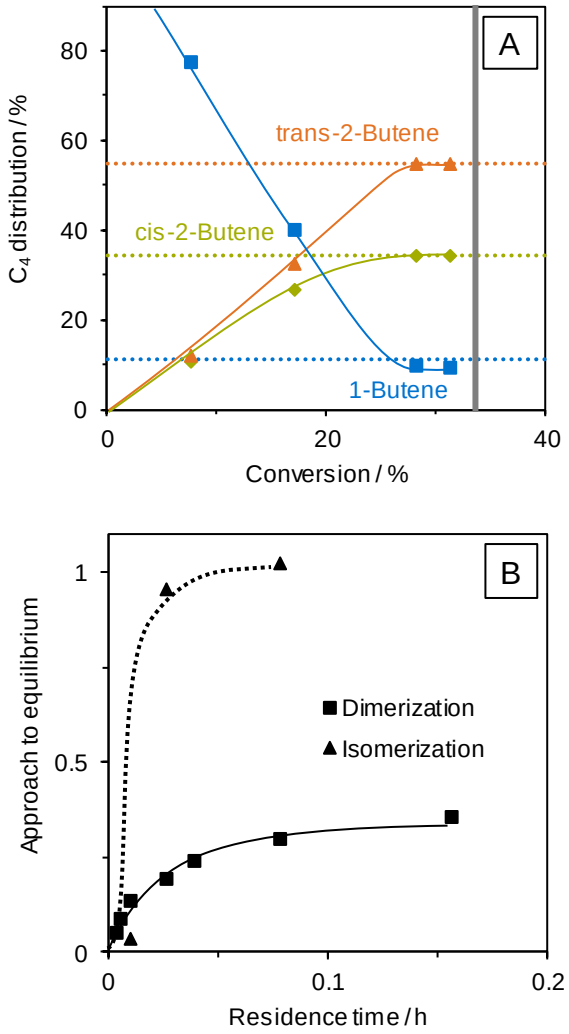

Figure 1-3. A) Reactant isomerization behavior over 6 wt.% Ni-Ca-LTA. The dotted lines give the equilibrium at 50 bar and 160 °C. B) Approach-to-equilibrium for dimerization and isomerization. Reaction conditions: T = 160 °C, p = 50 bar, WHSV = 6-245 h^{-1}.

Impact of 2-butene on the deactivation of Ni-Ca-LTA

The limiting butene conversion of 35 % (leveling off at a rate of $5 \cdot 10^{-5}$ mol_C /g/s, Figure 1-1) and chemically equilibrated double bond isomerization, taken together, suggest that 2-butene hinders further dimer formation (Figure 1-3). To test this hypothesis, pure cis-2-butene was fed and oligomerized (Figure 1-4). With cis-2-butene, rates were significantly lower and decreased much more rapidly (Figure 1-4 A), as well as higher selectivities to methylheptene and slightly higher selectivities to dimethylhexene (Figure 1-4 B) were observed. Therefore, following the reaction pathway of Scheme 1-1, 2-butene can only adsorb via 2'-adsorption

(Scheme 1-1, green color), leading to branched products only. The fact that n-octene was also formed even at lower conversions, suggests that a small fraction of 2-butene was isomerized to 1-butene, which in turn acted as precursor to n-octene.

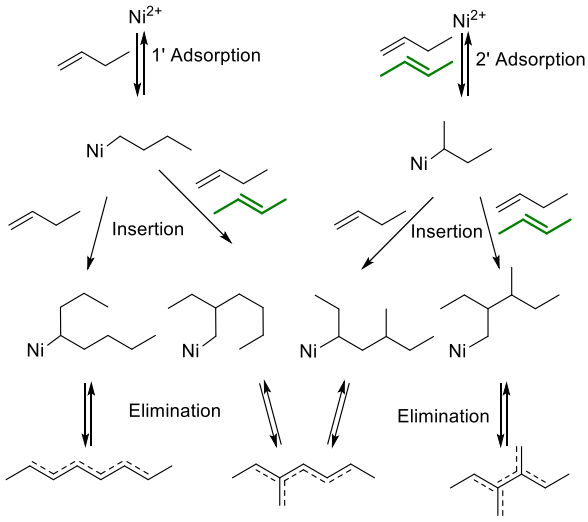

Scheme 1-1. Possible pathway for the formation of the dimer isomers from 1-butene (black) and 2-butene (green). Adapted from Cossee-Arlman mechanism.[39]

In order to understand the low activity of Ni-Ca-LTA in the dimerization of 2-butenes, the feed was switched between 1- and 2-butene (Figure 1-5). The first transient from 1-butene to cis-2-butene (Figure 1-5 A) led to a rapid decrease in butene conversion rate. In a second experiment, the reactor was first fed with 2-butene and subsequently switched to 1-butene. This transient increased the dimerization activity, but to a level that was approximately one order of magnitude lower than that starting from 1-butene (Figure 1-5 B, and comparison to Figure 1-5 A). Thus, we conclude that 2-butene induced irreversible changes to the most active sites of Ni-Ca-LTA.

Based on the above results, we conclude that 1-butene isomerizes to 2-butene, inducing rapid deactivation, especially at higher conversions. The higher concentration of 2-butene compared to 1-butene (90 % 2-butene and 10 % 1-butene at conversions above 30 %, Figure 1-3 A) leads also an increase in the selectivity to products formed from the 2'-adsorption pathway, i.e., methylheptene and dimethylhexene (Figure 1-2 B). However, the selectivity to n-octene is still higher than that to dimethylhexene, indicating a significantly faster dimerization for 1-butene than for 2-butene.

The low activity in 2-butene dimerization is hypothesized to be caused by the formation of a stable Ni-alkyl species either via the 2'-adsorption or via the insertion of another alkene

(1-butene or 2-butene) into the secondary carbon of the adsorbed 2-butene. Thus, the deactivation over time observed in Figure 1-1 is concluded to be caused by the high concentration of 2-butene (ca. 2/3 of butene at 20% butene conversion), leading to the formation of a surface species that is unable to desorb.

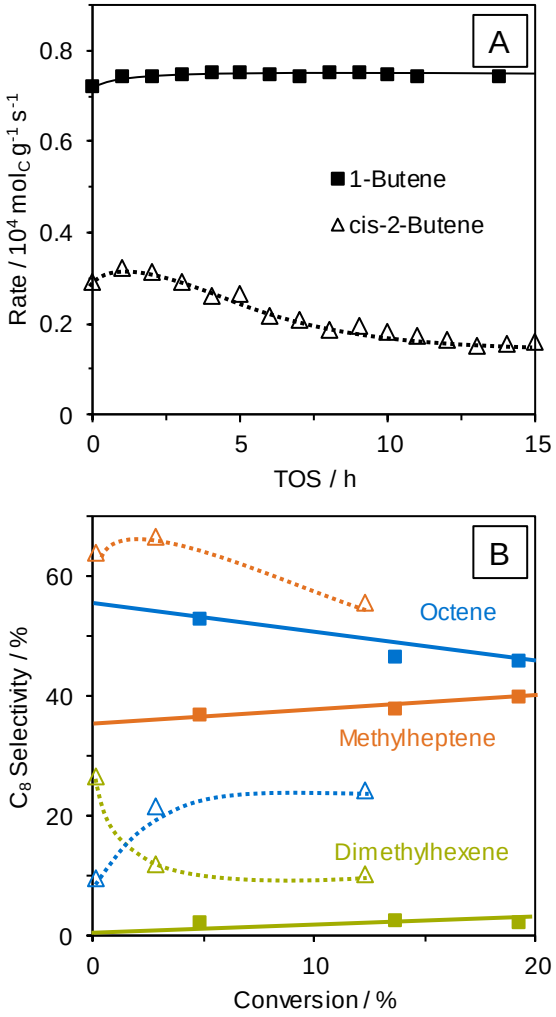

Figure 1-4. Conversion rate, in terms of the moles of carbon (A), and product distributions (B) of 1-butene and cis-2-butene dimerization reaction over 6 wt.% Ni-Ca-LTA at 160 °C, 50 bar, WHSV graph A = 12.5 h^{-1}; WHSV graph B =12-245 h^{-1}. Conversion of cis-2-butene is shown as empty triangles, reaction of 1-butene is presented as filled squares, and so are the corresponding products. Colors of products: n-octene (blue), methylheptene (orange), dimethylhexene (green).

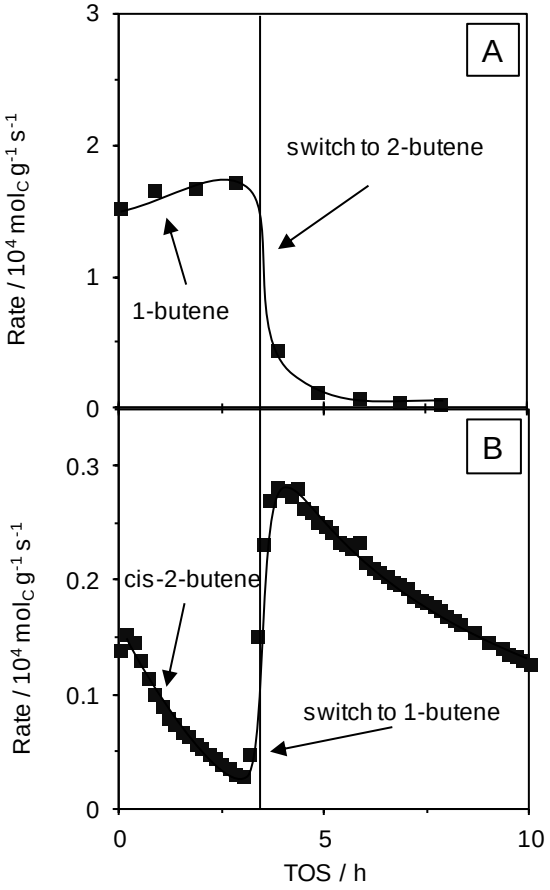

Figure 1-5. Effect of cis-2-butene on butene consumption rate over a 6 wt.% Ni-Ca-LTA, at T = 160 °C and P = 50 bar, starting with 1-butene and switched to cis-2-butene (WHSV = 50 h^{-1}) (A), and experiment started with cis-2-butene and switched to 1-butene (WHSV = 50 h^{-1}) (B).

To analyze the carbonaceous deposits resulting from exposure to 2-butenes, spent catalysts were dissolved in HF and the remainder was subsequently dried at 90 °C. The organic residue was dissolved in hexane and analyzed by gas chromatography. A higher concentration of C_{16+} was observed after 2-butene dimerization, while concentrations of hydrocarbons between C_{12} and C_{16+} were similar to those obtained after 1-butene dimerization. This suggests that 2-butene dimerization forms larger oligomers that block and deactivate Ni^{2+} sites.

Kinetics of 1-butene dimerization

The reaction orders obtained for the formation of octene and methylheptene (Figure 1-6), with respect to 1-butene, were approximately 2 (Figure S1-7 C and D). This points to the C-C coupling of the two weakly adsorbed butenes as the rate determining step (r.d.s.), in agreement to studies on ethene dimerization.[21, 44-46] The measured activation energies for the

formation of the specific dimers, as well as for the different oligomers, are shown in Table 1-1 (Arrhenius plots are shown in Figure S1-7 A and B in SI). The reaction order and activation energy were not measured for dimethylhexene, since it is a secondary product. Among the dimers, the values of apparent activation energies (E_a) determined for methylheptene and octene were similar (76 and 72 kJ/mol, respectively) and indicate that both products stem from a pathway with a similar transition state. The values were similar to the ones obtained by Zhang et al. with Ni-ZSM-5.[47] As previously shown in Scheme 1, the formation of dimethylhexene requires the 2'adsorption and 2'insertion of 1-butene or 2-butene. Therefore, prior to the formation of dimethylhexene, isomerization of 1-butene into 2-butene must take place.

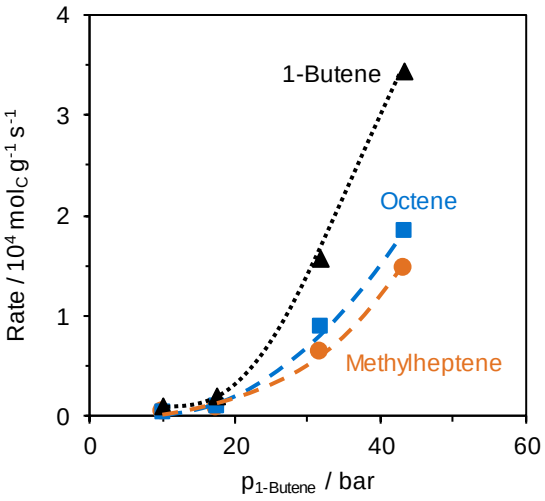

Figure 1-6. Reaction of 1-butene consumption and formation of methylheptene and octene over 6 wt.% Ni-Ca-LTA.. T = 160 °C, p = 50 bar, WHSV = 15-156 h^{-1}; 1-Butene feed mix diluted with propane: $c_{1\text{-butene}}$ = 20 – 86 wt.%.

Table 1-1. Energy of activation for the butene consumption, as well as for the formation of products at conversion levels between 0.5 and 3.5 %. WHSV = 150 h^{-1}, p = 50 bar, T = 140-180 °C. Arrhenius plots are shown in SI (Figure S1-7).

	E_A **[kJ mol^{-1}]**
C_4 consumption	73
Methylheptene	76
Octene	72

IR spectra of adsorbed and reacted butenes

IR spectroscopy is used to characterize the adsorbed species and monitor the gradual isomerization of adsorbed butenes as reaction proceeds. The basic nature of the catalysts stabilizes carbonates, which change in nature and concentration during reaction. We hypothesize that these carbonates are largely spectators to the catalytic transformations. However, their presence will moderate the acid-base properties of the investigated catalysts.

Exposing the activated zeolites to 1-butene and subsequent evacuation led to IR spectra of adsorbed 1-butene on Ca-LTA and Ni-Ca-LTA that are compiled together with the assignments in SI-5 (Table S1-4, Figure S1-8, and Figure S1-9). The spectra of 1-butene adsorbed on Ca-LTA and Ni-Ca-LTA showed bands at 1300-1700 cm^{-1} (Figure S1-8), which are characteristic of C=C stretching, C-H bending and carbonate or carboxylate vibrations. The assignments and the discussion on the carbonate bands are provided in SI-5. The IR spectra of 1-butene adsorption on Ca-LTA and Ni-Ca-LTA in the 2700-3200 cm^{-1} region are shown in Figure S1-9. Admission of butene leads to C-H stretching bands on both samples. The bands at above 3000 cm^{-1} are attributed to C-H stretching vibrations at C=C bonds, while the bands below 3000 cm^{-1} are attributed to C-H vibrations at C-C bonds of physisorbed alkenes.[48-49]

After activation of Ni-Ca-LTA, 1-butene was adsorbed at constant pressure (1 mbar) and IR spectra (Figure 1-7) showed bands characteristic of bidentate carbonate as described in SI-5. The most pronounced bands between 1620 and 1660 cm^{-1} are assigned to π-bonded butene on Ni^{2+}. Directly after exposing the sample to a stream of 1-butene, a band at 1622 cm^{-1} with a shoulder at 1658 cm^{-1} (attributed to gaseous 1-butene[50]) was observed. The wavenumber at 1622 cm^{-1} tentatively is attributed to π-bonded 1-butene.[48, 51-52] After 10 min, a band at 1641 cm^{-1} evolved. It is attributed to an adsorbed alkene with an internal double bond (π-bound 2-butene or a branched octene), since the higher wavenumber indicates a stronger C=C bond for 2-butene than for the external C=C bond observed for 1-butene (1622 cm^{-1}).[50, 53] This is further supported by the variations of the relative intensity of the CH vibrations at 1440, 1408, 3061 and 3005 cm^{-1} (Figure 1-7), indicating an increasing number of =CH vibrations in the surface species.

The changes observed in the concentration of methyl groups of the adsorbed hydrocarbons allowed us to follow double bond isomerization and/or dimerization reactions of 1-butene. An increase in the intensity of CH_3 group vibration (1390 cm^{-1}, Figure 1-7 A), especially within the first 30 min, and in the CH_3 bending vibration (2873 and 2967 cm^{-1}, Figure 1-7 B), suggests that several CH_3 groups were formed, as the combined result of isomerization and alkene

addition. Because the intensity of the CH_2 bands (2841 and 2939 cm^{-1}) remained constant throughout the experiment, we conclude that double bond isomerization and the formation of surface alkyl species are the main surface reactions under these conditions. Within the 30 min of exposure, two additional bands appeared at 1585 and 1295 cm^{-1}. The lower wavenumber is attributed to a delocalized C=C bond stretching vibration, tentatively assigned to π-allyl formation.[54] In addition, the band at 1295 cm^{-1} is assigned to the stretching of a carbenium ion (ν_{as} C^+-C).[55-57] The allyl species is hypothesized to lead to isomerization, while the carbenium ion is suggested to be a key intermediate in the dimerization (Scheme 1-2).

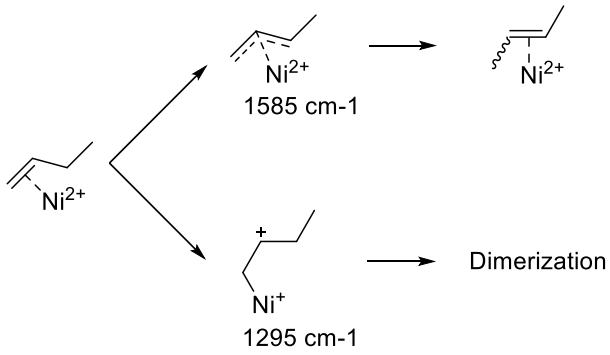

Scheme 1-2. Surface intermediates detected upon butene adsorption on Ni-Ca-LTA and their proposed reactivity.

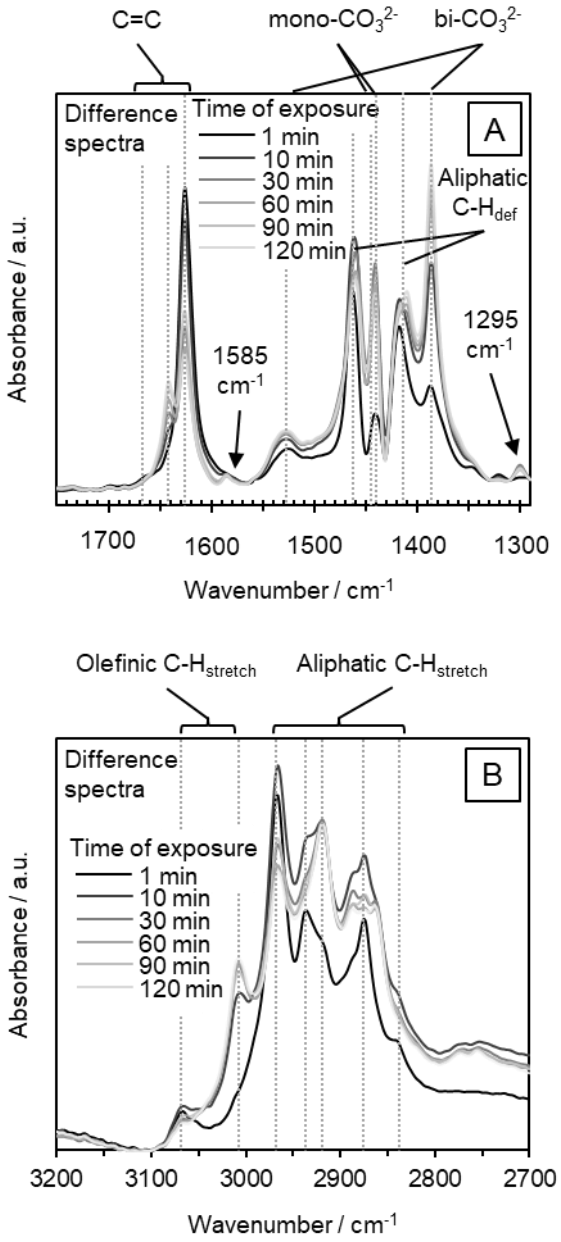

Figure 1-7. IR spectra of 6 wt.% Ni-Ca-LTA at 40 °C exposed to 1 mbar of 1-butene after 1-30 minutes A) 1300-1700 cm^{-1} range, B) 2700-3200 cm^{-1} range.

Enthalpic contribution of adsorption of butenes on Ni-Ca-LTA

The heat of adsorption of 1-butene on Ni-Ca-LTA was of 63 kJ mol^{-1} (Figure S1-10). A Langmuir approach was used to fit the isotherm, with a maximum surface coverage of 0.73 $mmol_{1\text{-butene}}/g$ and an adsorption constant K of $4.9 \cdot 10^{-3}$ bar^{-1} (SI-6) at 40 °C. This adsorption constant at 40 °C gives the adsorption constant of $6.0 \cdot 10^{-6}$ bar^{-1} at 160 °C, according to van't Hoff equation (SI-6). This adsorption constant translates to Ni^{2+} sites nearly saturated with 1-

butene, as predicted by Langmuir adsorption isotherm ($P_{1\text{-butene}}$ = 42.5 bar). The high adsorption enthalpy of 63 kJ mol^{-1} indicates a strong interaction of the alkene with the Ni, leading to the formation of a Ni alkene complex, potentially increasing the electron density at Ni^{2+}. It should be noted in passing that this hypothesized interaction was not manifested in XANES at the Ni-K edge energy (8333 eV).

The adsorption of 2-butene was also examined (Figure S1-11). A successive weight increase was observed within the first 12 hours at 0.03 mbar of 2-butene. The initial adsorption enthalpy was, however, approximately 63 $kJmol^{-1}$ and hence similar than for 1-butene.

Catalytic pathway of butene dimerization on Ni-Ca-LTA

The product distribution and the concluded formation of a Ni-alkyl complex (Scheme 1-1) are compatible with the proposed dimerization mechanism. The obtained product distribution indicates the dimerization is mainly taking place by 1'-adsorption of 1-butene and 1'-insertion or 2'-insertion of 1-butene, because n-octene and methylheptene were formed preferentially. In contrast, a metallacycle mechanism would involve the formation of the three dimers in comparable concentrations. Their ratio would depend on the adsorption and insertion orientation of the π-bound alkenes.[58-59] The very low formation rates of dimethylhexene and its non-existence at 0 % conversion led us to conclude that the metallacycle mechanism is not operative for Ni-Ca-LTA.

The product distribution obtained on Ni-Ca-LTA points to a stepwise mechanism for butene dimerization. We propose a dimerization pathway adapted from Cossee-Arlman mechanism (Scheme 1-3), which involves initially the formation of a Ni-alkyl complex as the active site throughout the entire catalytic cycle (Scheme 1-3). The full coverage of Ni by 1-butene and the reaction order of 2 with respect to 1-butene support the formation of a Ni-alkyl complex as the active site; this site is able to coordinate to two additional butene molecules that lead to the dimer. The catalytic cycle begins with the adsorption of 1-butene on the Ni-alkyl complex, preceded by the formation of a covalent bond with the Ni-alkyl complex (Step 1, Scheme 1-3), in chemical equilibrium with the gas phase butene. We view the allyl complex as the intermediate for the isomerization of π-bonded 1- and 2-butene on Ni (Scheme 1-2). In the next step, a second butene molecule weakly adsorbs via π bond interaction. Consecutively, the third step is the kinetically relevant C-C bond formation that forms the C_8 alkene product (step 3 in Scheme 1-3). Desorption of the C_8 alkene regenerates the Ni-$alkyl_{C4}$ complex, making it ready for the next catalytic cycle. Pseudo steady-state treatments on the

intermediates, together with assumptions of binding site and Ni-alkyl complex as the most abundant surface intermediates (step 1, Scheme 1-3), give the rate expression of (derivation at SI-4):

$$r = \frac{K_1 K_2 k_3 [C_4]^2}{1 + K_1[C_4] + K_2[C_4] + [C_8]/K_4} \approx k[C_4]^2$$

which simplifies to an apparent 2nd order dependence at low surface coverages in the limit of low product concentration. The K and k are the equilibrium constants for adsorption and elementary C-C bond formation rate constant of the kinetically relevant step, as also defined in Scheme 1-3.

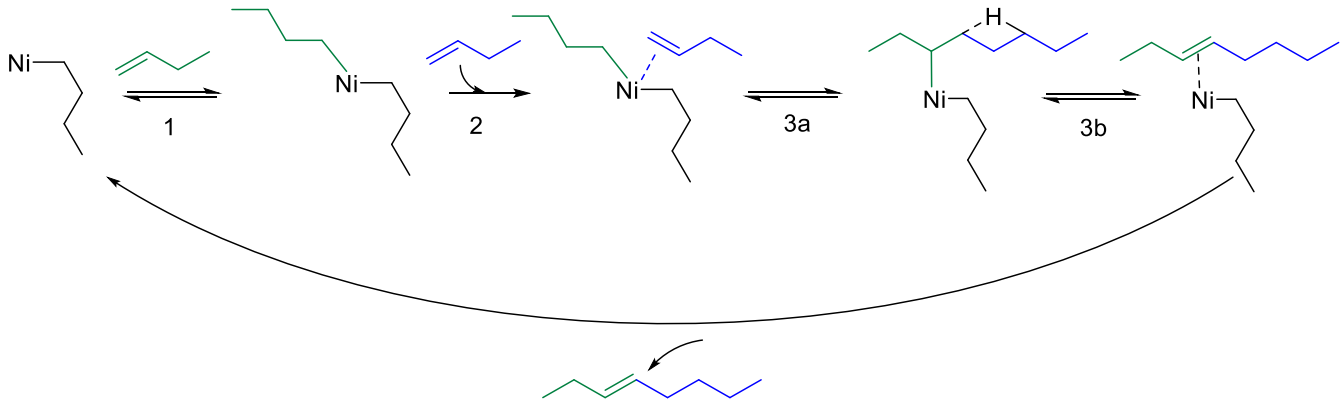

Scheme 1-3. Proposed reaction network for dimerization of linear butenes over Ni active site (Ni-alkyl in the zeolite). Firstly, 1-butene (green) would adsorb on the Ni-alkyl complex (1). A second butene molecule (blue) weakly adsorbs on the Ni-alkyl$_{C4}$ complex (2). Collectively, dimerization is taking place on the Ni-alkyl$_{C8}$ complex (3), being rate limiting. Finally, there is a subsequent internal hydride shift, leading to product desorption from the Ni site and formation of the Ni-alkyl$_{C4}$ complex for a new catalytic cycle.

It should be noted that, according to Scheme 1-3, an internal hydride shift (step 3a) is necessary, before the products can desorb from the Ni site and regenerate the active site to form a new Ni-alkyl complex. Brogaard et al.[20] have estimated that Ni-alkene-alkyl complexes of different alkyl chain length are quite close in free energy in the Cossee-Arlman pathway. Similarly, the proposed mechanism suggests the change to a larger adsorbate for the Ni-alkene-alkyl complex, evolving from a Ni-alkene-alkyl$_{C4}$ to a Ni—alkene-alkyl$_{C8}$. The reason for this modified Cossee-Arlman mechanism on Ni-zeolite is attributed to the absence of Brønsted acid sites.[20] The lack of Brønsted acidity also agrees well within the high yields to

linear and mono-branched C8 isomers, because dibranched dimer are favored by Brønsted acid catalyzed dimerization.[32-33]

While this is a plausible mechanistic pathway, the strong adsorption of butene on Ni^{2+} and the chemical potential of the reacting butene suggest that the reaction starts from a Ni-alkyl complex. This complex is equivalent to those observed in homogeneous systems,[8] having ligands coordinated to Ni metal altering the electronic charge of its d orbital. The observed second-order and the full coverage requires to postulate the presence of this Ni alkene complex that moderates the coordination of the reacting butenes with Ni^{2+}.

The insertion step defines the product selectivity upon the orientation of the adsorbed butene molecule. The possible orientations of the butene molecules within the cyclic transition state are shown in Scheme S1-1 in SI, as those proposed by theory with Ni homogeneous complexes.[44] In this case it is proposed a relatively low stability of the primary carbenium ion that would be formed upon a 2'-adsorption of 1-butene (Scheme S1-1 B in SI). Hence, it is preferred an initial 1'-adsorption of pure 1-butene. Once 2-butene is available from the double bond isomerization of 1-butene, 2'-adsorption of 2-butene leads to a better stabilized secondary carbenium ion, which opens another dimerization pathway via this intermediate. In all cases, however, the butene insertion step is associated with the highest activation barrier.

CONCLUSION

1-Butene dimerization on a Ni-Ca-LTA derived catalysts was highly selective to methylheptene and n-octene (95%), shifting the methylheptene/octene ratio from 0.7 to 1.4, in the conversion range up to 35 %. The main dimerization pathway is proposed to take place via initial 1'-adsorption of 1-butene on Ni and subsequent 1- or 2-insertion of a second butene, leading to the high selectivity to methylheptene and n-octene dimers.

Double bond isomerization of butene is also catalyzed by Ni^{2+} in Ni-Ca-LTA. The extent of dimerization plays an important role for the dimerization pathway. High concentrations of 2-butene favor the 2'-insertion into 1'-adsorbed species, increasing the selectivity to methylheptene. The 2'-adsorption is the only possible mode for internal alkenes, causing a high concentration of 2'-adsorbed species and lead to the formation of mono- and dibranched dimers. Double bond isomerization equilibrium was reached at about 30% conversion and limited the conversion rate to dimers by almost one order of magnitude. Adsorbed 2-butene or its dimerization products also lead to irreversible changes at the active sites and blocking them by formation of strongly bound oligomers.

IR spectroscopy shows that Ni-allyl and Ni-alkyl complexes are formed as most abundant intermediates during isomerization and dimerization. During isomerization, the adsorption-desorption is equilibrated and the reactants assume an allylic transition state.

Dimerization of linear butenes on Ni-Ca-LTA follows a Cossee-Arlman type mechanism. After formation of the Ni-alkyl complex, two butene molecules form a C-C bond. Ni sites are interacting with 1-butene, forming Ni-alkyl complexes, at which a second order kinetically-relevant C-C bond formation occurs that leads to octenes. These findings suggest the Ni^{2+} species that catalyzes the reaction exists in a very special chemical environment involving an additional coordinated butene.

EXPERIMENTAL

Catalyst preparation. Ca-LTA was obtained by stirring Ca-LTA-5A (Sigma-Aldrich, pre-calcined: 4 h, rate 5 °C/min, 500 °C) with water (20 g_{water} / $g_{zeolite}$) at 80 °C for 24 h (pH = 7-8 over total exchange time). The solid was recovered and washed thoroughly with deionized water. After drying at 100 °C for 10 hours, the precursor was calcined (8 h, rate: 5 °C/min, 500 °C, air). Ni-Ca-LTA with different Ni wt.% was prepared by aqueous ion exchange of Ca-LTA-5A with Ni^{2+}. The Ni^{2+} ion exchange was carried out with an aqueous $Ni(NO_3)_2$ (Sigma-Aldrich) solution (20 $g_{solution}$ / $g_{zeolite}$) at 80 °C for 24 h. The molarity of the solution varied between 0.00-0.06 M to obtain 0-6 wt.% Ni^{2+} in Ca-LTA (0 wt.% of Ni^{2+} was obtained in the case of no $Ni(NO_3)_2$ in solution). During Ni ion exchange, the pH value was 6-7 during the total time of exchange (Figure S12). The charge balance was approximately 100% with respect to Al atoms (Table S5). The solid was recovered and washed thoroughly with deionized water. After drying at 100 °C overnight, the precursor was calcined (8 h, rate: 5 °C/min, 500 °C, air).

Characterization methods. Two different methods were followed in the adsorption of 1-butene on Ni-Ca-LTA via IR: 1-butene was adsorbed, equilibrated and subsequently evacuated stepwise; and the time resolved adsorption of 1-butene at a constant pressure. In the first method, low pressure IR spectra were recorded on a Vertex 70 spectrometer from Bruker Optics, equipped with a liquid nitrogen cooled detector. A thin and self-supporting wafer was installed and activated for 1 h at 450 °C (rate: 10 °C/min) in vacuum. After cooling to 40 °C, butene was adsorbed to 0.5 mbar and then later evacuated ($P < 10^{-7}$ mbar). Scans were taken with a resolution of 0.4 cm^{-1}, with an average of 120 scans per spectrum. In the second approach, for IR spectroscopy under constant pressure, the samples were prepared as self-supporting wafer and first activated in vacuum at 450 °C (rate: 10 °C/min) in situ for 2 h. After pretreatment, the activated samples were cooled to 40°C. Subsequently, 1-butene was adsorbed at 1mbar. Spectra were recorded after 1-30 minutes on a Nicolet iS50AEM spectrometer from ThermoScientific, equipped with a liquid nitrogen cooled detector at a resolution of 4 cm^{-1}. Scans were taken from 1000-4500 cm^{-1} with an average of 500 scans per spectrum.

For determining the coke, spent catalysts (24 h on stream at 160 °C and 50 bar, WHSV = 50 h^{-1}) were dissolved in a sufficient amount (approx.. 20 ml) of HF at 80 °C. After evaporation of HF, the residue was collected in hexane and injected into a GC equipped with a 50 m HP-1 column and a flame ionization detector.

X-ray diffraction (XRD) measurements were performed in a PANalytical Empyreal System diffractometer, equipped with a Cu- Kα radiation source ($K\alpha_1$ line of 1.54 Å; 45 kV and 40 mA)). The diffractograms were measured by the usage of a sample spinner stage in a 2θ range between 5 ° and 70 ° (step size: 0.0131303/2θ) at ambient conditions.

X-ray absorption (XAS) spectra were recorded at DESY in Hamburg, Germany at PETRA III, P65. The monochromatic photon flux was at $2x10^{12}$ s^{-1} at 9 keV and a beam size of 0.5x1 mm^2. The sample was packed in a in-situ XAS setup capillary and activated in 10 % O_2 in He flow (5 ml/min) at 450 °C (rate: 10 °C/min) for 2 h. After cooling down to 160 °C, the system was flushed with He, before 1-butene flow (1.5 ml/min) was loaded for 4 h at 160 °C and ambient pressure. The spectra were recorded between 8160 and 8700 eV and evaluated in Athena software.[60] For the linear combination fit, NiO and Ni foil were applied as standards for Ni^{2+} and Ni^0, respectively.

For the determination of the particle size, the catalyst particles were enhanced (magnification: x2000) by a high resolution JEOL JSM-7500F scanning electron microscope (voltage: 2 kV) and subsequently measured. For the sample preparation a small amount of catalyst was sonicated in EtOH, dropped on the sample Cu grid and dried at ambient conditions.

The gravimetric sorption isotherms of 1-butene and 2-butene on Ni-Ca-LTA was measured in a Setaram TG-DSC 111 thermoanalyzer connected to a high vacuum system. About 20 mg of sample was placed in a quartz crucible and activated at 450 °C (rate: 10 °C/min) for 1 h in vacuum ($p < 10^{-4}$ mbar). After cooling to 40 °C, the sample was exposed to 1-butene in small pressure steps from 0.01 to 10 mbar. Both, the sample mass and the thermal flux were monitored. The heat of adsorption was directly obtained by integration of the observed heat flux signal. During the adsorption of 2-butene on Ni-Ca-LTA a successive weight increase was observed during the first 12 hours at 03 mbar of 2-butene. The adsorption enthalpy was directly obtained by integration of the heat flux signal for the same time interval as 1-butene.

The BET specific surface area and pore volume of the zeolite were determined by nitrogen physisorption. The isotherms were measured at liquid nitrogen temperature (77 K) using a PMI Automatic Sorptometer. The catalyst was activated in vacuum at 473 K for 2 h before measurement. Apparent surface area was calculated by applying the Brunauer-Emmett-Teller (BET) theory with a linear regression between $p/p_0 = 0.01 – 0.15$. The micro- and mesopores were determined from the t-plot linear regression for t = 5-6 Å.

Catalytic testing and reaction kinetics. Catalytic tests were conducted in a fixed bed plug flow reactor (PFR (id = 3.9 mm)), connected to an online GC analysis unit (Agilent HP 6890,

equipped with a 50 m HP-1 column). Prior to GC analysis, hydrogen is added to the product stream, which is hydrogenated over a Pt/Al_2O_3 catalyst. A mixture of 15 % i-butane and 85 % 1-butene is introduced by a syringe pump (ISCO model 500 D), temperature is controlled by a eurotherm 2416, pressure is controlled using a Tescom backpressure regulator.

Prior to weighing, the catalyst was dried at 100 °C for 1 h. The catalyst bed is diluted with SiC and fixed in the isothermal zone of the reactor. After activation for 2 h at 450 °C (rate: 10 °C/min) in air, the system is purged with nitrogen and pressurized to the desired pressure. Subsequently the system is flushed with the feed mixture (5 ml/min) for 2 min. After the desired flow rate is set, temperature program and GC measurements are started.

Standard measurement conditions were at 160 °C and 50 bar with a flow rate of butene mixture between 0.04 and 0.12 ml/min. These reaction conditions resulted in higher activity and lower deactivation. Catalyst loading was varied between 10 and 200 mg. WHSV was in the range 6 to 244 g g^{-1} h^{-1}.

Activation energy was determined between 140 and 180 °C at 50 bar with a WHSV of 150 h^{-1}. Reaction order was measured at 50 bar total pressure, 160 °C and WHSV of butene of 25 h^{-1}. The feed was diluted with propane, which led to concentrations of 1-butene between 32 and 86 wt.%.

i-Butane is inert under reaction conditions applied, and hence it was used as internal standard for normalization of GC areas. Conversion, selectivity and yield are calculated according to following equations:

$$X = \frac{n(butene)_{in} - n(butene)_{out}}{n(butene)_{in}}$$

$$S = \frac{n(product)_{out}}{n(butene)_{in} - n(butene)_{out}} \frac{|\nu_{butene}|}{\nu_{product}}$$

$$Y = \frac{n(product)_{out}}{n(butene)_{in}} \frac{|\nu_{butene}|}{\nu_{product}}$$

REFERENCES

(1) Weissermel, K.; Hans-Jürgen, A., *Industrial Organic Chemistry*. Wiley-VCH: Weinheim, 1997.
(2) Albrecht, S.; Kießling, D.; Wendt, G.; Maschmeyer, D.; Nierlich, F. Oligomerisierung von n-Butenen. *Chem. Ing. Tech.* **2005,** 6, 695-709.
(3) Hassan, S. M.; Panchenkov, G. M.; Kuznetsov, O. I. Studies on the Mechanism and Kinetics of Propylene Oligomerization and Hydrooligomerization on Zeolites. *Bull. Chem. Soc. Jpn.* **1977,** 10, 2597-2601.
(4) Ng, F. T. T.; Creaser, D. C. Ethylene Dimerization over Modified Nickel Exchanged Y-Zeolite. *Applied Catalysis A: General* **1994,** 327-339.
(5) Nkosi, B.; Ng, F. T. T.; Rempel, G. L. The Oligomerization of 1-Butene Using NaY Zeolite Ion-Exchanged with Different Nickel Precursor Salts. *Applied Catalysis A: General* **1997,** 1–2, 153-166.
(6) Nkosi, B.; Ng, F. T. T.; Rempel, G. L. The Oligomerization of Butenes with Partially Alkali Exchanged NiNaY Zeolite Catalysts. *Applied Catalysis A: General* **1997,** 1–2, 225-241.
(7) Schultz, R. G.; Engelbrecht, R. M.; Moore, R. N.; Wolford, L. T. Olefin Dimerization over Cobalt-Oxide-on-Carbon Catalysts: II. Butene and Hexene Dimerization. *J. Catal.* **1966,** 3, 419-424.
(8) Skupinska, J. Oligomerization of α-Olefins to Higher Oligomers. *Chem. Rev.* **1991,** 4, 613-648.
(9) Fischer, K.; Jonas, K.; Misbach, P.; Stabba, R.; Wilke, G. Zum „Nickel-Effekt". *Angew. Chem.* **1973,** 23, 1001-1012.
(10) Ziegler, K.; Holzkamp, E.; Breil, H.; Martin, H. Das Mülheimer Normaldruck-Polyäthylen-Verfahren. *Angew. Chem.* **1955,** 19-20, 541-547.
(11) Brückner, A.; Bentrup, U.; Zanthoff, H.; Maschmeyer, D. The Role of Different Ni Sites in Supported Nickel Catalysts for Butene Dimerization under Industry-Like Conditions. *J. Catal.* **2009,** 1, 120-128.
(12) Kumar, N.; Mäki-Arvela, P.; Yläsalmi, T.; Villegas, J.; Heikkilä, T.; Leino, A. R.; Kordás, K.; Salmi, T.; Yu Murzin, D. Dimerization of 1-Butene in Liquid Phase Reaction: Influence of Structure, Pore Size and Acidity of Beta Zeolite and MCM-41 Mesoporous Material. *Microporous Mesoporous Mater.* **2012,** 1, 127-134.
(13) Mlinar, A. N.; Baur, G. B.; Bong, G. G.; Getsoian, A. B.; Bell, A. T. Propene oligomerization over Ni-exchanged Na-X zeolites. *Journal of Catalysis* **2012,** 156-164.
(14) Wendt, G.; Kießling, D. Dimerisierung von n-Butenen an Nickelalumosilicat-Katalysatoren. *Chem. Tech. (Leipzig)* **1995,** 3, 136-143.
(15) Deimund, M. A.; Labinger, J.; Davis, M. E. Nickel-Exchanged Zincosilicate Catalysts for the Oligomerization of Propylene. *ACS Catalysis* **2014,** 11, 4189-4195.
(16) Canivet, J.; Aguado, S.; Schuurman, Y.; Farrusseng, D. MOF-Supported Selective Ethylene Dimerization Single-Site Catalysts through One-Pot Postsynthetic Modification. *JACS* **2013,** 11, 4195-4198.
(17) Madrahimov, S. T.; Gallagher, J. R.; Zhang, G.; Meinhart, Z.; Garibay, S. J.; Delferro, M.; Miller, J. T.; Farha, O. K.; Hupp, J. T.; Nguyen, S. T. Gas-Phase Dimerization of Ethylene under Mild Conditions Catalyzed by MOF Materials Containing (bpy)NiII Complexes. *ACS Catalysis* **2015,** 11, 6713-6718.
(18) Metzger, E. D.; Brozek, C. K.; Comito, R. J.; Dincă, M. Selective Dimerization of Ethylene to 1-Butene with a Porous Catalyst. *ACS Central Science* **2016,** 3, 148-153.
(19) Mlinar, A. N.; Keitz, B. K.; Gygi, D.; Bloch, E. D.; Long, J. R.; Bell, A. T. Selective Propene Oligomerization with Nickel(II)-Based Metal–Organic Frameworks. *ACS Catalysis* **2014,** 3, 717-721.

(20) Brogaard, R. Y.; Olsbye, U. Ethene Oligomerization in Ni-Containing Zeolites: Theoretical Discrimination of Reaction Mechanisms. *ACS Catalysis* **2016,** 2, 1205-1214.
(21) Agirrezabal-Telleria, I.; Iglesia, E. Stabilization of Active, Selective, and Regenerable Ni-Based Dimerization Catalysts by Condensation of Ethene within Ordered Mesopores. *J. Catal.* **2017,** 505-514.
(22) Andrei, R. D.; Popa, M. I.; Fajula, F.; Hulea, V. Heterogeneous Oligomerization of Ethylene over Highly Active and Stable Ni-AlSBA-15 Mesoporous Catalysts. *J. Catal.* **2015,** 76-84.
(23) Beucher, R.; Andrei, R. D.; Cammarano, C.; Galarneau, A.; Fajula, F.; Hulea, V. Selective Production of Propylene and 1-Butene from Ethylene by Catalytic Cascade Reactions. *ACS Catalysis* **2018,** 4, 3636-3640.
(24) Finiels, A.; Fajula, F.; Hulea, V. Nickel-Based Solid Catalysts for Ethylene Oligomerization - A Review. *Catalysis Science & Technology* **2014,** 8, 2412-2426.
(25) Moussa, S.; Arribas, M. A.; Concepción, P.; Martínez, A. Heterogeneous Oligomerization of Ethylene to Liquids on Bifunctional Ni-Based Catalysts: The Influence of Support Properties on Nickel Speciation and Catalytic Performance. *Catal. Today* **2016,** 78-88.
(26) Moussa, S.; Concepción, P.; Arribas, M. A.; Martínez, A. Nature of Active Nickel Sites and Initiation Mechanism for Ethylene Oligomerization on Heterogeneous Ni-beta Catalysts. *ACS Catalysis* **2018,** 3903-3912.
(27) Heveling, J.; Nicolaides, C. P.; Scurrell, M. S. Activity and Selectivity of Nickel-Exchanged Silica-Alumina Catalysts for the Oligomerization of Propene and 1-Butene into Distillate-Range Products. *Applied Catalysis A: General* **2003,** 1, 239-248.
(28) Beltrame, P.; Forni, L.; Talamini, A.; Zuretti, G. Dimerization of 1-Butene over Nickel Zeolitic Catalysts: A Search for Linear Dimers. *Applied Catalysis A: General* **1994,** 39-48.
(29) Cai, T. Studies of a New Alkene Oligomerization Catalyst Derived from Nickel Sulfate. *Catal. Today* **1999,** 1, 153-160.
(30) Sarazen, M. L.; Doskocil, E.; Iglesia, E. Catalysis on Solid Acids: Mechanism and Catalyst Descriptors in Oligomerization Reactions of Light Alkenes. *J. Catal.* **2016,** 553-569.
(31) Sarazen, M. L.; Doskocil, E.; Iglesia, E. Effects of Void Environment and Acid Strength on Alkene Oligomerization Selectivity. *ACS Catalysis* **2016,** 10, 7059-7070.
(32) Sarazen, M. L.; Iglesia, E. Stability of Bound Species During Alkene Reactions on Solid Acids. *Proceedings of the National Academy of Sciences* **2017,** 20, E3900-E3908.
(33) Sarazen, M. L.; Iglesia, E. Experimental and Theoretical Assessment of the Mechanism of Hydrogen Transfer in Alkane-Alkene Coupling on Solid Acids. *J. Catal.* **2017,** 287-298.
(34) Takeuchi, D.; Osakada, K. In *Organometallic Reactions and Polymerization*, Osakada, K., Ed. Springer Berlin Heidelberg: Berlin, Heidelberg, 2014; pp 169-215.
(35) Gal, I. J.; Jankovic, O.; Malcic, S.; Radovanov, P.; Todorovic, M. Ion-Exchange Equilibria of Synthetic 4A Zeolite with Ni2+, Co2+, Cd2+ and Zn2+ Ions. *Transactions of the Faraday Society* **1971,** 0, 999-1008.
(36) Amari, D.; Ginoux, J.-L.; Bonnetain, L. Textural Damage of Cation-Exchanged LTA Zeolites Studied by Gas Adsorption. *Zeolites* **1994,** 1, 58-64.
(37) Rabeah, J.; Radnik, J.; Briois, V.; Maschmeyer, D.; Stochniol, G.; Peitz, S.; Reeker, H.; La Fontaine, C.; Brückner, A. Tracing Active Sites in Supported Ni Catalysts during Butene Oligomerization by Operando Spectroscopy under Pressure. *ACS Catalysis* **2016,** 12, 8224-8228.
(38) Mlinar, A. N.; Shylesh, S.; Ho, O. C.; Bell, A. T. Propene Oligomerization Using Alkali Metal- and Nickel-Exchanged Mesoporous Aluminosilicate Catalysts. *ACS Catalysis* **2013,** 1, 337-343.
(39) Cossee, P. Ziegler-Natta Catalysis I. Mechanism of Polymerization of α-Olefins with Ziegler-Natta Catalysts. *J. Catal.* **1964,** 1, 80-88.
(40) Henry, R.; Komurcu, M.; Ganjkhanlou, Y.; Brogaard, R. Y.; Lu, L.; Jens, K.-J.; Berlier, G.; Olsbye, U. Ethene Oligomerization on Nickel Microporous and Mesoporous-Supported Catalysts: Investigation of the Active Sites. *Catal. Today* **2018,** 154-163.

(41) Mlinar, A. N.; Ho, O. C.; Bong, G. G.; Bell, A. T. The Effect of Noncatalytic Cations on the Activity and Selectivity of Nickel-Exchanged X Zeolites for Propene Oligomerization. *ChemCatChem* **2013,** 10, 3139-3147.
(42) Small, B. L.; Schmidt, R. Comparative Dimerization of 1-Butene with a Variety of Metal Catalysts, and the Investigation of a New Catalyst for C□H Bond Activation. *Chemistry – A European Journal* **2004,** 4, 1014-1020.
(43) Nadolny, F.; Hannebauer, B.; Alscher, F.; Peitz, S.; Reschetilowski, W.; Franke, R. Experimental and Theoretical Investigation of Heterogeneous Catalyzed Oligomerization of a Mixed C4 Stream over Modified Amorphous Aluminosilicates. *J. Catal.* **2018,** 81-94.
(44) Nikiforidis, I.; Görling, A.; Hieringer, W. On the Regioselectivity of the Insertion Step in Nickel Complex Catalyzed Dimerization of Butene: A Density-Functional Study. *J. Mol. Catal. A: Chem.* **2011,** 1–2, 63-70.
(45) F., H. Dimerisation and Double-Bond Isomerisation of Olefins with a Homogeneous Nickel II-Complex as Catalyst. *Journal of Applied Chemistry and Biotechnology* **1971,** 3, 90-91.
(46) Olav-Torgeir, O.; Hagbarth, W.; Ulf, B. Niederdruck-Oligomerisation von Mono-Olefinen mit löslichen Nickel/Aluminium-Bimetallkatalysatoren Teil III. Reaktionskinetische Untersuchungen über die Dimerisation und Trimerisation des Áthylens. *Helv. Chim. Acta* **1969,** 1, 215-223.
(47) Zhang, X.; Zhong, J.; Wang, J.; Zhang, L.; Gao, J.; Liu, A. Catalytic Performance and Characterization of Ni-Doped HZSM-5 Catalysts for Selective Trimerization of n-Butene. *Fuel Process. Technol.* **2009,** 7, 863-870.
(48) Eberly Jr, P. E. High-Temperature Infrared Spectroscopy of Olefins Adsorbed on Faujasites. *The Journal of Physical Chemistry* **1967,** 6, 1717-1722.
(49) Socrates, G., *Infrared and Raman characteristic group frequencies: tables and charts*. John Wiley & Sons: 2001.
(50) Coblentz Society, I. In *NIST Chemistry WEbBook, NIST Standard Reference Database Number 69*, Linstrom, P. J., Mallard, W. G., Eds. National Institute of Standards and Technology: Gaithersburg MD, 20899, 2017.
(51) Armaroli, T.; Finocchio, E.; Busca, G.; Rossini, S. A FT-IR Study of the Adsorption of C5 Olefinic Compounds on NaX Zeolite. *Vib. Spectrosc* **1999,** 1, 85-94.
(52) Kondo, J. N.; Liqun, S.; Wakabayashi, F.; Domen, K. IR Study of Adsorption and Reaction of 1-Butene on H-ZSM-5. *Catal. Lett.* **1997,** 2, 129-133.
(53) Larkin, P. J., *Infrared and Raman Spectroscopy - Principles and Spectral Interpretation*. Elsevier: 2011.
(54) Chang, C. C.; Conner, W.; Kokes, R. Butene Isomerization over Zinc Oxide and Chromia. *The Journal of Physical Chemistry* **1973,** 16, 1957-1964.
(55) Olah, G. A.; Baker, E. B.; Evans, J. C.; Tolgyesi, W. S.; McIntyre, J. S.; Bastien, I. J. Stable Carbonium Ions. V.1a Alkylcarbonium Hexafluoroantimonates. *JACS* **1964,** 7, 1360-1373.
(56) Olah, G. A.; DeMember, J. R.; Commeyras, A.; Bribes, J. L. Stable Carbonium Ions. LXXXV. Laser Raman and Infrared Spectroscopic Study of Alkylcarbonium Ions. *JACS* **1971,** 2, 459-463.
(57) Stepanov, A. G.; Luzgin, M. V.; Romannikov, V. N.; Sidelnikov, V. N.; Paukshtis, E. A. The Nature, Structure, and Composition of Adsorbed Hydrocarbon Products of Ambient Temperature Oligomerization of Ethylene on Acidic Zeolite H-ZSM-5. *J. Catal.* **1998,** 2, 466-477.
(58) Forestière, A.; Olivier-Bourbigou, H.; Saussine, L. Oligomerization of Monoolefins by Homogeneous Catalysts. *Oil & Gas Science and Technology - Rev. IFP* **2009,** 6, 649-667.
(59) Pillai, S. M.; Ravindranathan, M.; Sivaram, S. Dimerization of Ethylene and Propylene Catalyzed by Transition-Metal Complexes. *Chem. Rev.* **1986,** 2, 353-399.
(60) Ravel, B.; Newville, M. ATHENA, ARTEMIS, HEPHAESTUS: Data Analysis for X-Ray Absorption Spectroscopy Using IFEFFIT. *Journal of Synchrotron Radiation* **2005,** 4, 537-541.

1. Chapter - Supporting Information:

Dimerization of linear butenes on zeolite supported Ni^{2+}

SI-1 Synthesis and characterization of Ni-Ca-LTA catalysts

The XRD patterns of the differently loaded Ni-Ca-LTA catalysts, as well as of a reference Ca-LTA sample, showed that all LTA remained intact without forming another crystalline phase (Figure S1-1). The significant broadening of the peaks suggests that crystallinity was continuously lost with increasing ion-exchange degree. Diffraction lines corresponding to NiO are not observed.

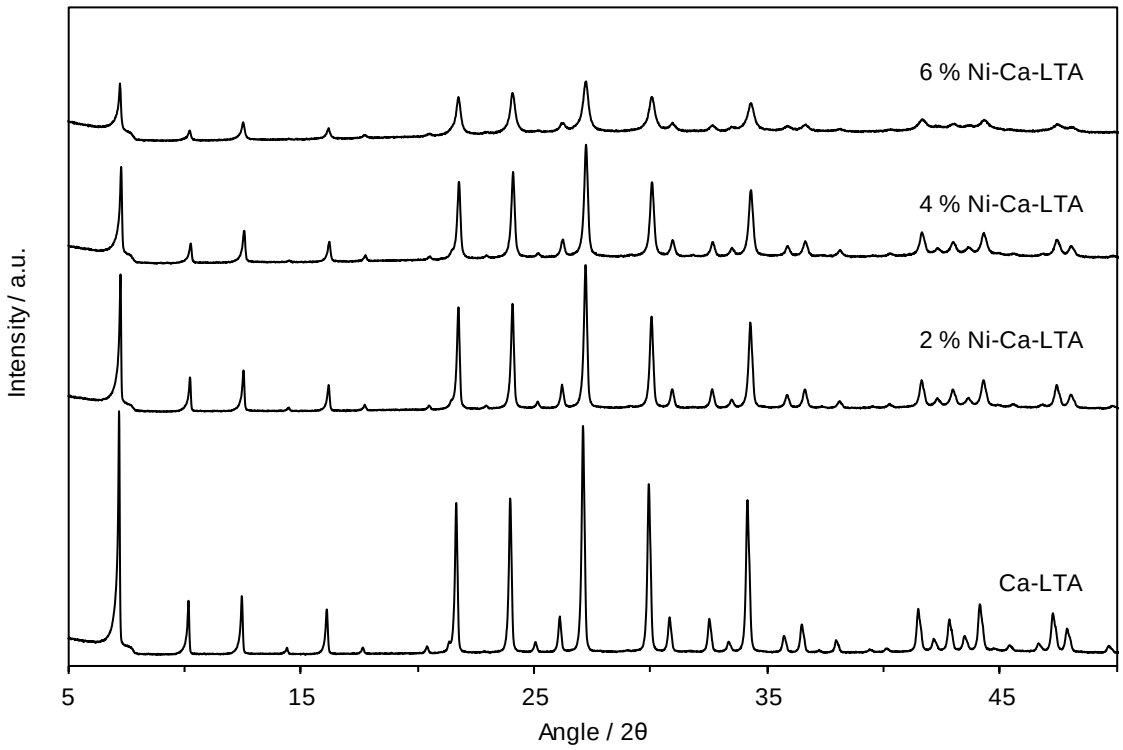

Figure S1-1. X-ray diffraction patterns of LTA based catalysts.

Ion exchange with increasing concentrations of Ni^{2+} resulted also in an increase in mesoporosity, as deduced by the increasing intensity of the hysteresis in the sorption isotherms of N_2 (Table S1-1 and Figure S1-2). In parallel, the micropore volume and BET surface area decreased. Changes in the particle size were not observed by SEM (Figure S1-3 and Table S1-2), suggesting that the generation of the mesopores has occurred by partial dissolution of crystalline matter.

Table S1-1. Mesoscopic properties of Ca-LTA and Ni exchanged Ca-LTA.

	BET $[m^2 g^{-1}]$	**Micropore volume** $[cm^3 g^{-1}]$	**Mesopore surface area** $[m^2 g^{-1}]$
Ca-LTA	605.85	0.24	44.29
2 wt.% Ni-Ca-LTA	453.91	0.18	51.23
4 wt.% Ni-Ca-LTA	434.95	0.16	94.49
6 wt.% Ni-Ca-LTA	338.52	0.09	114.76

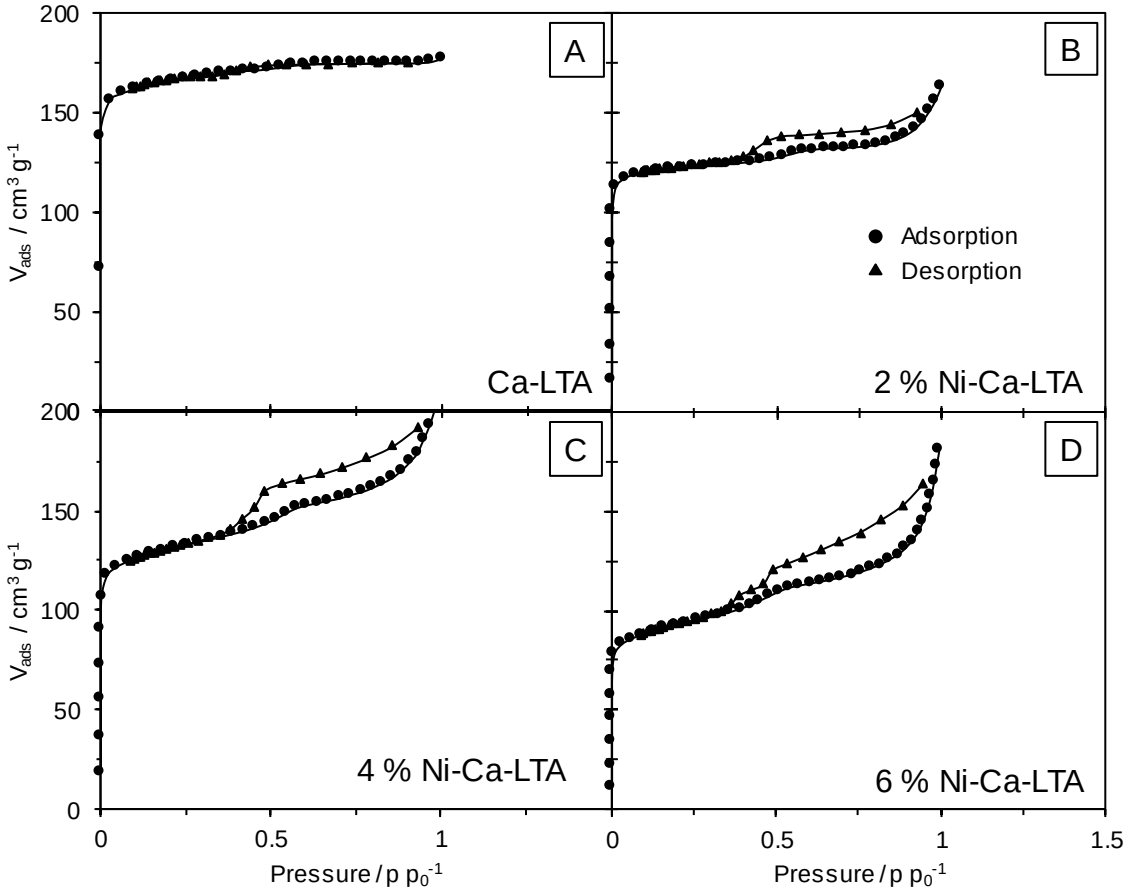

Figure S1-2. N_2 sorption curves for A) Ca-LTA, B) 2 % Ni-Ca-LTA, C) 4 % Ni-Ca-LTA and D) 6 wt.% Ni-Ca-LTA.

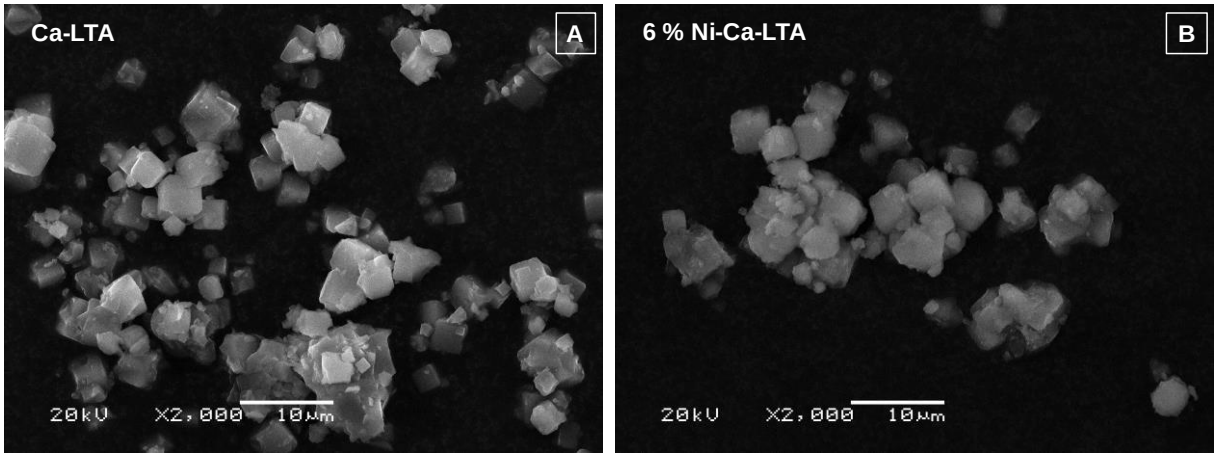

Figure S1-3. Examples for SEM pictures taken for parent and Ni exchanged Ca-LTA.

Table S1-2. Average particle size of pure and Ni exchanged Ca-LTA as determined from SEM measurements.

Ca-LTA	4 % Ni-Ca-LTA	6 wt.% Ni-Ca-LTA
2.55 ± 1.00 µm	3.14 ± 0.92 µm	3.47 ± 0.87 µm

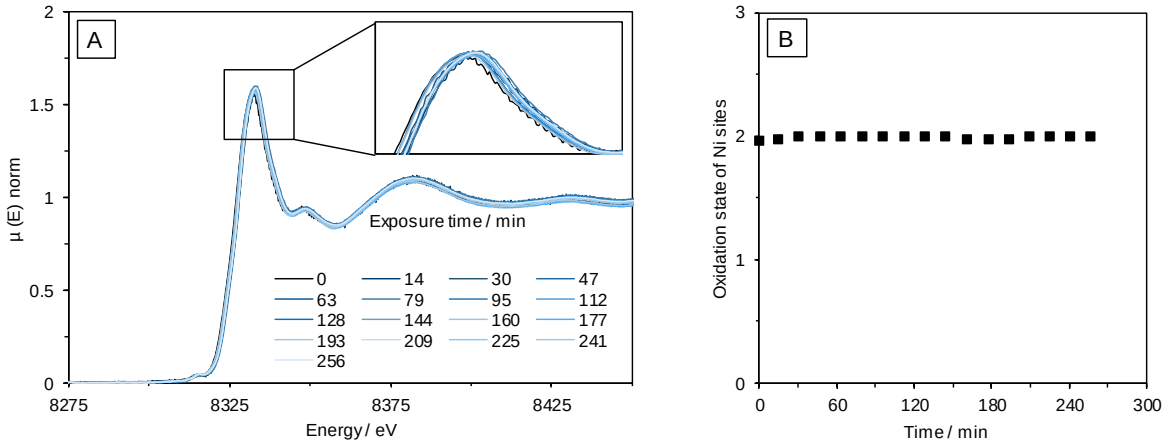

Figure S1-4. A) XANES measurements of 6 wt.% Ni-Ca-LTA under the influence of 1-butene flow at 1 bar and 160 °C monitored over 4 h. B) Linear combination fit results of Ni oxidation state in LTA.

SI-2 Catalytic testing of Ni-Ca-LTA catalysts

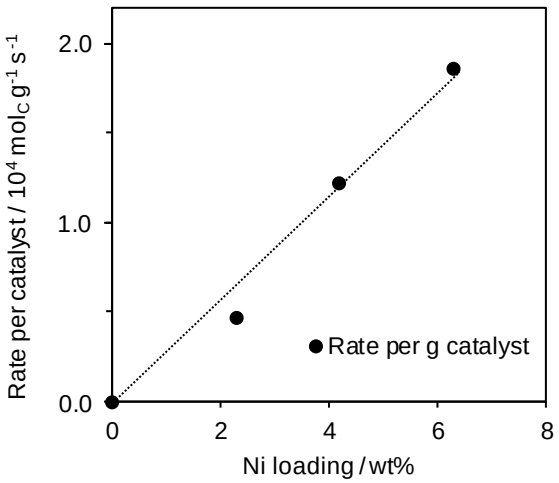

Figure S1-5. Conversion of 1-butene and rate per gram over Ca-LTA catalysts with different loadings of Ni at 50 bar, 160 °C and WHSV = 50 h^{-1}.

Table S1-3. Selectivity distribution of the different Ni-Ca—LTA catalysts

Catalyst (Ni wt. %)	$X_{1\text{-But.}}$ (%)	$S_{Oct.}$(%)	S_{MH} (%)	S_{DMH} (%)	S_{Trim} (%)
Ni-Ca-LTA (2%)	6.3	52.3	36.7	2.5	8.5
Ni-Ca-LTA (6%)	4.9	53.1	37.0	2.2	7.7
Ni-Ca-LTA (4%)	12.6	46.0	42.0	3.7	8.3
Ni-Ca-LTA (6%)	13.7	46.7	38.0	2.5	12.8

SI-3 Thermodynamic equilibrium calculations

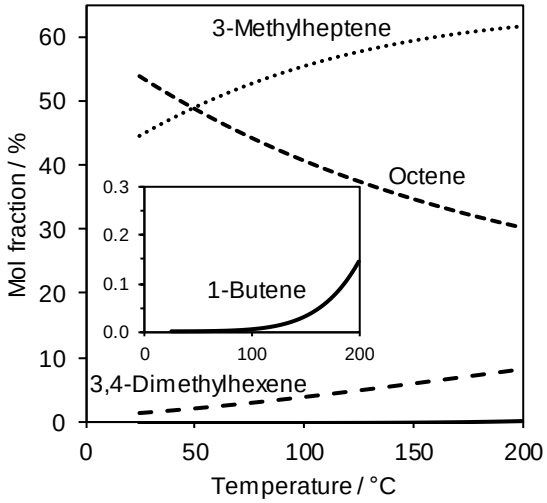

Figure S1-6. Thermodynamic equilibrium composition of dimerization at 50 bar (calculated with HSC chemistry).

Determination of approach to equilibrium

Measured conversion and isomerization are normalized to their thermodynamic equilibrium value. The values for the conversion are given as:

$$X_{appr.eq.} = \frac{X_{meas}}{X_{eq}}$$

$$\mathrm{X_{appr.eq.}} = \text{Approach to equilibrium of conversion}$$

$$\mathrm{X_{meas}} = \text{measured conversion}$$

$$\mathrm{X_{eq}} = \text{equilibrium conversion } (= 99.99)$$

The approach to equilibrium for isomerization is calculated as:

$$I_{appr.eq.} = \frac{I_{meas}}{I_{eq}}$$

$$\mathrm{I_{appr.eq.}} = \text{Approach to equilibrium of isomerization}$$

$$\mathrm{I_{meas}} = \text{measured isomerization } (\text{ratio } \frac{2-\text{butenes}}{1-\text{butene}})$$

$$\mathrm{I_{eq}} = \text{equilibrium isomerization } (\text{equilibrium ratio } \frac{2-\text{butenes}}{1-\text{butene}})$$

SI-4 Discrimination of reaction kinetics

The following reactions are given:

r_1 $\quad {}^*C_{4alkyl} + C_4 \rightleftharpoons C_{4\sigma}{}^*C_{4alkyl}$ (Eq. 1-1)

r_2 $\quad C_{4\sigma}{}^*C_{4alkyl} + C_4 \rightleftharpoons C_4C_{4\sigma}{}^*C_{4alkyl}$ (Eq. 1-2)

r_3 $\quad C_4C_{4\sigma}{}^*C_{4alkyl} \longrightarrow C_{8\sigma}{}^*C_{4alkyl}$ (Eq. 1-3)

r_4 $\quad C_{8\sigma}{}^*C_{4alkyl} \rightleftharpoons C_8 + {}^*C_{4alkyl}$ (Eq. 1-4)

Assuming the Most Abundant Reaction Intermediates (MARI) and vacant sites ([*]) are part of the site balance:

$$[{}^*C_{4alkyl}]_0 = [{}^*C_{4alkyl}] + [C_{4\sigma}{}^*C_{4alkyl}] + [C_4C_{4\sigma}{}^*C_{4alkyl}] + [C_{8\sigma}{}^*C_{4alkyl}]$$

Therefore, assuming equation 3 is rate limiting:

$$r_3 = k_3\left[C_4C_{4\sigma}^*C_{4alkyl}\right] = \frac{K_1K_2k_3[C_4]^2}{1 + K_1[C_4] + K_2[C_4] + [C_8]/K_4}\left[{}^*C_{4alkyl}\right]_0 \quad \text{(Eq. 1-5)}$$

At low conversions the concentration of octene is quite low, having an apparent reaction order of 2. Normalizing by the number of active Ni sites:

$$r_3 = k_3[C_4]^2 \quad \text{(Eq. 1-6)}$$

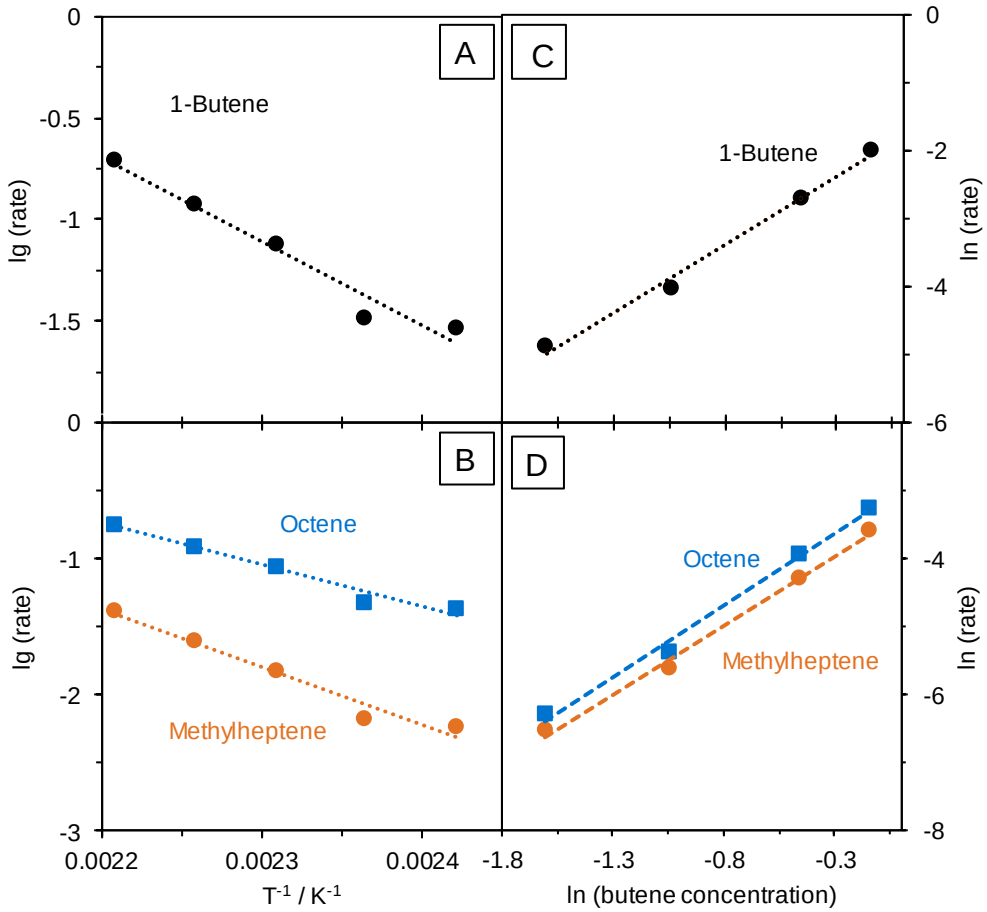

Figure S1-7. Arrhenius plot of butene consumption (A) and product formation (B) over a 6 wt.% Ni-Ca-LTA, T = 140-180 °C, p = 50 bar, WHSV = 312,5 h^{-1}, X = 0.5 – 3.5 %. And reaction order for 1-butene consumption (C) and the formation of the dimers (D), T = 160 °C, p = 50 bar, WHSV = 15-156 h^{-1}; 1-Butene feed mix diluted with propane: $c_{1\text{-butene}}$ = 20 – 86 wt.%.

SI-5 Butene adsorption on Ni-Ca-LTA

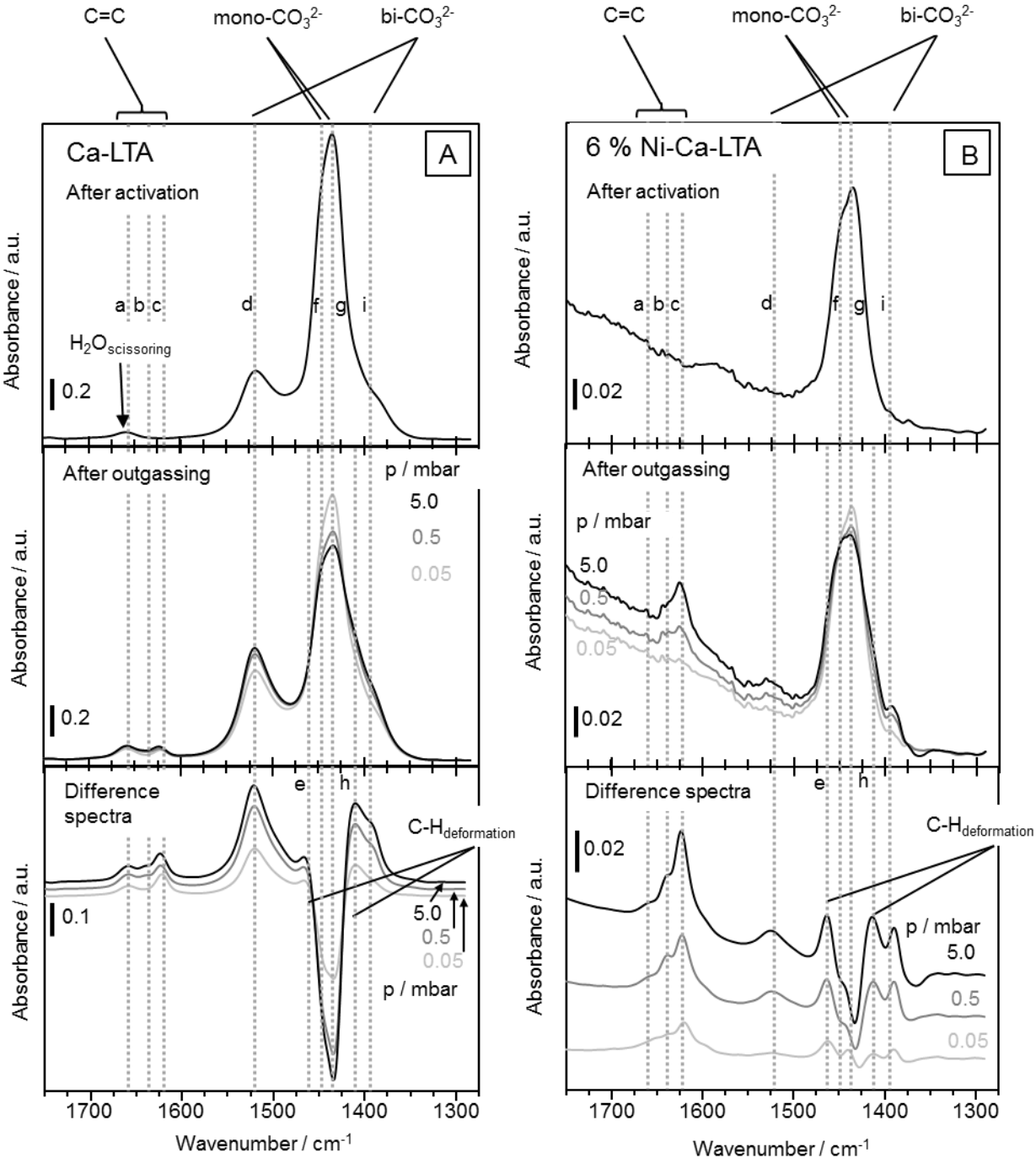

Figure S1-8. IR spectra of C=C stretching and C-H deformation region at 40 °C of (A) parent Ca-LTA and (B) Ni exchanged Ca-LTA (Ni/Ca ratio = 0.55) before (top) and after (middle) the exposure to different pressures of 1-butene and subsequent evacuation, as well as the difference spectra (bottom). For detailed band assignment, see Table S1-4.

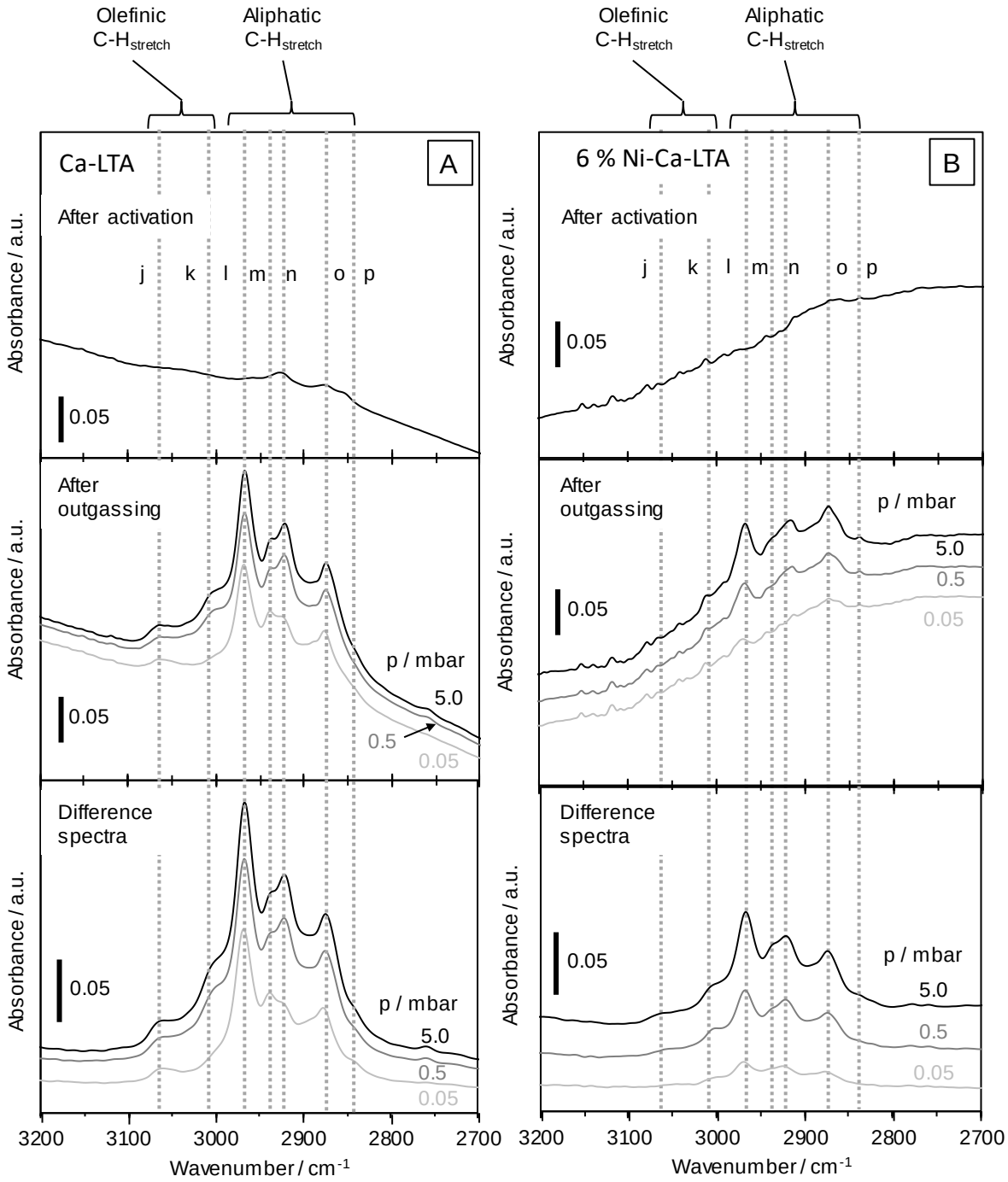

Figure S1-9. IR spectra of C-H vibration region at 40 °C of (A) parent Ca-LTA and (B) Ni exchanged Ca-LTA (Ni/Ca ratio = 0.55) before (top) and after (middle) the exposure to different pressures of 1-butene and subsequent evacuation, as well as the difference spectra (bottom). For detailed band assignment, see Table S1-4.

Table S1-4. Band assignment of infrared bands observed upon butene adsorption (Figure S1-8 and Figure S1-9).

	$\bar{\nu}$	Vibration mode		$\bar{\nu}$	Vibration mode
a	1658	v C=C, 1-butene$_{gas}$	j	3061	v =CH, 1-butene
b	1641	v C=C, 2-butene	k	3005	v =CH, 2-butene
c	1622	v C=C, 1-butene	l	2967	ν_{as} CH_3
d	1518	ν_{as} O-C-O bident. CO_3^{2-}	m	2939	ν_{as} CH_2
e	1467	δ_{as} CH	n	2920	v CH
f	1448	ν_{as} O-C-O monodent. CO_3^{2-}	o	2873	ν_{sy} CH_3
g	1435	ν_{sy} O-C-O monodent. CO_3^{2-}	p	2841	ν_{sy} CH_2
h	1408	δ_{sy} CH			
i	1390	ν_{sy} O-C-O bident. CO_3^{2-}			

The presence of Ca^{2+} leads to the formation of mono- and bidentate carbonates on the surface of the zeolite. [1-5] The bands at 1518 and 1392 cm^{-1} correspond to the O-C-O antisymmetric and symmetric stretching vibrations of bidentate carbonate and the bands at 1448 and 1435 cm^{-1} correspond to the O-C-O antisymmetric and symmetric stretching vibrations of the monodentate carbonate.[5-8] Prior, to the adsorption of butene the corresponding scissoring mode of residual molecular water(1667 cm^{-1}) was observed.[5-6]

After exposure to 1-butene and subsequent outgassing, new bands between 1648 and 1625 cm^{-1} (alkene C=C stretching vibration) indicate the presence of physisorbed (or π-bound) 1-butene.[9] Additional shoulders appeared at 1460 and1408 cm^{-1}, attributed to C-H deformation vibrations. [10] The difference spectrum between adsorbed 1-butene on Ca-LTA and the clean activated sorbent (Figure S1-8 A, bottom) shows that the intensity of the bidentate carbonate

bands (1518 and 1392 cm^{-1}) and C-H deformations increased, while the monodentate carbonate bands decreased (1448 and 1435 cm^{-1}). This is tentatively attributed to butene adsorbing on the carbonate and inducing its conversion to the bidentate carbonate. The IR spectra of the activated Ni-Ca-LTA (Figure S1-8 B, top) and after the exposure to 1-butene showed similar transformation of bidentate to monodentate carbonate.

SI-6 Adsorption kinetics of butene

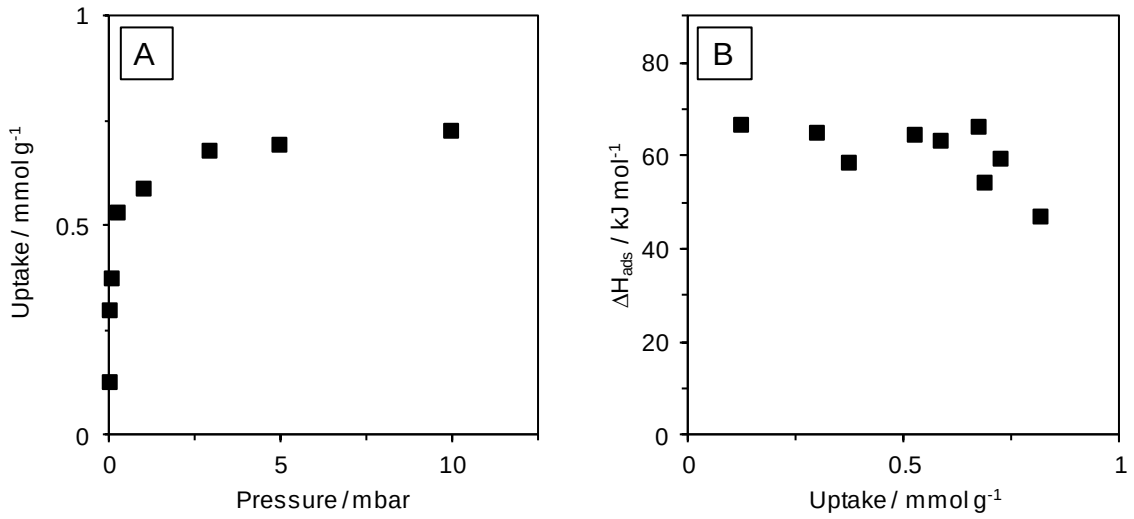

Figure S1-10. 1-Butene adsorption on Ni containing Ca-LTA at 40 °C. A) Butene uptake as function of pressure and B) The resulting adsorption enthalpy.

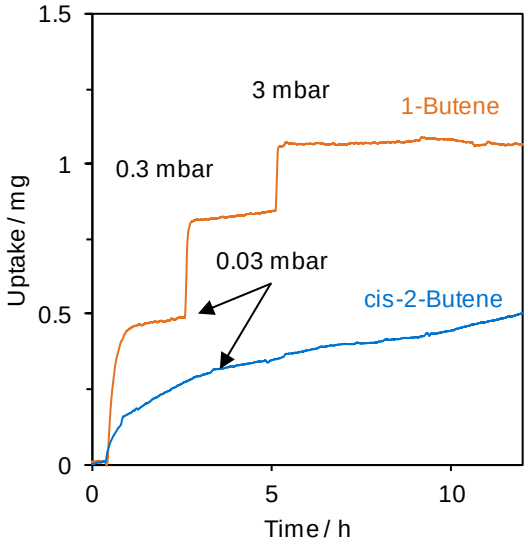

Figure S1-11. Adsorption of 1- and cis-2-butene on 6 % Ni-Ca-LTA at 40 °C (Pretreatment: 450 °C, 1 h, vacuum).

From the coverage (θ_1) under TGA conditions ($T_1 = 40$ °C, $p_1 = 10$ mbar) and the assumption of a Langmuir adsorption, it can be formed:

$$\theta_1 = \frac{V}{V_{max}} = \frac{K_1 p_1}{1 + K_1 p_1} \quad \text{(Eq. 1-7)}$$

$$\frac{1}{V} = \frac{1}{V_{max} K_1 p_1} + \frac{1}{V_{max}} \quad \text{(Eq. 1-8)}$$

$$K_1 = \frac{V}{(V_{max} - V)p} \quad \text{(Eq. 1-9)}$$

With the measured data, the average value of K_1 is achieved:

$$K_1 = 4.9 \cdot 10^{-3}\ bar^{-1} \quad \text{(Eq. 1-10)}$$

From the van't Hoff equation:

$$ln\left(\frac{K_2}{K_1}\right) = -\frac{\Delta H}{R}\left(\frac{1}{T_2} - \frac{1}{T_1}\right) \quad \text{(Eq. 1-11)}$$

It can be formed:

$$ln(K_2) = -\frac{\Delta H}{R}\left(\frac{1}{T_2} - \frac{1}{T_1}\right) + ln(K_1) \quad \text{(Eq. 1-12)}$$

With $T_2 = 160$ °C, $p_2 = 42.4$ bar of 1-butene and $\Delta H = 63$ kJ/mol K_2 can be calculated:

$$K_{2p} = 6.0 \cdot 10^{-6} bar^{-1} \quad \text{(Eq. 1-13)}$$

And hence, the coverage at reaction conditions (θ_2) is:

$$\theta_2 = \frac{K_2 p_2}{1 + K_2 p_2} = 0.996 \quad \text{(Eq. 1-14)}$$

SI-7 Reaction mechanisms for butene dimerization

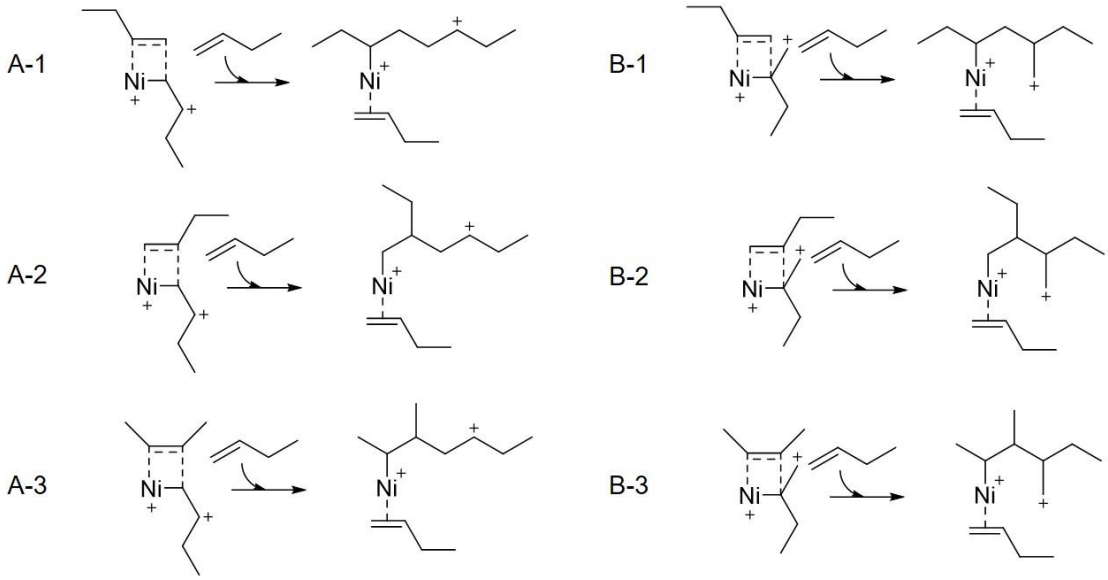

Scheme S1-1. Possible coordinations of the butene molecules in the transition step and the resulting dimers. A: initial 1'-adsorption; B: initial 2'-adsorption. X-1: 1'-insertion of a 1-butene molecule; X-2: 2'-insertion of a 1-butene molecule; X-3: insertion of a 2-butene molecule.

SI-8 Synthesis and elemental characterization

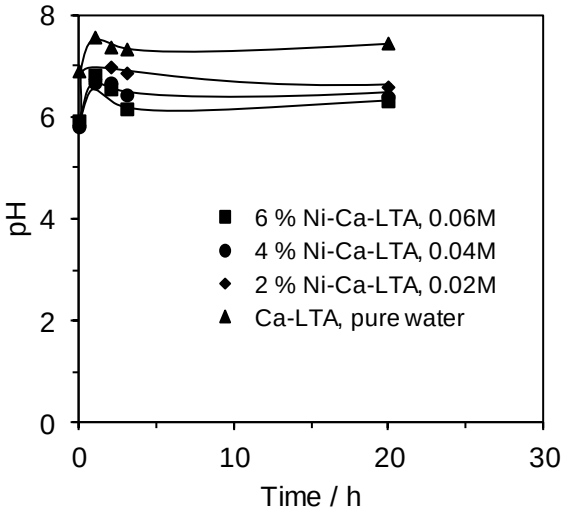

Figure S1-12. pH values measured at several times of exchange.

The pH value of the exchange solution was monitored over the time of exchange (Figure S1-12). No significant changes were recorded, whereas higher Ni concentrations resulted in slightly lower pH values.

Table S1-5. Charge balance (calculated as $\frac{\sum cation\ charges}{n(aluminum\ centers)}$) of Ni-Ca-LTA with different Ni loadings.

Ni loading / wt%	Al loading / mmol g^{-1}	Ni loading / mmol g^{-1}	Na loading / mmol g^{-1}	Ca loading / mmol g^{-1}	Charge balance / %
0	7.01	0.00	1.89	2.64	102.5
2	6.93	0.40	1.34	2.34	98.2
4	6.86	0.72	1.08	2.09	97.7
6	6.93	1.08	0.94	1.97	101.6

The charge balance is calculated as the quotient of the sum of all positive cation charges and the Al content (i.e. the sum of the negative charges). For the case that this quotient equals to 1, this indicates that all negative charges, which are induced by the Al centers, are balanced by cations and that all cations are dispersed and not present as clusters.

References

(1) Forster, H.; Schumann, M. Infrared Spectroscopic Studies on Carbon Dioxide Adsorption in Alkali-Metal and Alkaline-Earth-Metal Ion-Exchanged A-type Zeolites. Part 1.-General Features of CO2 Interaction with A-Type Zeolites. *Journal of the Chemical Society, Faraday Transactions 1: Physical Chemistry in Condensed Phases* **1989,** 5, 1149-1158.
(2) Köck, E.-M.; Kogler, M.; Bielz, T.; Klötzer, B.; Penner, S. In Situ FT-IR Spectroscopic Study of CO2 and CO Adsorption on Y2O3, ZrO2, and Yttria-Stabilized ZrO2. *The Journal of Physical Chemistry C* **2013,** 34, 17666-17673.
(3) Gallei, E.; Stumpf, G. Infrared Spectroscopic Studies of the Adsorption of Carbon Dioxide and the Coadsorption of Carbon Dioxide and Water on CaY- and NiY-Zeolites. *J. Colloid Interface Sci.* **1976,** 2, 415-420.
(4) Coblentz Society, I. In *NIST Chemistry WEbBook, NIST Standard Reference Database Number 69*, Linstrom, P. J., Mallard, W. G., Eds. National Institute of Standards and Technology: Gaithersburg MD, 20899, 2017.
(5) Montanari, T.; Busca, G. On the Mechanism of Adsorption and Separation of CO2 on LTA Zeolites: An IR Investigation. *Vib. Spectrosc* **2008,** 1, 45-51.
(6) Bermejo-Deval, R.; Walter, R. M. H.; Gutierrez, O. Y.; Lercher, J. A. On the Role of the Alkali Cations on Methanol Thiolation. *Catalysis Science & Technology* **2017,** 19, 4437-4443.
(7) Morterra, C.; Magnacca, G. A Case Study: Surface Chemistry and Surface Structure of Catalytic Aluminas, as Studied by Vibrational Spectroscopy of Adsorbed Species. *Catal. Today* **1996,** 3, 497-532.
(8) Busca, G.; Lorenzelli, V. Infrared Spectroscopic Identification of Species Arising from Reactive Adsorption of Carbon Oxides on Metal Oxide Surfaces. *Materials Chemistry* **1982,** 1, 89-126.
(9) Kondo, J. N.; Liqun, S.; Wakabayashi, F.; Domen, K. IR Study of Adsorption and Reaction of 1-Butene on H-ZSM-5. *Catal. Lett.* **1997,** 2, 129-133.
(10) Manzanares I, C.; Blunt, V. M.; Peng, J. Spectroscopy of C-H Stretching Vibrations of Gas-Phase Butenes: Cis-2-Butene, Trans-2-Butene, 2-Methyl-2-Butene, and 2,3-Dimethyl-2-Butene. *The Journal of Physical Chemistry* **1993,** 16, 3994-4003.

2. Chapter:

On the Role of Co-Cations in Nickel Exchanged LTA Zeolite for Butene Dimerization

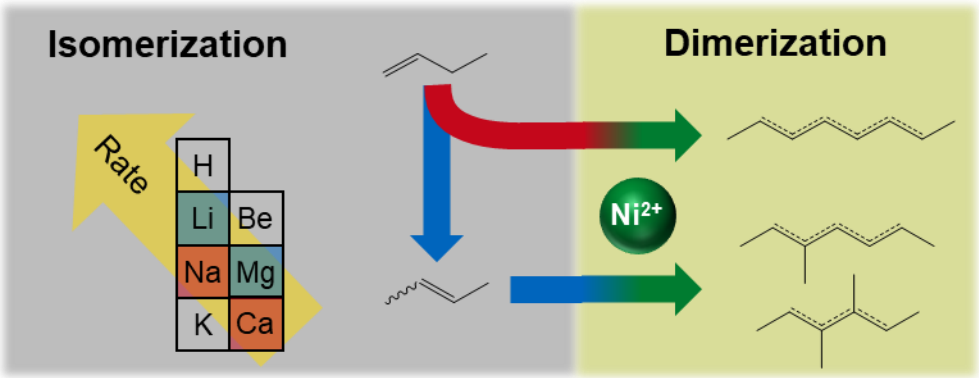

This chapter is based on:

Andreas Ehrmaier, Yue Liu, Stephan Peitz, Maricruz Sanchez-Sanchez, Ricardo Bermejo de Val, Johannes Lercher,[2] *"On the Role of Co-Cations in Nickel Exchanged LTA Zeolite for Butene Dimerization", Microporous Mesoporous Mater., 2019, In press*

[2] A.E. prepared and characterized the catalysts, planned, designed and performed the experiments, analyzed and interpreted the data and wrote the manuscript. Y.L., M.S., S.P. contributed to the scientific discussion. R.B., J.L. guided the experiments, contributed to the scientific discussion and corrected the manuscript anytime.

ABSTRACT

Partially Ni^{2+} exchanged Li^{+}, Mg^{2+}, Ca^{2+} and Na^{+} LTA zeolites were investigated for 1-butene dimerization, all showing selectivities higher than 90 % into n-octenes and methylheptene isomers. The presence of the co-cations influences the rate of 1-butene double bond isomerization, while the Ni concentration determines the rates of dimerization. With higher electronegativity of the co-cation, the relative rate of isomerization increased, increasing so the selectivity to branched dimers. The higher Sanderson electronegativity of Li^{+} and Mg^{2+}, with respect to Na^{+}, is hypothesized to better stabilize the π-allyl Ni-complex-intermediate during butene isomerization. In consequence, the selectivity of alkene dimerization on Ni-exchanged zeolites can be tailored by acid-base properties of the alkali and alkali-earth cations.

INTRODUCTION

Linear and mono-branched octenes are preferred in the dimerization of 1-butene,[1-13] as they are important intermediates in the synthesis of high value products, such as in plasticizers for polyvinyl chloride [14] and as a co-monomer for low density polyethene.[15] Ni catalysts exhibit the highest activity and selectivity to linear olefins, favoring the formation of dimers.[2, 16-17] While homogeneous Ni-alkyl complexes are reported to follow either the Cossee-Arlman, metallacycle or proton-transfer mechanisms in the dimerization of α-alkenes,[14, 18-19] Ni dispersed in mesoporous and microporous aluminosilicates, [20-24] as well as coordinated in organic frameworks, [6-7, 11, 13, 25-29 30] are proposed mainly to follow a Cossee-Arlman type mechanism. This has been recently corroborated with Ni exchanged on Ca-LTA in the absence of Brønsted acid sites (BAS) during 1-butene dimerization, supported by the dimer product distribution and mechanistic studies.[31]

The Ni^{2+} ion-exchange of zeolites results in the charge compensation of two Al framework atoms. High Al concentrations in the zeolite framework (Si/Al ~1-3) have a high concentration of neighboring Al sites and, therefore, conceptually also a high concentration of sites able to exchange Ni^{2+}. However, Ni^{2+} is not able to compensate all exchange positions in the zeolite, resulting in the presence of BAS. Brønsted acid sites form carbenium ions with olefins and catalyze undesired side reactions, including isomerization and cracking. [32-35] The removal of these BAS requires its exchange with monovalent cations. Alkali (or alkali-earth) cations exchanged in zeolites are known to be inactive for butene isomerization and dimerization,[36-37] but change the accessibility of the pores.[38] Bell et al.[8, 39] reported, for example, that the presence of co-cations such as Li^{+}, Na^{+}, K^{+}, Mg^{2+}, Ca^{2+}, Sr^{2+} in zeolite X alters the accessibility of Ni^{2+} and changes its activity for propene dimerization. For larger alkenes, it is hypothesized that the co-cations induce side reactions that may modify catalytic activity and selectivity. [40]

In this work, we investigate the impact of Li^{+}, Mg^{2+}, Ca^{2+} and Na^{+} in Ni^{2+} ion-exchanged zeolite LTA on activity and selectivity of 1-butene dimerization, showing how the cations influence alkene isomerization rates and, hence, dimerization selectivity.

RESULTS AND DISCUSSION

Synthesis and characterization of Ni-Ca-LTA catalysts

The concentration of Ni in the zeolite increased linearly with the concentration of the Ni nitrate in solution (ca. 1.1 mmol/g Ni, 6 wt.% Ni; Figure S2-1) during the ion-exchange of Ca-LTA. The increase in Ni loading resulted in a decrease in the concentration of other cations, maintaining a charge balance of ~100 % (Figure S2-2). The Ni ion-exchange with Ca-LTA decreased Ca^{2+} from 2.6 to 2.0 mmol/g and Na^{+} from 1.9 to 0.9 mmol/g. However, the Li^{+} and Mg^{2+} ion-exchange of parent Ca-LTA resulted mainly in a decrease of the Na^{+} concentration below 0.5 mmol/g (Figure S2-1 B and C, respectively), resulting in 1.3 and 2.0 mmol/g of Mg^{2+} (Mg-Ca-LTA) and Li^{+} (Li-Ca-LTA), respectively. Subsequent Ni^{2+} exchange led to partial removal of the co-cations to final concentrations of 0.6 mmol/g of Mg^{2+} (Ni-Mg-Ca-LTA) and 0.2 mmol/g of Li^{+} (Ni-Li-Ca-LTA). Small changes were observed in the concentration of Ca^{2+} (approximately 1.7-1.9 mmol/g) in LTA. The concentration of Na^{+} decreased below 0.3 mmol/g for both Ni-Mg-Ca-LTA and Ni-Li-Ca-LTA. These results indicate a higher stability of the Ca^{2+} than of the other alkali and alkali-earth metal cations during ion-exchange.

The successive ion-exchange treatments led to structural changes in the zeolite framework, monitored by X-ray diffraction. In all materials ion-exchange caused significant broadening of the LTA diffraction lines, indicating decreasing crystalline domain size (Figure S2-3). The Mg^{2+} ion-exchange had a stronger effect on the zeolite structure than the Li^{+}. In all cases, the introduction of Ni^{2+} led to a further loss of crystallinity.

SEM micrographs were used to characterize potential effects on the zeolite crystal morphology. Exemplary pictures and the average particle sizes are shown in Figure S2-4, indicating clearly the absence of a measurable impact on particle size and morphology (Figure S2-5). On the other hand, N_2 sorption (Figure S2-6) shows the loss of micropore and simultaneous generation of mesopore volume upon Ni ion-exchange. This implies that mesopores have been generated by partial dissolution of crystalline matter. The partial breakdown of the zeolite structure is accompanied by a decrease in BET surface area (Figure S2-7).

The effect of Ni^{2+} ion exchange on catalytic activity

Typically, the catalytic activity was studied in a fixed bed flow reactor at 160 °C, 50 bar and a WHSV of 100 h^{-1}. The weight normalized rate of butene dimerization of Ni-Ca-LTA increased linearly with the Ni concentration (Figure 2-1). Similar trends were observed with Ni-Li-Ca-LTA and Ni-Mg-Ca-LTA. In Ni-Ca-LTA all the crystal disintegration is induced by Ni^{2+}, resulting in the dispersion of the nickel sites at a higher degree of structural collapse, increasing the dimerization rate upon higher Ni^{2+} concentration in the aluminosilicate. The mesoscopic properties of the Ni ion-exchange catalysts suggest the Ni sites catalyzing the dimerization are located either in the amorphous phase or at the pore mouth of LTA. Nevertheless, changes in mesoscopic properties (Figure S2-8) do not show a clear correlation between the rate per Ni^{2+} and the textural properties (mesopore surface area, micropore volume, BET surface area and BJH pore diameter). The minor rate differences observed at lower Ni^{2+} exchange (2 and 4 wt.%) with the different co-cations in Figure 2-1 could be due to subtle differences in the mesoscopic properties, however, at 6 wt. % the rate differences are reduced, since all catalysts had similar mesoscopic properties, supporting the similar initial rates observed in Figure 2-4. Therefore, the 6 wt.% Ni samples of the three catalyst series were used for further studies.

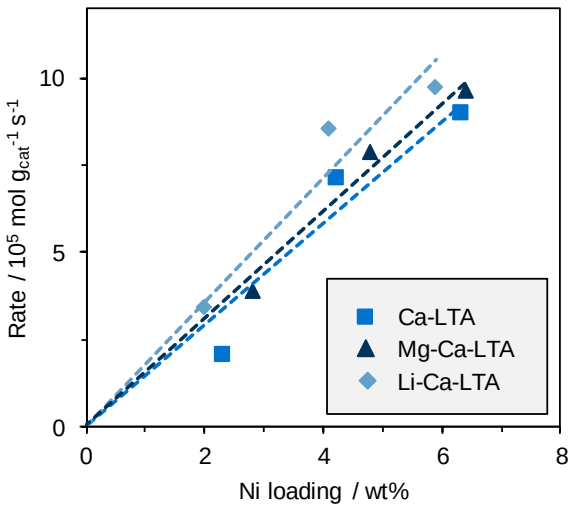

Figure 2-1. Rate per Ni as a function of the Ni loading with Ni exchanged Ca-LTA, Mg- and Li-Ca-LTA catalysts in dimerization of 1-butene (160 °C, 50 bar, WHSV = 100 h^{-1}).

Effect of co-cations on isomerization and dimerization activity

We have shown previously that isomerization of 1-butene into 2-butene occurs competitively during 1-butene dimerization with Ni-Ca-LTA, causing changes in the dimer selectivity.[31] Double bond isomerization also occurred on Ni-Li-Ca-LTA and Ni-Mg-Ca-LTA (Figure 2-2). The isomer distribution varied with the butene conversion in each catalyst. The equilibrium between 1-butene and *cis*- and *trans*-2-butene was reached at butene conversion levels of 28 % for Ni-Ca-LTA, 21 % for Ni-Mg-Ca-LTA and 20% for Ni-Li-Ca-LTA. All three ion exchanged zeolites were not active in the isomerization of 1-butene into 2-butene in the absence of Ni^{2+}.[36-37] Thus, isomerization takes place on the Ni^{2+} cation, as recently confirmed [31] and as observed for ethene dimerization with Ni^{2+} cations in zeolite BEA.[41]

The dimer selectivity as a function of conversion is shown in Figure 2-3. In all three catalysts, octene and methylheptene were primary products, while dimethylhexene was a secondary product. At conversions below 5 % in butene, n-octene was the dominating product. However, equal selectivity between octene and methylheptene was reached at different butene conversions (grey bar, Figure 2-3), following: Ni-Li-Ca-LTA < Ni-Mg-Ca-LTA < Ni- Ca-LTA. In agreement with a higher rate of isomerization for Ni-Li-Ca-LTA and Ni-Mg-Ca-LTA catalysts (498 and 493 10^4 mol_C g^{-1} s^{-1},respectively, Table 2-1) than for Ni-Ca-LTA (349 10^4 mol_C g^{-1} s^{-1} , Table 2-1), higher concentrations of branched dimers were formed with the former catalysts. It is noted in passing, that the rates of isomerization are two orders of magnitude higher than the rates of dimerization (Table 2-1). Thus, the dimer selectivity is significantly influence by the butene isomerization, as shown by the increase in methylheptene and dimethylhexene with the concentration of 2-butene formed, at the expense of the rate of n-octene formation. Indeed, a lower concentration of 2-butene in Ni-Ca-LTA results into a lower rate of dimethylhexene (0.02 10^4 mol_C g^{-1} s^{-1} for Ni-Ca-LTA and 0.04 10^4 mol_C g^{-1} s^{-1} for Mg and Li containing zeolites). The minor impact on the formation of n-octene and dimethylhexene suggest that the competitive rates do not depend markedly on the concentration of 2-butene.

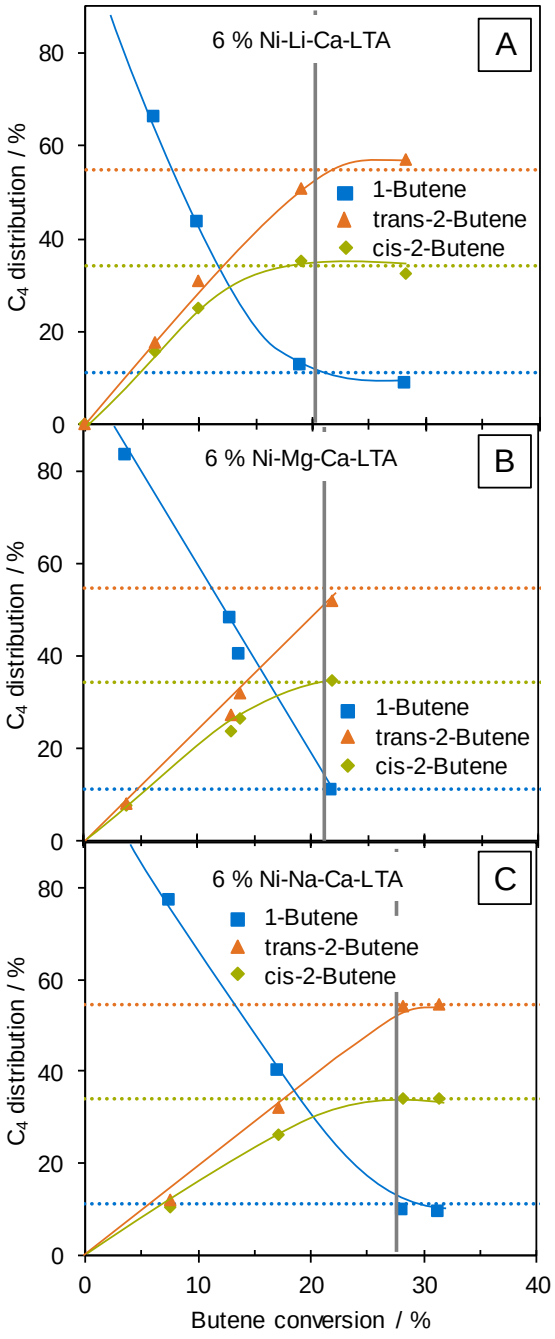

Figure 2-2. Effect of co-cations on 1-butene isomerization vs. butene conversion (T = 160 °C, p = 50 bar, WHSV = 6 – 125 h^{-1}). The dotted lines give the respective equilibrium values at 160 °C and 50 bar, the grey bar demonstrates conversion level, where the C_4 equilibrium is reached.

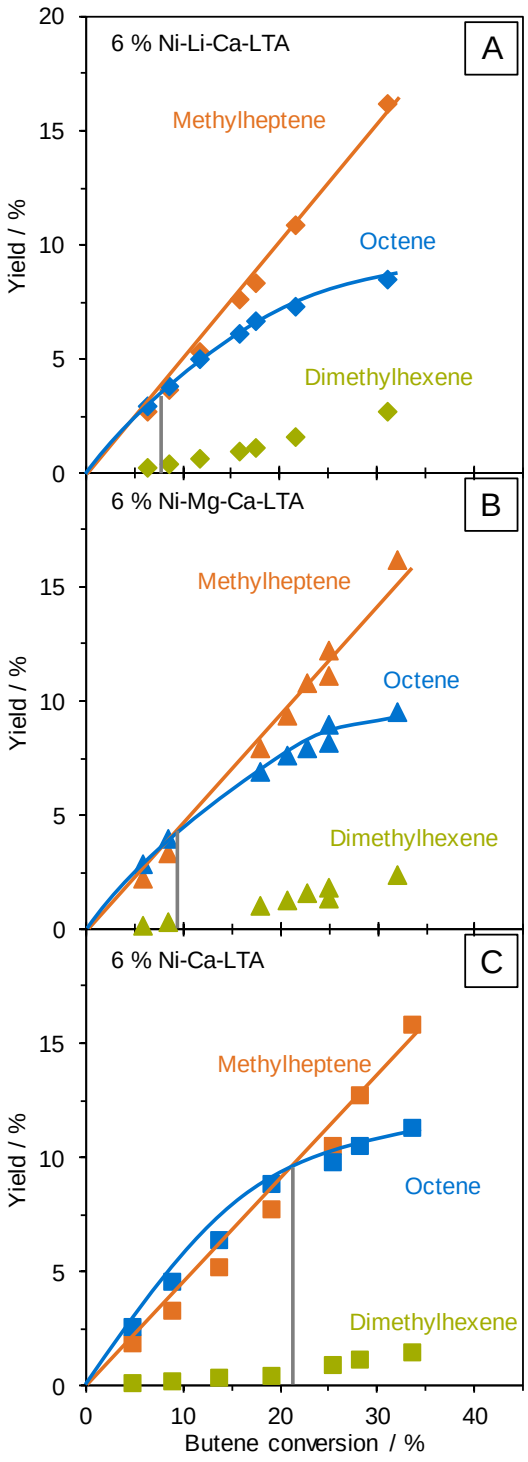

Figure 2-3. Yield as function of butene conversion over 6 % Ni containing LTA based catalysts with different co-cations. T = 160 °C, p = 50 bar, WHSV = 6-245 h^{-1}. A) 6 % Ni-Ca-LTA, B) 6 % Ni-Mg-Ca-LTA, C) 6 % Ni-Li-Ca-LTA. Grey bars show equal concentration of octene and methylheptene.

Table 2-1. Isomerization and dimerization rates over Ni exchanged LTA catalysts with different co-cations at $X_{Dimerization}$ = 2 % (T = 160 °C, p = 50 bar, $WHSV_{Isomerization}$ = 185 h^{-1}, $WHSV_{Dimerization}$ = 312 h^{-1}).

	Isomerization	Dimerization rate				$\frac{Rate_{Isom}}{Rate_{Dim}}$
	Isomerization rate	Butene consumption	DMH	MH	n-Octene	
	[10^4 mol_C g^{-1} s^{-1}]	[10^4 mol_C g^{-1} s^{-1}]	[10^5 mol_C g^{-1} s^{-1}]			
Ni-Ca-LTA	349	1.41	0.2	5.5	8.3	248
Ni-Mg-Ca-LTA	493	1.49	0.4	5.9	8.6	331
Ni-Li-Ca-LTA	498	1.29	0.4	5.2	7.4	386

A detailed description of the reaction network is shown in Scheme 2-1. As reported [31], the main dimerization route follows the 1'-adsorption. After the formation of a Ni-alkyl, another butene coordinates to the Ni site and forms the dimer. The C-C bond formation with the second butene can take place at the primary (1'-insertion, 1-butene) or secondary (2'-insertion, 1-butene or 2-butene) carbon, leading to the formation of n-octene or 3-methylheptene, respectively. The presence of 2-butene alters the reaction pathways, since adsorption and insertion are taking place on the C_2-atom, increasing the 2'-adsorption pathway (Scheme 2-1, right pathway, green). Consequently, the concurrent isomerization of 1-butene into 2-butene conceptually changes the product distribution to an increased selectivity towards branched dimers with butene conversion, as shown in Figure 2-3. It is noted in passing, that dimerization of 2-butene is one order of magnitude slower than with 1-butene, as shown with transient experiments of both butenes.[31] Even though the concentration of 1-butene at thermodynamic equilibrium is an order of magnitude lower than at 0 % butene conversion (11 % for 1-butene at thermodynamic equilibrium), the high selectivity to octene and methylheptene (above 95 %) reflects the higher rates of 1-butene dimerization.

High stability of the formed Ni-alkyl species has been hypothesized either via the 2'-adsorption or via the insertion of another alkene (1-butene or 2-butene) into the secondary carbon of the adsorbed 2-butene, leading to the deactivation of the Ni-Ca-LTA. In agreement

with their high activity for double bond isomerization, Mg^{2+} and Li^{+} containing LTA show rapid deactivation compared to Ni-Ca-LTA (Figure S2-9).

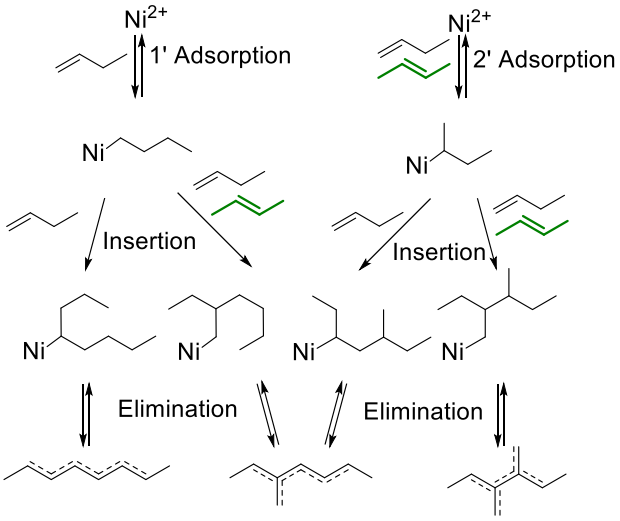

Scheme 2-1. Dimerization pathways of 1-butene and 2-butene (green) leading to linear, mono- and di-branched octenes.

The inverse temperature dependence of the rate (Arrhenius plots) is shown for n-octene and methylheptene in Figure S2-10 and the corresponding apparent activation energies are listed in Table S2-2. Apparent activation energies were not determined for dimethylhexene, being a secondary product after the isomerization of 1-butene into 2-butene. The similarities in the initial rates and apparent activation energies point to a similar dimerization pathway for all catalysts. Therefore, we hypothesize that dimerization is solely catalyzed by Ni^{2+} sites and is hardly affected by other co-cations.

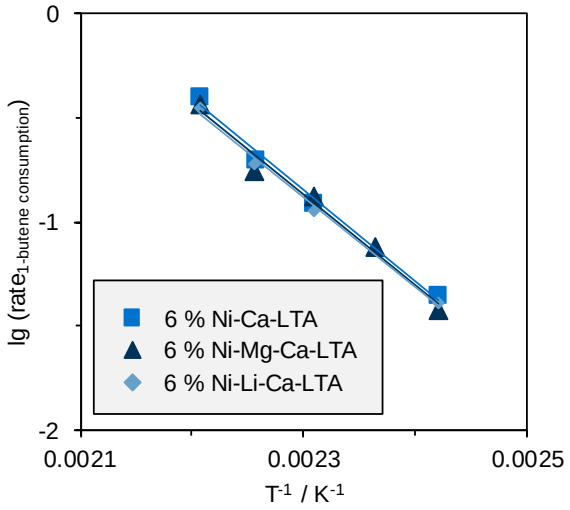

Figure 2-4. Arrhenius type plots of the fitted initial rates in 1-butene conversion (WHSV = 312 h^{-1}; T = 140 – 180 °C, p = 50 bar).

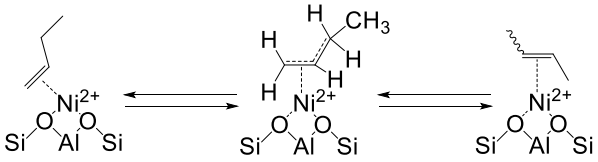

Scheme 2-2. Isomerization of 1-butene over a Ni^{2+} site.

Isomerization of 1-butene to *cis*- and *trans*-2-butene was concluded to occur via a π-allyl bound Ni-complex (Scheme 2-2).[31] At similar textural properties for all 6 wt.% Ni catalysts, we suggest that the different isomerization activities originate from the different electronic environment induced by the co-cations present on the Ni-alkyl complex. However, it is noted in passing that in the absence of Ni^{2+} isomerization and dimerization were not observed with Ca-LTA, Li-Ca-LTA and Mg-Ca-LTA. We hypothesize that these cations influence, however, the stabilization of the π-allyl bound Ni-complex. Among the co-cations, Li and Mg have higher Sanderson electronegativity (0.89[42] and 1.32[42], respectively) than Na (0.84[42]). The similar rates in isomerization with Mg and Li containing LTA demonstrates comparable stabilization effects in agreement with earlier literature [43-44]. Thus, the higher electronegativity of Mg^{2+} and Li^{+} is suggested to stabilize the formation of the π-allyl bound Ni-complex

intermediate, increasing the isomerization rate of 1-butene into 2-butene. Na^+, on the other hand, is less electronegative, resulting in a slower isomerization rate.

Adsorption studies

It has been shown, previously, that the presence of co-cations (alkali and alkali-earth) of diverse size in zeolite X alters the accessibility to Ni^{2+} and changes its activity for propene dimerization. [8, 39] Although these co-cations can vary the olefin uptake and the rates of isomerization of 1-butene into 2-butene, the dimerization rates were identical. Therefore, we measured the 1-butene uptakes (Table 2-2, the corresponding isotherms are shown in Figure S2-11 and Figure S2-12) to assess the changes in accessibility to 1-butene and demonstrate these do not alter the dimerization activity. The highest 1-butene uptake was observed on the Ca-LTA (1.1 mmol/g). The presence of co-cations and Ni^{2+}, decreases the micropore volume and surface area, and increases the mesopore surface area (Figure S2-6 and Figure S2-7). Therefore, the adsorption capacity on parent Ca-LTA was much larger than on the other metal exchanged samples.

Among the 6 wt.% Ni containing samples, Mg^{2+} and Li^+ containing LTA adsorbed a higher concentration of 1-butene (1.1-1.0 mmol/g) than Ni-Ca-LTA (0.7 mmol/g). Although the Ni ion-exchange generated partial structural collapse and the dispersion of the Ni in the induced mesopores, the remaining micropores were still available for 1-butene adsorption. Thus, the zeolite micropores in the absence of active Ni sites but in the presence of co-cations can vary the accessibility for 1-butene. The 6 % Ni-Ca-LTA has approximately 0.9 mmol/g monovalent cations, while Ni-Li-Ca-LTA and Ni-Mg-Ca-LTA (both 6 wt.% Ni) have 0.4 and 0.2 mmol/g (Table S2-1). Upon higher monovalent cation concentration, these cations have been suggested to be located at the center of the 8-membered rings in LTA,[38, 45-46] minimizing the accessibility to the supercage of LTA framework (M^{2+} occupy the positions at the 6-MR windows, which are non-accessible). [38, 45-46] Hence, the presence of Na^+ at the center 8-membered rings in LTA decreases the adsorption capacity to 1-butene.

Table 2-2. Results of thermogravimetric analysis of 1-butene adsorption behavior on different materials.

	Butene uptake maximum [mmol g^{-1}]	ΔH_{ads} [kJ mol^{-1}]
Ca-LTA	2.1	78
6 % Ni- Ca-LTA	0.7	63
6 % Ni-Li-Ca-LTA	1.1	56
6 % Ni-Mg-Ca-LTA	1.0	53

The adsorption enthalpies of 1-butene on Li- and Mg-Ni-Ca-LTA were of 56 and 53 kJ/mol (Table 2-2), respectively, while a higher adsorption enthalpy was observed with Ni-Ca-LTA (63 kJ/mol, Table 2-2). Interestingly, the highest value was observed with Ca-LTA having the highest Na^+ concentration (78 kJ/mol on Ca-LTA). It is hypothesized that the higher micropore volume and the absence of mesopores in Ca-LTA increases the confinement, inducing stronger interactions with 1-butene.[47] In the case of the Ni^{2+} exchanged LTA, similar mesoscopic structures were obtained after ion-exchange. Interestingly, Ni-Ca-LTA has a higher concentration of Na^+ than Ni-Mg-Ca-LTA and Ni-Li-Ca-LTA (2.0, 0.3 and 0.3 mmol/g, respectively). It is speculated that that the larger cation size of Na^+, decreases the pore size and enhances so the interaction with 1-butene.[48-49]

CONCLUSION

The presence of co-cations, such as Na^+, Li^+ and Mg^{2+} was found to alter the catalytic activity of Ni exchanged Ca-LTA based catalysts for 1-butene dimerization. Both butene double bond isomerization and dimerization takes place in the Ni^{2+} cations. Even though in presence of Ni^{2+} 1-butene dimerization rates were equal for all catalysts with, regardless of the co-cation, the rates of 1-butene isomerization into 2-butene were higher in the presence of Li^+ and Mg^{2+} co-cations. The co-cations with higher Sanderson electronegativity (0.89 and 1.32 for Li and Mg) than Na (0.84) [42] are suggested to enhance the stabilization of the π-allyl bound Ni-complex intermediate, increasing the isomerization rates into 2-butenes. Thus, thermodynamic equilibrium between butene isomers was reached at lower butene conversions when Li^+ and Mg^{2+} co-cations (X_{eq} ~ 20%) replaced with Na^+ (X_{eq} ~ 28%). In consequence, the dimer distribution varied at butene conversions above 5 %, leading to a higher concentration of branched dimers with Li^+ and Mg^{2+} co-cations. Hence, future design of Ni-ion exchange zeolites for α-alkene dimerization should involve the presence of co-cations with low electronegativity, preventing the formation of Brønsted acid sites that lead to undesired reactions and diminishing the rates of 1-butene isomerization into 2-butene.

EXPERIMENTAL

Catalyst preparation. Ca-LTA was obtained by stirring Ca-LTA-5A (Sigma-Aldrich, pre-calcined: 4 h, rate 5 °C/min, 500 °C) with water (20 g_{water} / $g_{zeolite}$) at 80 °C for 24 h (pH = 7-8 during the time of exchange). The solid was recovered and washed thoroughly with deionized water. After drying at 100 °C for 10 hours, the precursor was calcined (8 h, rate: 5 °C/min, 500 °C, air). The solid was recovered and washed thoroughly with deionized water. After drying at 100 °C for 10 hours, the precursor was calcined (8 h, rate: 5 °C/min, 500 °C, air). The solid was recovered and washed thoroughly with deionized water. After drying at 100 °C overnight, the precursor was calcined (8 h, rate: 5 °C/min, 500 °C, air).

For the Mg or Li containing catalysts, the pre-calcined (see above) commercial zeolite Ca-LTA-5A was exchanged with an aqueous $MgCl_2$ or LiCl solution (0.5 M, 40 $g_{solution}/g_{zeolite}$), respectively. The ion exchange was performed for 4 h at 80 °C and was repeated 4 times. After the last exchange step, the solid was recovered and washed thoroughly with water, dried overnight, and calcined (8 h, rate: 5 °C/min, 500 °C, air). The nickel exchange was performed as described above.

Characterization methods. Atomic absorption spectroscopic measurements (AAS) were performed in a Solar M5 Dual Flame graphite furnace AAS from ThermoFisher. After drying at 250 °C for 24 h, the samples were dissolved in a mixture of HF and nitric acid and injected in the graphite furnace. A previous calibration was applied to determine the concentration of each of the metals.

X-ray diffraction measurements were performed in a PANalytical Empyreal System diffractometer, equipped with a Cu- Kα radiation source ($K\alpha_1$ line of 1.54 Å; 45 kV and 40 mA)). The diffractograms were measured by the usage of a sample spinner stage in a 2θ range between 5 ° and 70 ° (step size: 0.0131303/2θ) at ambient conditions.

The gravimetric sorption isotherms of 1-butene on Ni-Ca-LTA as well as on Ca-LTA were measured in a Setaram TG-DSC 111 thermoanalyzer connected to a high vacuum system. About 20 mg of sample was placed in a quartz crucible and activated at 450 °C (rate: 10 °C/min) for 1 h in vacuum ($p < 10^{-4}$ mbar). After cooling down to 40 °C, the equilibration of the sorbate was performed in small pressure steps from 0.01 to 10 mbar. Both, the sample mass and the thermal flux were monitored. The heat of adsorption was directly obtained by integration of the observed heat flux signal at uptakes below 0.7 mmol/g.

The BET specific surface area and pore volume of the zeolite were determined by nitrogen physisorption. The isotherms were measured at liquid nitrogen temperature (77 K) using a PMI Automatic Sorptometer. The catalyst was activated in vacuum at 473 K for 2 h before measurement. Apparent surface area was calculated by applying the Brunauer-Emmett-Teller (BET) theory with a linear regression between p/p_0 = 0.01 – 0.15. The micro- and mesopores were determined from the t-plot linear regression for t = 5-6 Å.

Catalytic testing and reaction kinetics. Catalytic tests were conducted in a fixed bed PFR (id = 3.9 mm), connected to an online GC analysis unit (Agilent HP 6890, equipped with a 50 m HP-1 column). Prior to GC analysis, hydrogen is added to the product stream, which is hydrogenated over a Pt/Al_2O_3 catalyst. A mixture of 15 % i-butane and 85 % 1-butene is introduced by a syringe pump (ISCO model 500 D), temperature is controlled by a Eurotherm 2416, pressure is controlled using a Tescom backpressure regulator.

Prior to weighing, the catalyst was dried at 100 °C for 1 h. The catalyst bed was diluted with SiC and fixed in the isothermal zone of the reactor. After activation for 2 h at 450 °C (rate: 10 °C/min) in air, the system was purged with nitrogen and pressurized to the desired pressure. Subsequently the system was flushed with the feed mixture (5 ml/min) for 2 min. After the desired flow rate is set, temperature program and GC measurements were started.

Standard measurement conditions were at 160 °C and 50 bar with a flow rate of butene mixture between 0.04 and 0.12 ml/min. Catalyst loading was varied between 10 and 200 mg. WHSV was in the range of 6 to 244 g g^{-1} h^{-1}.

Activation energies were determined between 150 and 180 °C at 50 bar with a WHSV of 150 h^{-1}. The feed was diluted with propane, which led to concentrations of 1-butene between 32 and 86 wt.%. Each measurement was performed over a fresh catalyst. As rapid deactivation was observed on all catalysts, the rates were fitted to t=0 (start of the reaction). With these rate values, the energy of activation was determined.

i-Butane is inert under reaction conditions applied, and was used as internal standard for normalization of GC areas. Conversion, selectivity and yields are calculated according to the following equations:

$$X = \frac{n(butene)_{in} - n(butene)_{out}}{n(butene)_{in}}$$

$$S = \frac{n(product)_{out}}{n(butene)_{in} - n(butene)_{out}} \frac{|\nu_{butene}|}{\nu_{product}}$$

$$Y = \frac{n(product)_{out}}{n(butene)_{in}} \frac{|\nu_{butene}|}{\nu_{product}}$$

REFERENCES

[1] S. Albrecht, D. Kießling, G. Wendt, D. Maschmeyer, F. Nierlich, Oligomerisierung von n-Butenen, Chem. Ing. Tech., 77 (2005) 695-709.
[2] K. Fischer, K. Jonas, P. Misbach, R. Stabba, G. Wilke, Zum „Nickel-Effekt", Angew. Chem., 85 (1973) 1001-1012.
[3] S.M. Hassan, G.M. Panchenkov, O.I. Kuznetsov, Studies on the Mechanism and Kinetics of Propylene Oligomerization and Hydrooligomerization on Zeolites, Bull. Chem. Soc. Jpn., 50 (1977) 2597-2601.
[4] R. Henry, M. Komurcu, Y. Ganjkhanlou, R.Y. Brogaard, L. Lu, K.-J. Jens, G. Berlier, U. Olsbye, Ethene Oligomerization on Nickel Microporous and Mesoporous-Supported Catalysts: Investigation of the Active Sites, Catal. Today, 299 (2018) 154-163.
[5] Y.T. Kim, J.P. Chada, Z. Xu, Y.J. Pagan-Torres, D.C. Rosenfeld, W.L. Winniford, E. Schmidt, G.W. Huber, Low-Temperature Oligomerization of 1-Butene with H-Ferrierite, J. Catal., 323 (2015) 33-44.
[6] N. Kumar, P. Mäki-Arvela, T. Yläsalmi, J. Villegas, T. Heikkilä, A.R. Leino, K. Kordás, T. Salmi, D. Yu Murzin, Dimerization of 1-Butene in Liquid Phase Reaction: Influence of Structure, Pore Size and Acidity of Beta Zeolite and MCM-41 Mesoporous Material, Microporous Mesoporous Mater., 147 (2012) 127-134.
[7] A.N. Mlinar, G.B. Baur, G.G. Bong, A.B. Getsoian, A.T. Bell, Propene Oligomerization over Ni-Exchanged Na-X Zeolites, J. Catal., 296 (2012) 156-164.
[8] A.N. Mlinar, S. Shylesh, O.C. Ho, A.T. Bell, Propene Oligomerization Using Alkali Metal- and Nickel-Exchanged Mesoporous Aluminosilicate Catalysts, ACS Catalysis, 4 (2013) 337-343.
[9] F.T.T. Ng, D.C. Creaser, Ethylene Dimerization over Modified Nickel Exchanged Y-Zeolite, Appl. Catal. A, 119 (1994) 327-339.
[10] B. Nkosi, F.T.T. Ng, G.L. Rempel, The Oligomerization of 1-Butene Using NaY Zeolite Ion-Exchanged with Different Nickel Precursor Salts, Appl. Catal. A, 161 (1997) 153-166.
[11] B. Nkosi, F.T.T. Ng, G.L. Rempel, The Oligomerization of Butenes with Partially Alkali Exchanged NiNaY Zeolite Catalysts, Appl. Catal. A, 158 (1997) 225-241.
[12] R.G. Schultz, R.M. Engelbrecht, R.N. Moore, L.T. Wolford, Olefin Dimerization over Cobalt-Oxide-on-Carbon Catalysts: II. Butene and Hexene Dimerization, J. Catal., 6 (1966) 419-424.
[13] G. Wendt, D. Kießling, Dimerisierung von n-Butenen an Nickelalumosilicat-Katalysatoren, Chem. Tech. (Leipzig), 47 (1995) 136-143.
[14] A. Behr, Z. Bayrak, S. Peitz, G. Stochniol, D. Maschmeyer, Oligomerization of 1-Butene with a Homogeneous Catalyst System Based on Allylic Nickel Complexes, RSC Advances, 5 (2015) 41372-41376.
[15] K. Weissermel, A. Hans-Jürgen, Industrial Organic Chemistry, Wiley-VCH, Weinheim, 1997.
[16] J. Skupinska, Oligomerization of α-Olefins to Higher Oligomers, Chem. Rev., 91 (1991) 613-648.
[17] K. Ziegler, E. Holzkamp, H. Breil, H. Martin, Das Mülheimer Normaldruck-Polyäthylen-Verfahren, Angew. Chem., 67 (1955) 541-547.
[18] H. F., Dimerisation and Double-Bond Isomerisation of Olefins with a Homogeneous Nickel II-Complex as Catalyst, Journal of Applied Chemistry and Biotechnology, 21 (1971) 90-91.
[19] Y.V. Kissin, D.L. Beach, Oligomerization of Ethylene with a Homogeneous Sulfonated Nickel Ylide–Aluminum Alkoxide Catalyst, J. Polym. Sci., Part A: Polym. Chem., 27 (1989) 147-155.

[20] R.D. Andrei, M.I. Popa, F. Fajula, V. Hulea, Heterogeneous Oligomerization of Ethylene over Highly Active and Stable Ni-AlSBA-15 Mesoporous Catalysts, J. Catal., 323 (2015) 76-84.
[21] R. Beucher, R.D. Andrei, C. Cammarano, A. Galarneau, F. Fajula, V. Hulea, Selective Production of Propylene and 1-Butene from Ethylene by Catalytic Cascade Reactions, ACS Catalysis, 8 (2018) 3636-3640.
[22] A. Finiels, F. Fajula, V. Hulea, Nickel-Based Solid Catalysts for Ethylene Oligomerization - A Review, Catalysis Science & Technology, 4 (2014) 2412-2426.
[23] S. Moussa, M.A. Arribas, P. Concepción, A. Martínez, Heterogeneous Oligomerization of Ethylene to Liquids on Bifunctional Ni-Based Catalysts: The Influence of Support Properties on Nickel Speciation and Catalytic Performance, Catal. Today, 277 (2016) 78-88.
[24] S. Moussa, P. Concepción, M.A. Arribas, A. Martínez, Nature of Active Nickel Sites and Initiation Mechanism for Ethylene Oligomerization on Heterogeneous Ni-beta Catalysts, ACS Catalysis, (2018) 3903-3912.
[25] A. Brückner, U. Bentrup, H. Zanthoff, D. Maschmeyer, The Role of Different Ni Sites in Supported Nickel Catalysts for Butene Dimerization under Industry-Like Conditions, J. Catal., 266 (2009) 120-128.
[26] M.A. Deimund, J. Labinger, M.E. Davis, Nickel-Exchanged Zincosilicate Catalysts for the Oligomerization of Propylene, ACS Catalysis, 4 (2014) 4189-4195.
[27] J. Canivet, S. Aguado, Y. Schuurman, D. Farrusseng, MOF-Supported Selective Ethylene Dimerization Single-Site Catalysts through One-Pot Postsynthetic Modification, J. Am. Chem. Soc., 135 (2013) 4195-4198.
[28] S.T. Madrahimov, J.R. Gallagher, G. Zhang, Z. Meinhart, S.J. Garibay, M. Delferro, J.T. Miller, O.K. Farha, J.T. Hupp, S.T. Nguyen, Gas-Phase Dimerization of Ethylene under Mild Conditions Catalyzed by MOF Materials Containing (bpy)NiII Complexes, ACS Catalysis, 5 (2015) 6713-6718.
[29] E.D. Metzger, C.K. Brozek, R.J. Comito, M. Dincă, Selective Dimerization of Ethylene to 1-Butene with a Porous Catalyst, ACS Central Science, 2 (2016) 148-153.
[30] A.N. Mlinar, B.K. Keitz, D. Gygi, E.D. Bloch, J.R. Long, A.T. Bell, Selective Propene Oligomerization with Nickel(II)-Based Metal–Organic Frameworks, ACS Catalysis, 4 (2014) 717-721.
[31] A. Ehrmaier, Y. Liu, S. Peitz, A. Jentys, Y.-H.C. Chin, M. Sanchez-Sanchez, R. Bermejo-Deval, J. Lercher, Dimerization of Linear Butenes on Zeolite-Supported Ni2+, ACS Catalysis, 9 (2019) 315-324.
[32] M.L. Sarazen, E. Doskocil, E. Iglesia, Catalysis on Solid Acids: Mechanism and Catalyst Descriptors in Oligomerization Reactions of Light Alkenes, J. Catal., 344 (2016) 553-569.
[33] M.L. Sarazen, E. Doskocil, E. Iglesia, Effects of Void Environment and Acid Strength on Alkene Oligomerization Selectivity, ACS Catalysis, 6 (2016) 7059-7070.
[34] M.L. Sarazen, E. Iglesia, Stability of Bound Species During Alkene Reactions on Solid Acids, Proceedings of the National Academy of Sciences, 114 (2017) E3900-E3908.
[35] M.L. Sarazen, E. Iglesia, Experimental and Theoretical Assessment of the Mechanism of Hydrogen Transfer in Alkane-Alkene Coupling on Solid Acids, J. Catal., 354 (2017) 287-298.
[36] S.V. Bordawekar, R.J. Davis, Probing the Basic Character of Alkali-Modified Zeolites by CO2 Adsorption Microcalorimetry, Butene Isomerization, and Toluene Alkylation with Ethylene, J. Catal., 189 (2000) 79-90.
[37] F. Yagi, H. Tsuji, H. Hattori, IR and TPD (Temperature-Programmed Desorption) Studies of Carbon Dioxide on Basic Site Active for 1-Butene Isomerization on Alkali-Added Zeolite X, Microporous Mater., 9 (1997) 237-245.
[38] R. Szostak, Hanbook of Molecular Sieves, Van Nostrand Reinhold, New York, 1992.
[39] A.N. Mlinar, O.C. Ho, G.G. Bong, A.T. Bell, The Effect of Noncatalytic Cations on the Activity and Selectivity of Nickel-Exchanged X Zeolites for Propene Oligomerization, ChemCatChem, 5 (2013) 3139-3147.

[40] A. Ehrmaier, R. Bermejo-Deval, M. Sanchez-Sanchez, Y. Liu, J.A. Lercher, S. Peitz, G. Stochniol, Selective Oligomerization of Olefins, in: EPOrg (Ed.), EVONIK Degussa GmbH Technische Universität München2018.
[41] R. Joshi, G. Zhang, J.T. Miller, R. Gounder, Evidence for the Coordination–Insertion Mechanism of Ethene Dimerization at Nickel Cations Exchanged onto Beta Molecular Sieves, ACS Catalysis, 8 (2018) 11407-11422.
[42] R.T. Sanderson, Principles of electronegativity Part I. General nature, J. Chem. Educ., 65 (1988) 112.
[43] P. Atkins, T. Overton, Shriver and Atkins' Inorganic Chemistry, OUP Oxford2010.
[44] A.F. Holleman, E. Wiberg, N. Wiberg, Lehrbuch der anorganischen Chemie, de Gruyter1995.
[45] A. García-Sánchez, E. García-Pérez, D. Dubbeldam, R. Krishna, S. Calero, A Simulation Study of Alkanes in Linde Type A, Adsorption Science & Technology, 25 (2007) 417-427.
[46] R.Y. Yanagida, A.A. Amaro, K. Seff, Redetermination of the Crystal Structure of Dehydrated Zeolite 4A, J. Phys. Chem., 77 (1973) 805-809.
[47] A. Bhan, R. Gounder, J. Macht, E. Iglesia, Entropy Considerations in Monomolecular Cracking of Alkanes on Acidic Zeolites, J. Catal., 253 (2008) 221-224.
[48] F. Eder, J.A. Lercher, Alkane Sorption in Molecular Sieves: The Contribution of Ordering, Intermolecular Interactions, and Sorption on Brønsted Acid Sites, Zeolites, 18 (1997) 75-81.
[49] F. Eder, M. Stockenhuber, J.A. Lercher, Brønsted Acid Site and Pore Controlled Siting of Alkane Sorption in Acidic Molecular Sieves, J. Phys. Chem. B, 101 (1997) 5414-5419.

2. Chapter - Supporting Information:

On the Role of Co-Cations in Nickel Exchanged LTA Zeolite for Butene Dimerization

SI-1 Synthesis and characterization of Ni-LTA catalysts with different co-cations

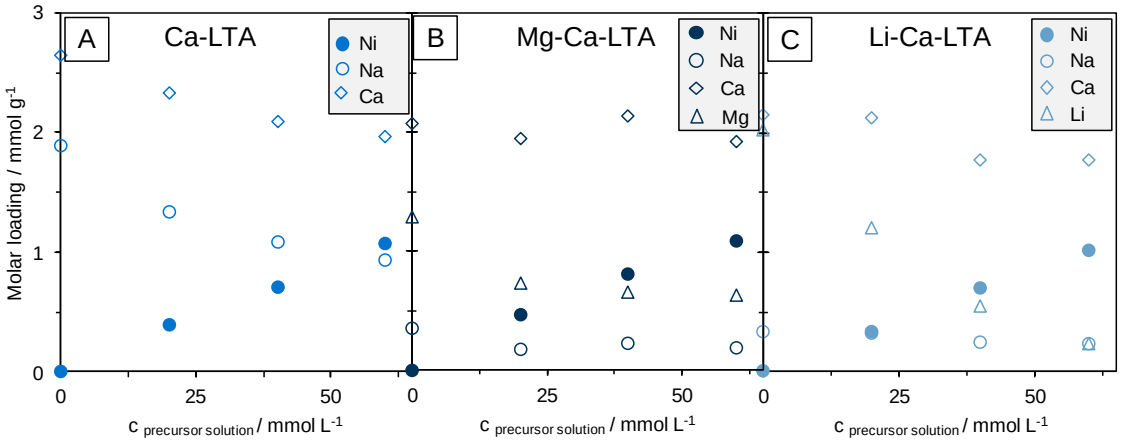

Figure S2-1. Cation loading of Ca-LTA based catalysts with various loadings of nickel and co-cations. A) Na-Ca-LTA, B) Li-Ca-LTA, and C) Mg-Ca-LTA.

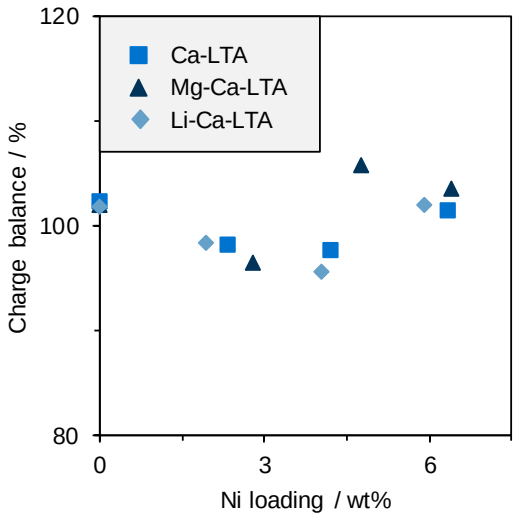

Figure S2-2. Charge balance of Ni and co-cation exchanged LTA catalysts.

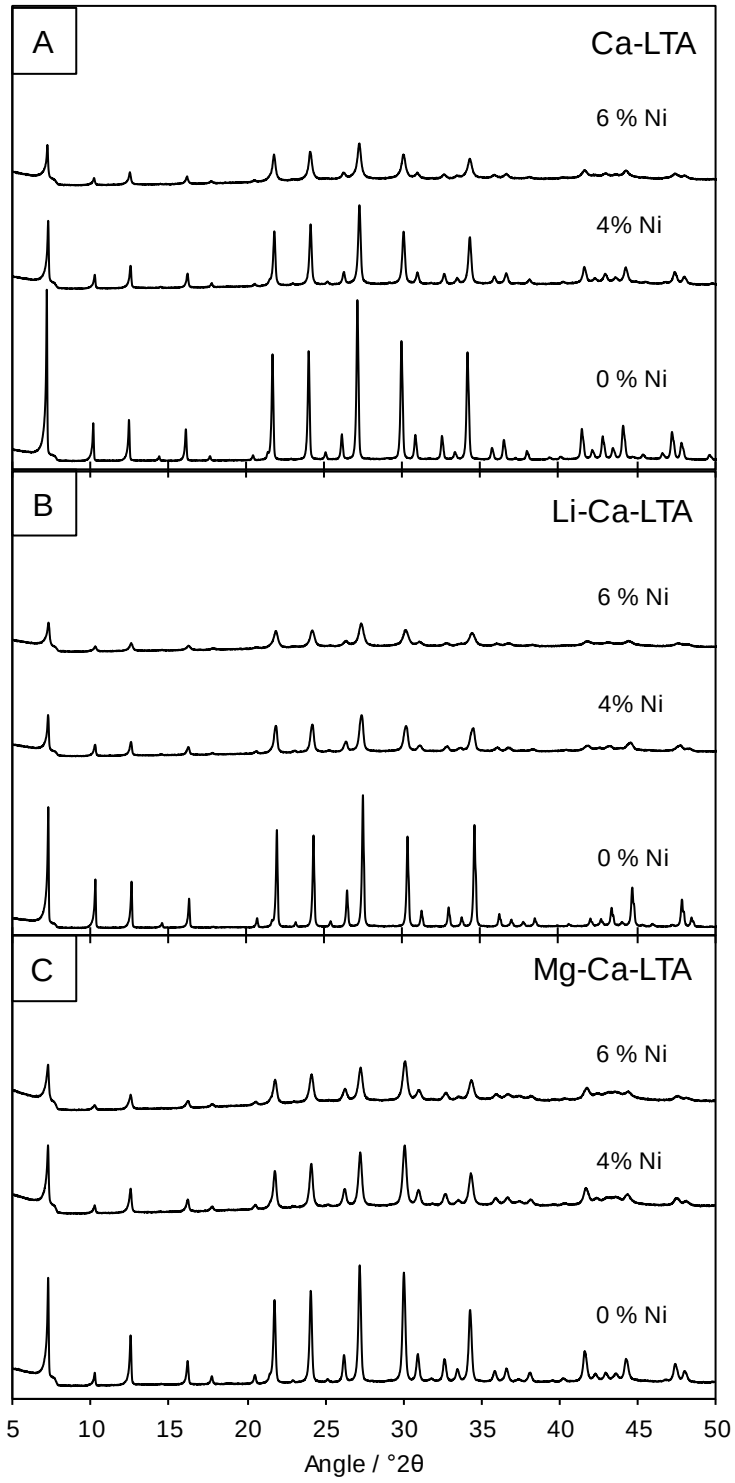

Figure S2-3. XRD patterns of different amounts of Ni exchanged to LTA catalysts with various other cations.

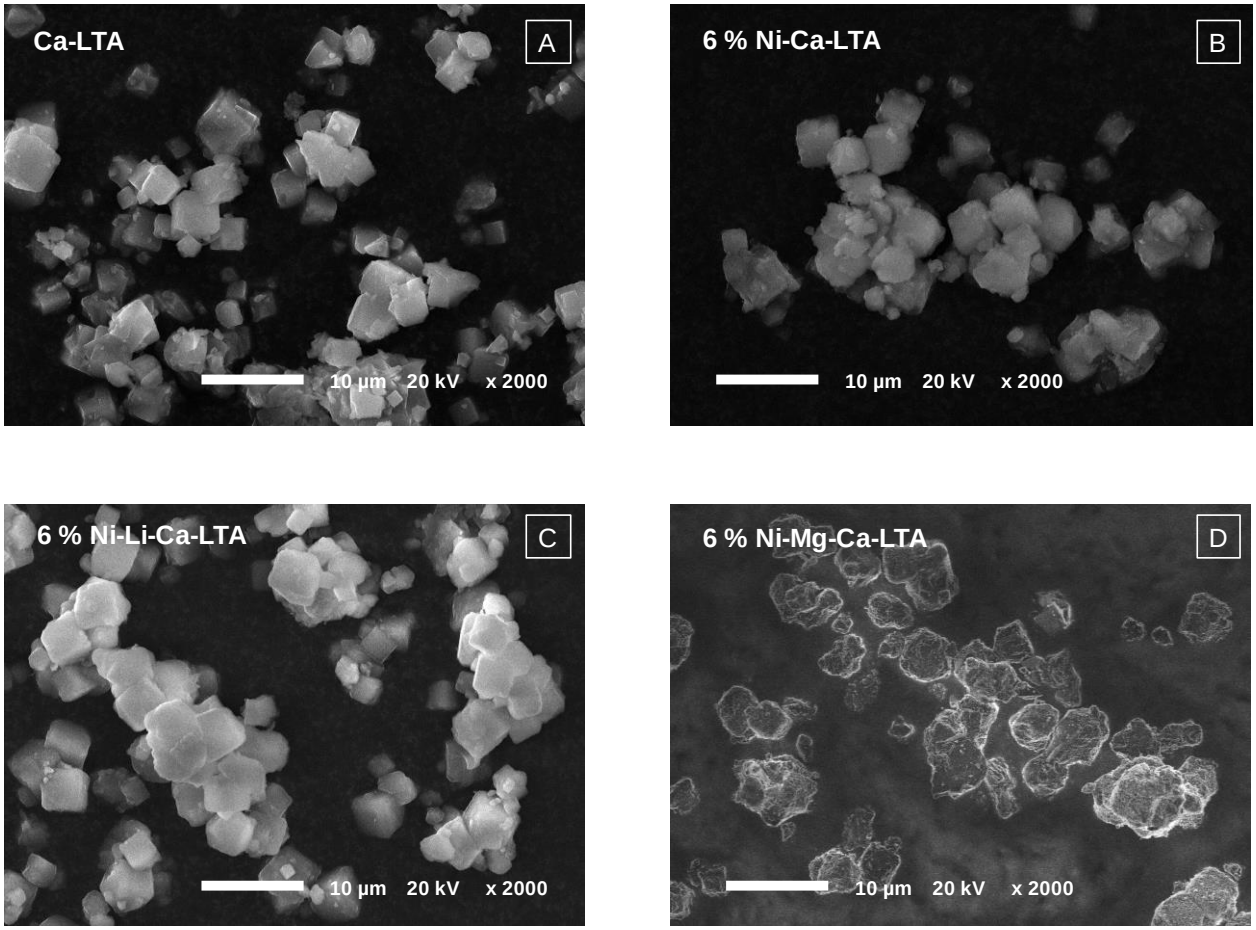

Figure S2-4. Exemplary SEM images of different co-cation containing Ni-LTA catalysts.

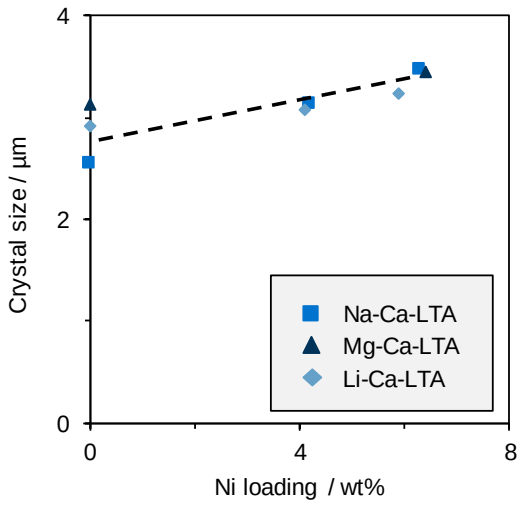

Figure S2-5. Average particle size measured from SEM images.

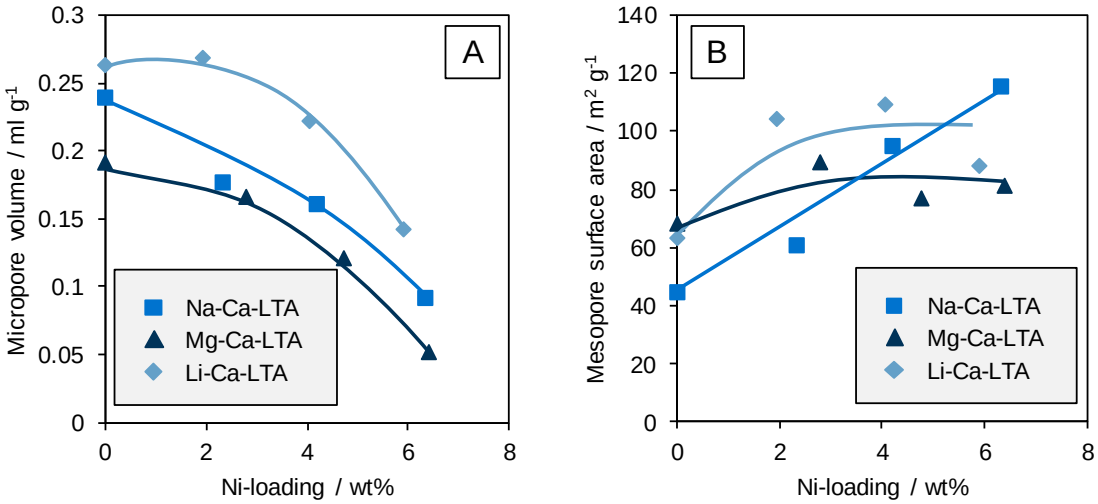

Figure S2-6. Mesoscopic properties (A: Micropore volume; B: Mesopore surface area) of catalysts with different Ni and co-cation loadings.

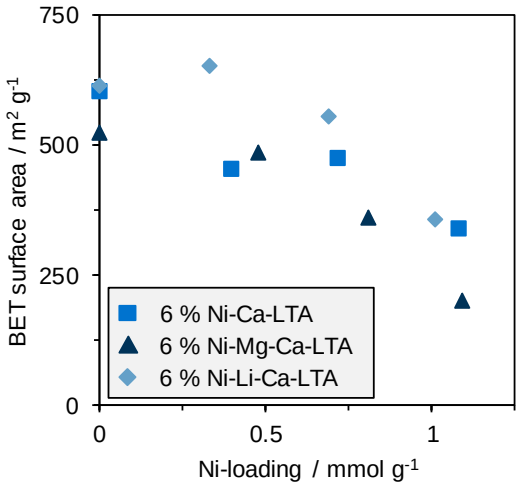

Figure S2-7. BET surface area of co-cation containing LTA catalysts with different Ni loadings.

SI-2 Catalytic testing of Ni-LTA catalysts with different co-cations

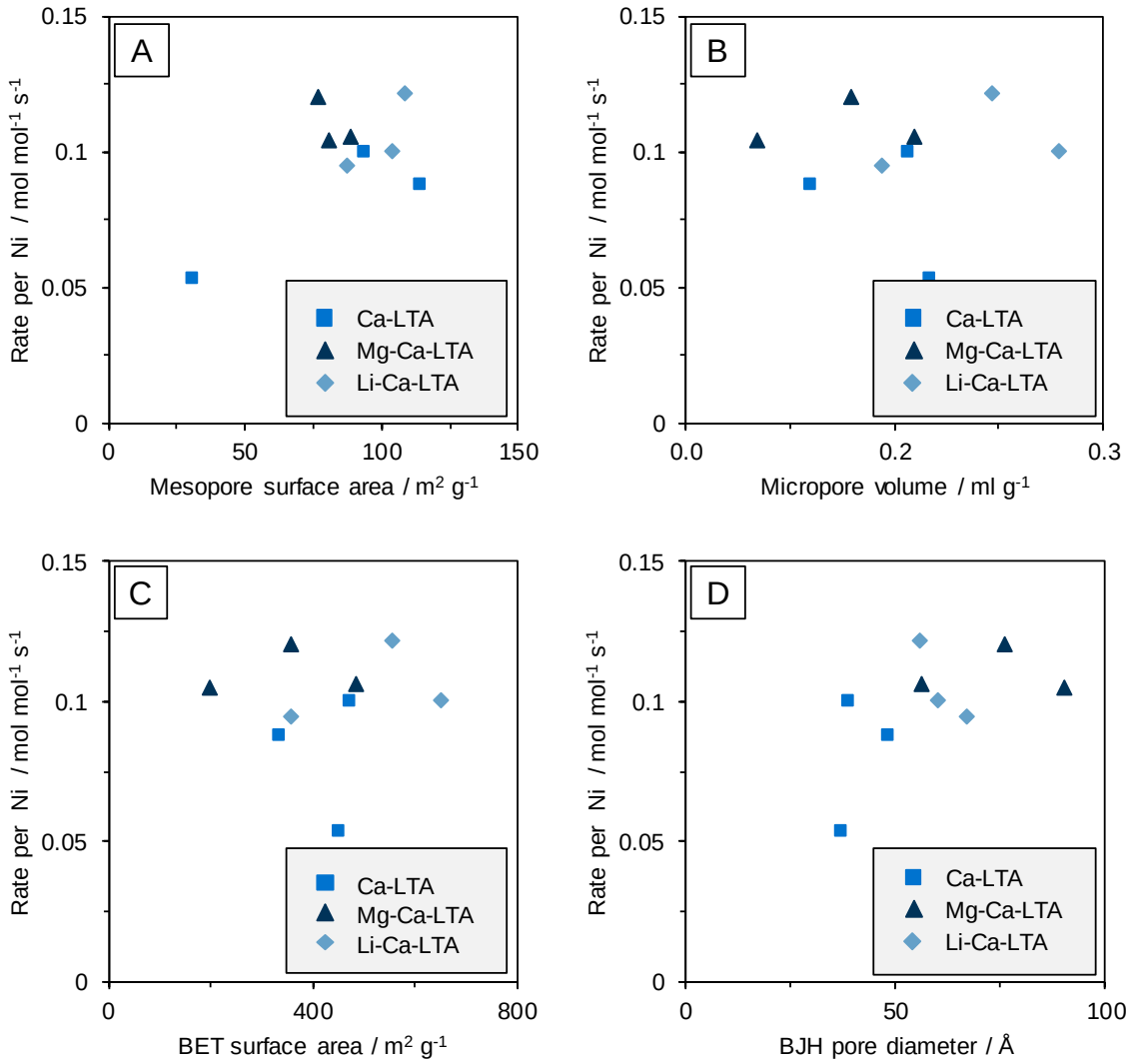

Figure S2-8. Effect of mesoscopic properties on the butene conversion rate over differently Ni exchanged Ca-LTA with various co-cations (160 °C, 50 bar, WHSV = 100 h^{-1}). A) Mesopore surface area. B) Micropore volume. C) BET surface area. D) Pore diameter.

Table S2-1. Cationic composition of 6 % Ni containing catalyst samples.

	Ni^{2+} $[\frac{mmol}{g}]$	Na^{+} $[\frac{mmol}{g}]$	Li^{+} $[\frac{mmol}{g}]$	Mg^{2+} $[\frac{mmol}{g}]$	Ca^{2+} $[\frac{mmol}{g}]$	Σ M^{+}	Σ M^{2+}	Σ M^{x+}	Charge balance
6 % Ni-Ca-LTA	1.1	0.9	0	0	2.0	**0.9**	**3.1**	**4.0**	1.02
6 % Ni-Li-Ca-LTA	1.0	0.2	0.2	0	1.8	**0.4**	**2.8**	**3.2**	1.02
6 % Ni-Mg-Ca-LTA	1.1	0.2	0	0.6	1.9	**0.2**	**3.6**	**3.8**	1.04

*Maximum error of 5%

SI-3 Reaction kinetics of Ni-LTA catalysts with different co-cations

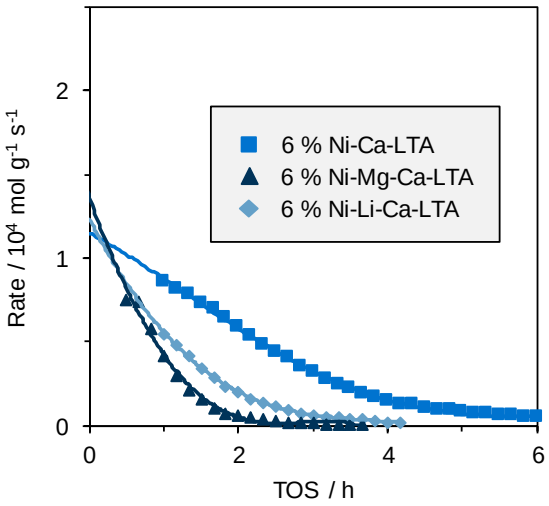

Figure S2-9. Catalytic activity of 6 % Ni containing LTA catalysts with different co-cations and the extrapolation fits to t=0 (160 °C, p = 50 bar WHSV = 312 h^{-1}).

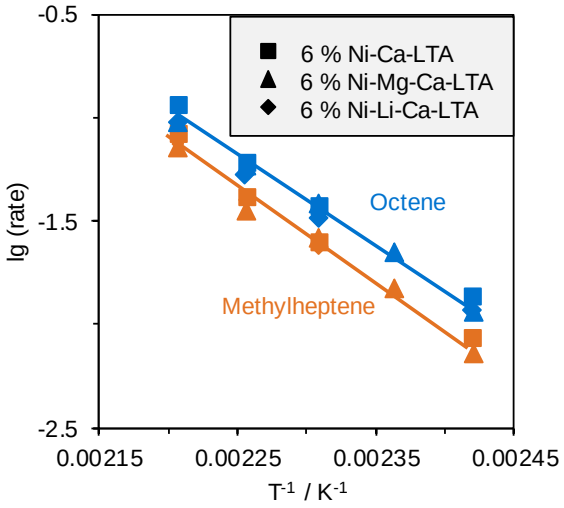

Figure S2-10. Arrhenius type plots of the fitted initial rates of formed products upon butene dimerization (WHSV = 312 h^{-1}; T = 140 – 180 °C, p = 50 bar).

Table S2-2. Apparent activation energies at t=0 of 1-butene consumption and product formation over different co-cation containing catalysts.

	E_A butene consumption [kJ mol^{-1}]	E_A MH formation [kJ mol^{-1}]	E_A O formation [kJ mol^{-1}]
6 % Ni-Ca-LTA	84	87	81
6 % Ni-Li-Ca-LTA	82	84	80
6 % Ni-Mg-Ca-LTA	84	85	81

SI-4 Butene adsorption studies on Ni-LTA catalysts with different co-cations

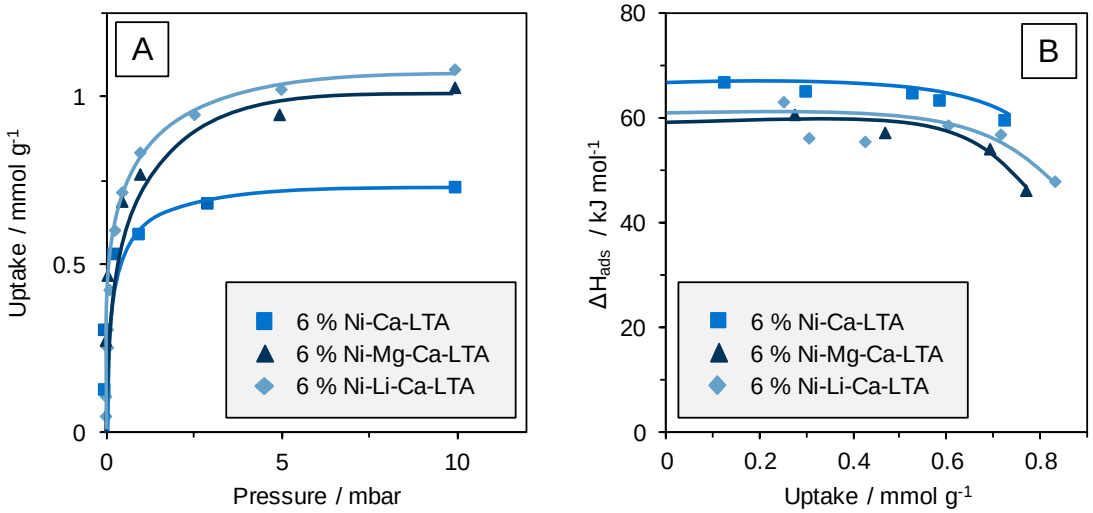

Figure S2-11. A) Stepwise butene uptake at 40 °C and B) the corresponding adsorption enthalpies of each single point. Enthalpy average values were obtained up to 0.7 mmol/g.

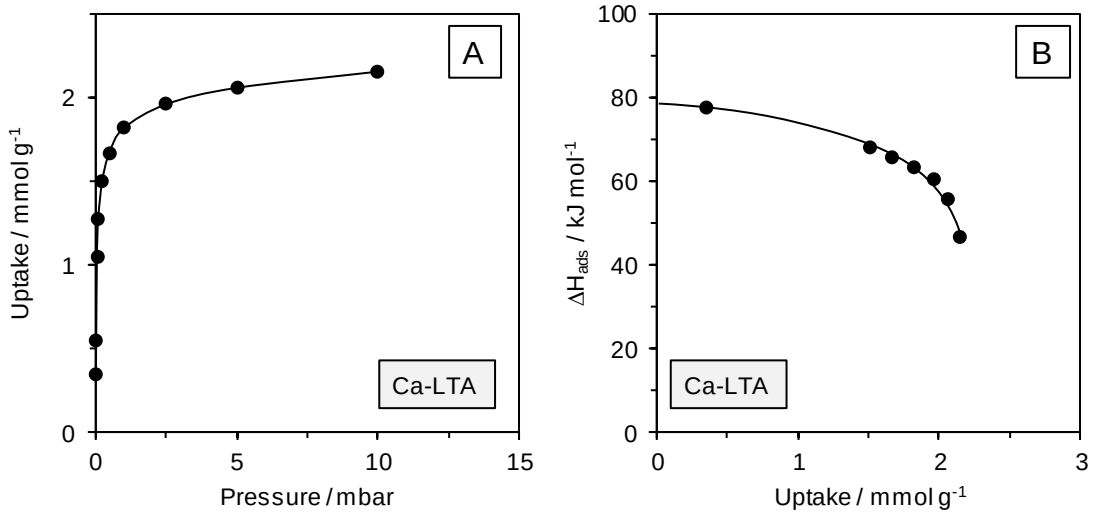

Figure S2-12. A) Stepwise butene uptake at 40 °C and B) the corresponding adsorption enthalpies of each single point on parent Ca-LTA.

3. Chapter:

The Effect of Co-Cations on Amorphous Supported Ni Catalysts in Butene Dimerization

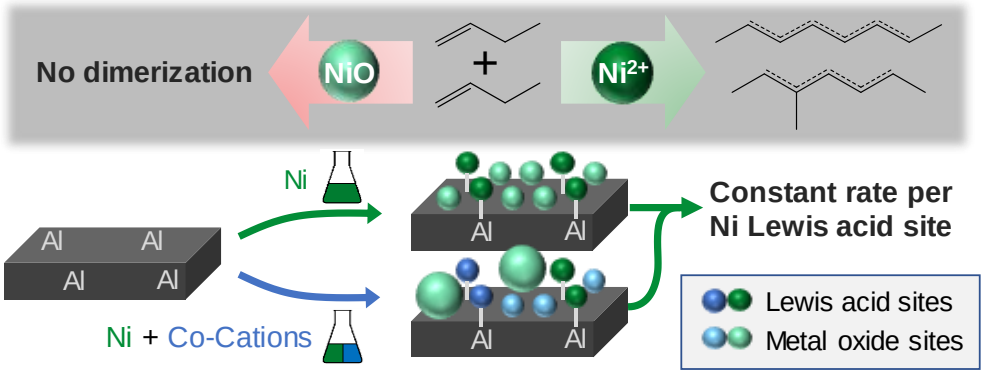

This chapter is based on:

Andreas Ehrmaier, Laura Löbbert, Maricruz Sanchez-Sanchez, Ricardo Bermejo de Val, Johannes Lercher,[3] *"The Effect of Co-Cations on Amorphous Supported Ni Catalysts in Butene Dimerization", In preparation*

[3] A.E. prepared and characterized the catalysts, planned, designed and performed the experiments, analyzed and interpreted the data and wrote the manuscript. L.L. helped with the experiments and contributed to the scientific discussion. R.B., J.L. guided the experiments, contributed to the scientific discussion and corrected the manuscript anytime.

ABSTRACT

The co-impregnation of various alkali or alkaline earth cations with Ni on an amorphous silica-alumina support increases the selectivity to linear octenes in the dimerization of 1-butene. The addition of alkali or alkaline earth cations was observed by X-ray diffraction to increase the formation of NiO clusters on the surface, being non-active in 1-butene dimerization. Adsorption of pyridine via IR shows the addition of the Ni and co-cations decreases the number of Brønsted acid sites from the SiO_2-Al_2O_3 support and generates additional Lewis acid sites, being the Ni sites active in both 1-butene dimerization and isomerization into 2-butene. It is suggested that the cations with lower Sanderson electronegativity (Na^+ and Ca^{2+}) stabilize less the π-allylic intermediate than harder cations (Li^+ and Mg^{2+}) during 1-butene isomerization, which in turn, decreases the concentration of 2-butenes and increases the formation of linear alkenes.

INTRODUCTION

The valorization of raffinates (butenes) from naphtha cracking processes is of high interest in the synthesis of high-value products.[1-3] These butenes are converted into branched dimers, used as gasoline additives,[3] or linear dimers,[4-6] applied as feedstock for the production of PVC plasticizers,[2, 7-9] catalyzed by Brønsted acids or transition metal catalysts, respectively. For the latter, Ni dispersed on amorphous silica alumina materials is used, obtaining selectivities of approx. 60 % to linear dimers (methylheptene and octene) and 40 % to branched dimers (dimethylhexenes).[10]

SiO_2-Al_2O_3 support provides both Lewis and Brønsted acid sites, enabling the dispersion and strong interaction with Ni cations. These cations are the active sites in the dimerization of 1-butene into linear dimers, following the Cossee-Arlman mechanism.[11-12] However, isolated Brønsted acid sites (BAS) catalyze the synthesis of branched dimers, via the formation of secondary carbenium ions and further isomerization into 2-butene.[13-14] Therefore, to achieve high selectivity into linear octenes these BAS can be titrated with other non-active cations.[15-17] The addition of alkali and alkaline earth metals into meso- and microporous aluminosilicates has shown to increase the selectivity to linear dimers with C_3 or higher olefins. [12, 18] Nonetheless, the constraint and accessibility induced by these cations in the meso- and microporous aluminosilicates have been claimed to solvate the transition state of the linear dimers. Howbeit, alkali and alkaline earth cations provide additional electronic properties and are able to adjust the chemical properties of the Ni active sites. [19-20] Thus, further assessment of these cations is needed without porous constraints to differentiate its intrinsic properties in olefin dimerization.

In this work, we explore the effect of alkali and alkali-earth co-cations on a nickel amorphous silica alumina catalyst. These co-cations alter the nature and concentration of acid sites, and in turn, modify the activity and tune the dimer selectivities of the industrial dimerization catalyst.

RESULTS AND DISCUSSION

Synthesis and characterization of Ni supported on SiO_2-Al_2O_3 catalysts with different co-cation contents

The loadings of Ni and the respective co-cations are shown in Table 3-1, having equal amounts of Ni and different amounts of co-cations (Na, Ca, Li, Mg) impregnated on the SiO_2/Al_2O_3. After the subsequent calcination, NiO clusters were observed by means of X-ray diffraction (Figure S3-1). The NiO crystallite size was calculated with the Scherrer equation (Figure S3-2). Smaller NiO crystallites were observed on the Ni-SiO_2/Al_2O_3 than with the corresponding co-cations. An increase in the NiO crystallite size with the co-cation concentration is observed, suggesting a stronger interaction of the co-cations with the SiO_2/Al_2O_3 support. Ni impregnation on SiO_2 led to relatively large NiO crystallites in the absence of co-cations, showing a weak interaction between the Ni and the SiO_2/Al_2O_3 support.

Table 3-1. Loadings of Ni and the respective co-cations of the catalysts used in this work.

Catalyst	Ni loading	Co-cation loading	Catalyst	Ni loading	Co-cation loading
	mmol g^{-1}	mmol g^{-1}		mmol g^{-1}	mmol g^{-1}
Ni-SiAl	1.0		Ni-SiO_2	1.0	
1Na-Ni-SiAl	1.0	0.7	2Na-Ni-SiAl	1.0	2.3
1Ca-Ni-SiAl	1.0	1.1	2Ca-Ni-SiAl	1.0	2.5
1Li-Ni-SiAl	1.0	1.4	2Li-Ni-SiAl	1.0	2.8
1Mg-Ni-SiAl	1.0	0.8	2Mg-Ni-SiAl	1.0	2.9

The impregnation of the Ni^{2+} cation in the absence of the co-cations induced the highest modification on the mesoscopic properties of the SiO_2/Al_2O_3 support (Figure S3-3), decreasing the BET surface area from 645 to 403 m^2/g, the micropore volume from 0.034 to 0.013 cm^3/g and the mesopore surface area from 689 to 422 m^2/g (Figure S3-4). A minor decrease is observed in the BET surface, mesopore surface area and micropore volume with

the co-cation concentration (Figure S3-3 A and D), while the pore diameter remains completely constant (Figure S3-3 B).

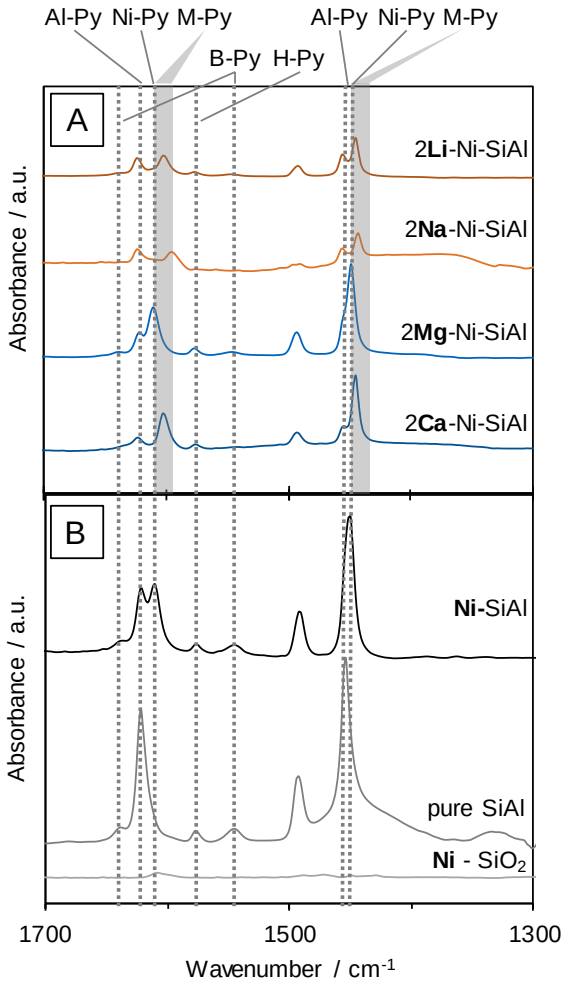

Figure 3-1. IR spectra of 1 mbar pyridine adsorbed at T = 150 °C on Ni catalysts containing ~2.5 mmol/g of different co-cations (A) and on co-cation free Ni-SiO_2/Al_2O_3 (B, top) as well as on the pure silica-alumina support (B, middle) or on Ni-SiO_2 (B, bottom). Al-Py: pyridine adsorbed to Al LAS; Ni-Py: pyridine adsorbed to Ni LAS; M-Py: pyridine adsorbed to co-cation LAS, B-Py: pyridine adsorbed to BAS; H-Py: H-bonded pyridine.

The nature and concentration of the surface acid sites were determined by IR via adsorption of pyridine (Figure 3-1, the 1.25 mmol/g loaded samples are shown in Figure S3-5). Pyridine adsorption on the parent silica-alumina support (Figure 3-1 B, middle) lead to the formation of protonated pyridinium ions with the Brønsted acid sites (B-Py) at 1540 and 1637 cm^{-1}.[21] In addition, pyridine bound to weak hydroxyls was observed at 1575 cm^{-1} (H-Py).[21-24] The band at 1621 cm^{-1} is assigned to the 8a vibrational mode of pyridine coordinatively bound to Lewis

acid sites, while the band at 1454 cm^{-1} is a cumulative band from pyridine adsorbed to Lewis acid H-bonded sites. [21, 25-26] As there are no other Lewis acid sites present, we would like to attribute these interactions to Al bound pyridine (Al-Py). The impregnation with Ni (Figure 3-1 B, top) did not change the total amount of Lewis or the Brønsted acid sites (Figure S3-6) drastically, but caused a significant change of the nature of the Lewis acid sites (Figure 3-1 B). In addition to the band at 1621 cm^{-1}, a new band was observed at 1610 cm^{-1}, indicative of lower Lewis acid strength (Lewis acid strength increases with wavenumber for the coordinative bound pyridine).[22] This band is assigned to pyridine coordinated to a Ni Lewis acid site (Ni-Py). A small shift was also detected from 1454 to 1450 cm^{-1}, indicative of an overlap between the Lewis acid sites of the support (Al-Py) and the Ni cations (Ni-Py), respectively. The adsorption of pyridine to the NiO on pure SiO_2 (Figure 3-1 B, bottom) revealed no adsorbed species, indicating that pyridine does not adsorb on NiO clusters and that the SiO_2 support does not have Lewis or Brønsted acidity.

The co-impregnation with additional cations (Figure 3-1 A) led to small changes in the IR spectra. The 1621 cm^{-1} band, assigned to the LAS of the SiO_2/Al_2O_3 support (Al-Py), decreased on all samples. The IR band assigned to the pyridine coordinated to Ni cations (Ni-Py, 1610 cm^{-1}) remained on all samples. However, an additional third band in that region at lower wavenumbers was observed, being assigned to the interaction of pyridine with the co-cations. The highest redshift was observed with the Na^+ co-cation (19 cm^{-1}), followed by Ca^{2+}, Li^+ (being both of 10 cm^{-1}) and Mg^{2+} (almost no red-shift) co-cations. The observed redshift is strongly correlated to the Sanderson electronegativity of the different co-cations (Figure S3-7), being the highest with Mg^{2+} (1.32) than Li^+, Na^+ and Ca^{2+} (0.89, 0.84 and 0.95, respectively).[27]

A significant decrease of the total acid site concentrations was observed upon addition of the co-cations (Figure 3-2). Brønsted acid sites decreased from 69 µmol/g with Ni-SiO_2/Al_2O_3 to 0 µmol/g with higher co-cation loading. Increasing loadings of all co-cations generated a decrease of the total concentration of Lewis acid sites, from 574 µmol/g with Ni-SiO_2/Al_2O_3 to 134-346 µmol/g with higher co-cation loading. Thereby, a lower concentration of LAS was observed in the presence of monovalent cations (134 and 170 µmol/g with Na^+ and Li^+) than with divalent cations (239 and 346 µmol/g with Ca^{2+} and Mg^{2+}). The deconvolution of the bands in the 8a vibrational mode (1600 cm^{-1} region, assuming all the of the brands in this region have the same molar extinction coefficient) allowed the differentiation between the Al based Lewis acid sites and the Ni- and co-cation-based Lewis acid sites. The respective concentrations are shown in Figure 3-2 (deconvolution areas are shown in Table S3-1). After the Ni exchange, almost 2/3 of the Lewis acidity arose from Ni sites. With increasing

concentrations of the co-cations, both, the Al based (Al-Py), as well as the Ni based Lewis acid sites (Ni-Py) decrease, while the co-cation based sites increase. However, the main difference is observed on the concentration of alkali and alkali-earth cations (Figure 3-2 M-Py), which is higher for the latter ones.

Among all 2.5 mmol/g co-cation loaded samples, a neglectable concentration of Brønsted acid sites was observed for all cations, suggesting the total exchange of the protons by the cations on the surface of the SiO_2-Al_2O_3.

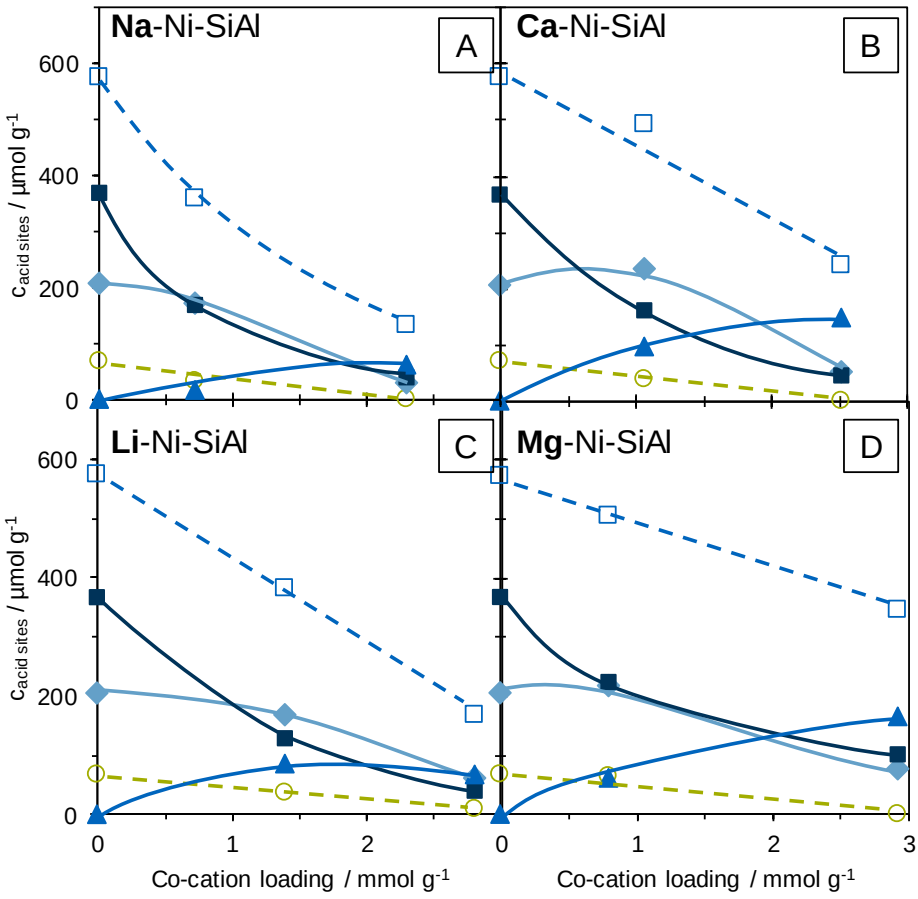

Figure 3-2. Concentrations of Lewis (□) and Brønsted (○) acid sites of 6 % Ni supported catalysts as a function of different concentrations of co-cations (A: Na-Ni-SiAl; B: Ca-Ni-SiAl; C: Li-Ni-SiAl; D: Mg-Ni-SiAl). Additionally, the concentration of Lewis acid sites is deconvoluted to Al-Lewis acid sites (Al-Py, ◆), Ni-Lewis sites (Ni-Py, ■) and co-cation based Lewis acid sites (M-Py, ▲).

Dimerization of 1-butene on Ni supported catalysts

The catalysts were tested for 1-butene dimerization in a flow reactor system at 160 °C and 50 bar. In the absence of Ni and co-cations, the support SiO_2-Al_2O_3 was active in the dimerization of 1-butene, forming only branched octenes (methylheptene and dimethylhexene) and deactivating rapidly (Figure S3-8). Upon addition of Ni, the rates in dimerization increased from 26 to 112 $mmol_C\ g^{-1}\ s^{-1}$, (Figure S3-8 and Figure 3-3) showing the Ni cations are active for dimerization. Ni-SiO_2 was not active (Figure S3-9), indicating that large NiO particles do not catalyze the dimerization of 1-butene. Operando spectroscopy measurements during butene dimerization have confirmed the deactivation of Ni upon particle agglomeration on SiO_2/Al_2O_3.[8]

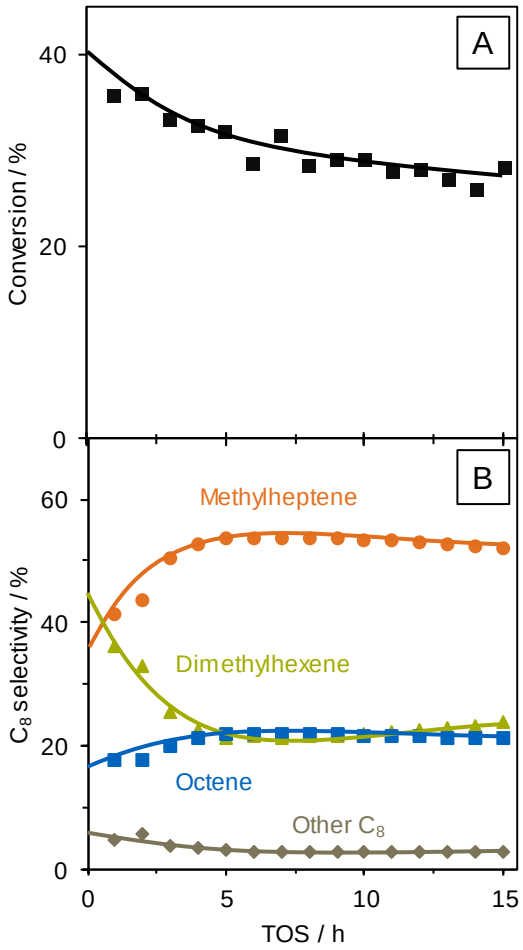

Figure 3-3. Conversion (A) and dimer selectivity (B) of dimerization of 1-butene over a 6 % Ni – SiO_2/Al_2O_3 supported catalyst (T = 160 °C, p = 50 bar, WHSV = 168 h^{-1}; MHSV = 12 $mol_{Butene}\ mol_{BAS}^{-1}\ s^{-1}$).

Figure 3-3 shows the conversion of 1-butene (Figure 3-3 A), as well as the selectivity within the dimer fraction (Figure 3-3 B) for Ni–SiO_2/Al_2O_3. Catalyst deactivation was observed, decreasing the conversion from 36 % to 27 % within 15 hours. A similar selectivity to dimethylhexene (DMH) and methylheptene (MH) was observed within the first hour (36 % and 41 %, respectively), decreasing the selectivity of DMH (down to 23 %) and increasing the selectivity of MH (up to 52 %). The selectivity of octene increased from 18 % to 21 %. The initial higher selectivity to dimethylhexene and lower selectivity to methylheptene and octene suggests the dimer formation is catalyzed by Brønsted and Ni acid sites. The proton catalyzed pathway occurs over a carbenium ion (Scheme S3-1), being of higher stability on a secondary carbon and leading to the formation of branched dimers,[14] as shown with the SiO_2/Al_2O_3 support containing Brønsted acid sites (Figure S3-8). [28] The rapid change in selectivity implies the inhibition of these Brønsted acid sites. In that regard, the acid site concentration was measured after the reaction with pyridine adsorption via infrared spectroscopy (Figure 3-4). After reaction, no Brønsted acid sites were observed. In addition, the concentration of LAS decreased significantly from 574 µmol/g to 0.3 µmol/g, indicating that both the Bronsted and Ni acid sites are inhibited by oligomerized products. X-ray diffraction measurements of the sample before and after reaction revealed no significant changes except a slight increase in NiO clusters upon sintering (Figure S3-10).

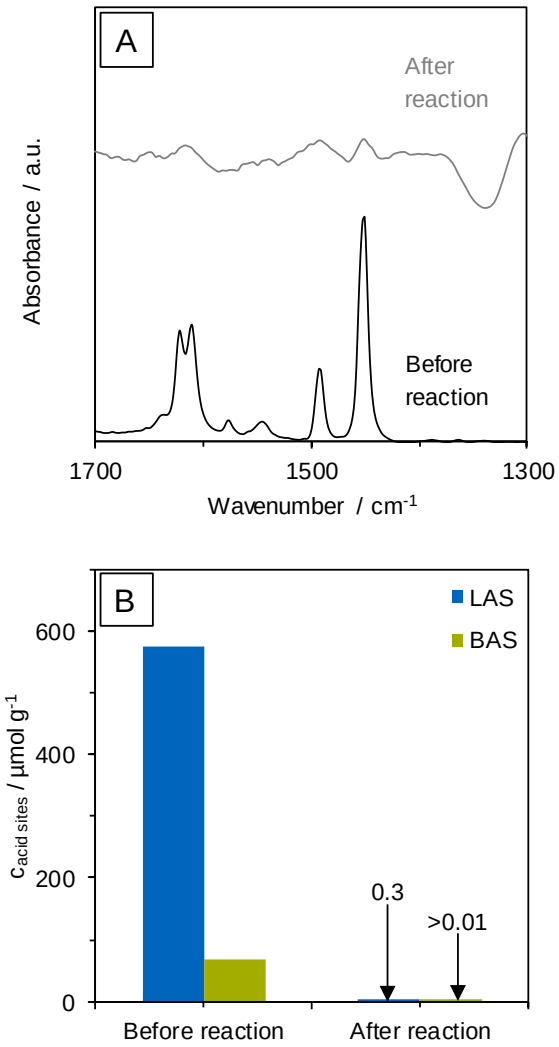

Figure 3-4. A) IR spectra of adsorbed pyridine (1 mbar at 150 °C) and B) concentration of acid sites of a 6 % Ni – SiO_2/Al_2O_3 catalyst before and after performing the dimerization reaction of 1-butene (T = 160 °C, 50 bar, WHSV = 168 h^{-1}).

Effect of co-cations on Ni-SiO_2/Al_2O_3 in 1-butene dimerization

The Ni-SiO_2/Al_2O_3 catalysts in the presence of the different co-cations were also tested for 1-butene dimerization (Figure S3-11). The dimerization rates decreased in the presence of co-cations, going from 0.88 mmol g^{-1} s^{-1} with Ni – SiO_2/Al_2O_3 to ~ 0.01 mmol g^{-1} s^{-1}. A subsequent decrease in the activity with higher co-cation loading is observed among all catalysts, independent of the nature of the co-cation (Figure 3-5). The lower Sanderson electronegativity of the Na co-cation resulted in very low activity with higher loading (2Na-Ni-SiO_2/Al_2O_3). Mg

on SiO_2/Al_2O_3 (without Ni, Figure S3-12) showed no activity in dimerization, which evidences that the co-cations alone do not catalyze the 1-butene dimerization.

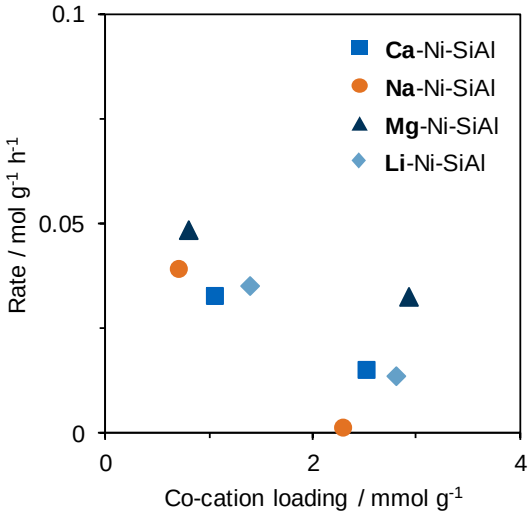

Figure 3-5. Rate of butene dimerization over different co-cation loaded catalysts with 6 % Ni on SiO_2-Al_2O_3 (T = 160 °C, p = 50 bar, WHSV = 6 h^{-1}).

Figure S3-13 shows the linear correlation between the increase in size of the NiO clusters (with the increase in co-cation loading from 1.25 to 2.5 mmol/g) and the decrease in dimerization activity, demonstrating that NiO clusters are also inactive in the SiO_2/Al_2O_3 system. Thus, it is suggested that the exchanged Ni^{2+} sites are the exclusive active centers for (metal based) dimerization. At high co-cation loading these will compete with the Ni^{2+} cations, decreasing the dispersion of the Ni^{2+} cations and the activity of the catalyst. Normalization of the 1-butene dimerization rates per Lewis acide Ni site shows a similar activity per site within the same co-cation concentration (Figure 3-6). Thus, the observed differences in dimerization rates result mainly from the Ni cations. This agrees well with our previous work reported with the co-cations in Ni exchanged LTA zeolite, [20] being the dimerization activity dependent only from the Ni concentration.

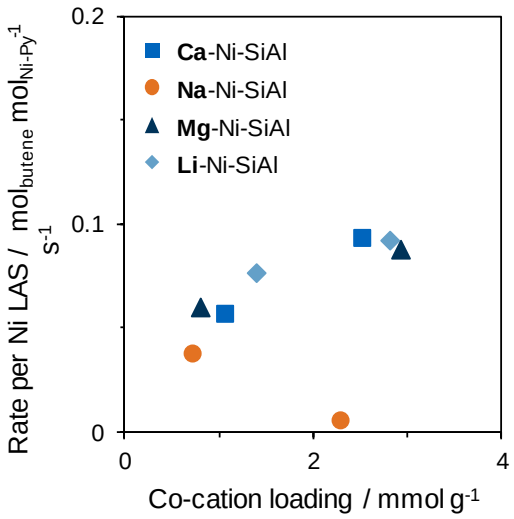

Figure 3-6. Butene dimerization rate per Ni-Lewis acid sites over 6 % Ni containing catalysts with different co-cations.

The dimer selectivity as a function of the butene conversion with the different catalysts is shown in Figure 3-7. An increase in branched products at higher conversion is observed on all catalysts. In the absence of co-cations, at the Ni-SiO_2/Al_2O_3 (Figure 3-7 A), the extrapolation to zero conversion shows all three dimers as primary products: n-octene, methylheptene and dimethylhexene. However, in the presence of co-cations (~2.5 mmol/g, Figure 3-7 B) just n-octene and methylheptene are primary products, while dimethylhexene is not formed at zero conversion, being a secondary product. The metal based dimerization follows a Cossee-Arlman type mechanism with an adsorption of a butene molecule and a subsequent insertion and coordination of another butene molecule into the Ni-C bond.[4, 29] Thereby, the initial adsorption could occur as 1'- or 2'-adsorption (Scheme S3-2, left pathway). As previously reported,[11] 1'-adsorption is needed for the formation of linear dimers (Scheme S3-2, left pathway). The subsequent coordination of the second 1-butene determines whether methylheptene or octene is formed. The initial 2'-adsorption of the butene molecule (Scheme S3-2, right pathway) would lead to branched dimers. Since no dimethylhexene is formed as primary product, this route can be ruled out for pure dimerization of 1-butene. In addition to the dimerization, the active sites are able to isomerize the reactant 1-butene to *cis*- and *trans*-2-butene.[11] 2-Butene will adsorb with an internal carbon (2-adsorption), opening this pathway for dimerization (Scheme S3-2, right pathway, red). and the formation of dimethylhexene as a secondary product.

Furthermore, the presence of 2-butene increases the probability of 2'-insertion on the 1'-adsorption pathway (Scheme S3-2, left pathway, red) resulting in higher selectivity to methylheptene.

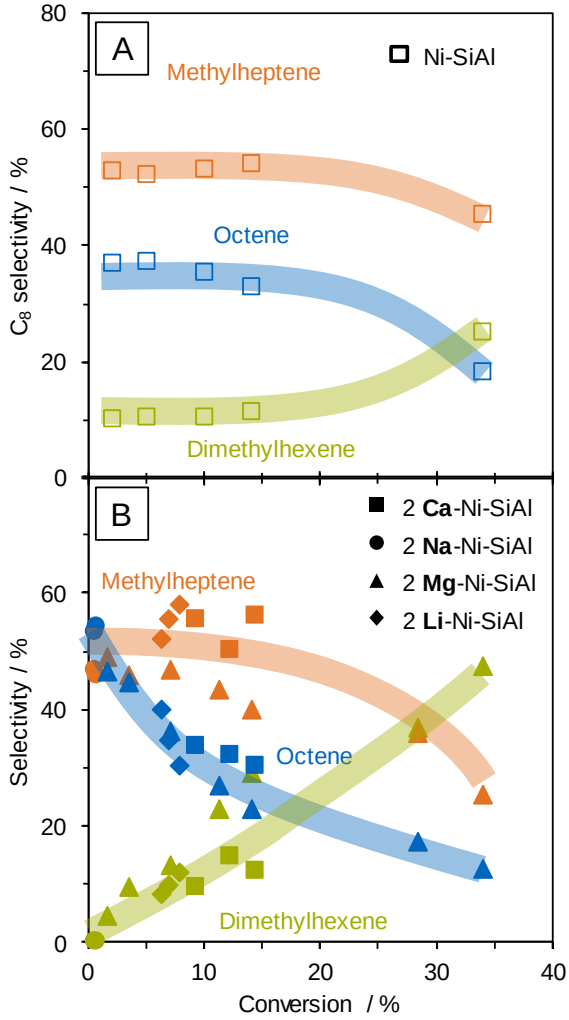

Figure 3-7. Selectivity of dimers as function of 1-butene conversion over co-cation free Ni (6 wt%) supported catalyst (A) and different co-cation loaded Ni (6 wt%) supported catalysts (B). T = 160 °C, p = 50 bar, $WHSV_A$ = 1388 h^{-1}, $WHSV_B$ = 6 – 50 h^{-1}.

Even though a general trend was followed over all co-cation catalysts, subtle differences were observed in the product distribution. Since n-octene is formed from the dimerization of 1-butene and dimethylhexene is the major product from the dimerization of 2-butene (Scheme S3-2),[11] the ratio of these two products can relate the isomerization of 1-butene into 2-butene. At 8% 1-butene conversion the O/DMH is higher with the Ca promoted catalyst (3.47) than over the Li and Mg promoted catalysts (2.55 and 2.21, respectively). This suggests that the Li

and Mg promoted Ni catalysts (2Li/Mg-Ni-SiO_2/Al_2O_3) possess the highest isomerization activity. These results support our previous findings with Ni ion-exchange on zeolite LTA in the presence of these co-cations, where the lowest selectivity to n-octene and the highest isomerization rate were observed with Li and Mg as a co-cations [20]. Nevertheless, it was suggested the co-cation stabilizes the Ni-π-allyl complex intermediate, enhanced by co-cations with higher Sanderson electronegativity, such as Mg and Li.

CONCLUSION

The impregnation of alkali (Na^+ or Li^+) or alkali-earth (Ca^{2+} or Mg^{2+}) co-cations with Ni^{2+} on an amorphous silica-alumina support changed the number and nature of acid site sites, being active in 1-butene dimerization. Brønsted acid sites were eliminated and a decrease in the concentration of the Lewis acid sites was observed upon the impregnation of the co-cations. The Lewis acid sites originate from Al sites of the support, as well as from Ni and the co-cations. However, only the Ni sites are active in both, 1-butene dimerization and isomerization. In addition, Ni cations can agglomerate and become inactive NiO clusters with increasing co-cation concentration, decreasing the overall activity of the catalyst.

The addition co-cations increases the overall selectivity to linear dimers (n-octene and methyl heptene) at low 1-butene conversions ($x < 10\%$), at the expense of the dimerization activity. The co-cations with lower Sanderson electronegativity (Na^+ and Ca^{2+}) enhance the selectivity to n-octene while harder cations (Li^+ and Mg^{2+}) increase the selectivity to dimethylhexene. It is suggested these co-cations stabilize better the π-allylic intermediate during 1-butene isomerization, increasing the concentration of 2-butene for dimerization. At higher conversions similar dimer selectivity is observed. Hence, the design of α-alkene dimerization catalysts should involve the presence of co-cations softer properties on $Ni\text{-}SiO_2/Al_2O_3$, preventing the formation of Brønsted acid sites and diminishing the rates of 1-butene isomerization into 2-butene.

EXPERIMENTAL

Catalyst preparation. The catalysts were prepared by incipient wetness impregnation (IWI) of an amorphous silica-alumina support (Sigma-Aldrich, silica-alumina catalyst support, Si/Al = 5.5) material with the aqueous solutions containing all the respective metal salts. The following metal salts were used in the impregnation: $Ni(NO_3)_2$ (SIGMA-ADLRICH; > 97.0 %), $Mg(NO_3)_2$ (SIGMA-ADLRICH; > 99.0 %), $Ca(NO_3)_2$ (MERCK; > 99.0 %), $LiNO_3$ (SIGMA-ADLRICH; > 99.0 %), and NaCl (SIGMA-ADLRICH; > 97.0 %). The concentration of the solution was tuned accordingly to the desired metal concentration. The respective co-cation was mixed in the Ni impregnation solution, resulting approximately in concentrations of 1 mmol/g Ni and/or ~1.25 mmol/g (nomenclature: 1X-Ni-SiO_2/Al_2O_3 , X=Na, Li, Ca, Mg) or ~2.5 mmol/g (nomenclature: 2X-Ni-SiO_2/Al_2O_3 , X=Na, Li, Ca, Mg) of the respective co-cations. After impregnation, the catalyst precursors were dried overnight at 80 °C and subsequently calcined (8 h, rate: 5 °C/min, 500 °C, air).

Characterization methods. Atomic absorption spectroscopic measurements (AAS) were performed in a Solar M5 Dual Flame graphite furnace AAS from ThermoFisher. After drying at 250 °C for 24 h, the samples were dissolved in a mixture of HF and nitric acid and injected in the graphite furnace. A previous calibration was applied to determine the concentration of each of the metals.

X-ray diffraction measurements were performed in a PANalytical Empyreal System diffractometer, equipped with a Cu- Kα radiation source ($K\alpha_1$ line of 1.54 Å; 45 kV and 40 mA)). The diffractograms were measured by the usage of a sample spinner stage in a 2θ range between 5 ° and 70 ° (step size: 0.0131303/2θ) at ambient conditions.

The BET specific surface area and pore volume of the zeolite were determined by nitrogen physisorption. The isotherms were measured at liquid nitrogen temperature (77 K) using a PMI Automatic Sorptometer. The catalyst was activated in vacuum at 473 K for 2 h before measurement. Apparent surface area was calculated by applying the Brunauer-Emmett-Teller (BET) theory with a linear regression between p/p_0 = 0.01 – 0.15. The micro- and mesopores were determined from the t-plot linear regression for t = 5-6 Å.

The adsorption of pyridine was followed by IR in a Nicolet 5700 FT-IR spectrometer from Thermo Electron corporation, equipped with a liquid nitrogen cooled detector. For the measurement, a self-supporting wafer was installed and activated at 450 °C (rate: 10 °C/min) for 1 h in vacuum. After cooling down to 150 °C, pyridine was equilibrated to 1 mbar for 30

min. Subsequently, the system was evacuated for another 30 min, before measurement. Scans were taken after activation and after outgassing at a resolution of .4 cm^{-1} with an average of 250 scans per spectrum. For the calculation of the acid site concentrations, molar extinction coefficients of 0.96 and 0.73 cm/µmol and were used for the characteristic bands of 1450 cm^{-1} (Lewis) and 1540 cm^{-1} (Brønsted),[30] respectively. For the deconvolution of the Lewis acid sites, the bands at 1600 cm^{-1} region were fitted, assuming similar extinction coefficients for all kinds of LAS. Subsequently, the total concentration was split according to the results of the 1600 cm^{-1} integration.

Catalytic testing and reaction kinetics. Catalytic tests were conducted in a fixed bed PFR (id = 3.9 mm), connected to an online GC analysis unit (Agilent HP 6890, equipped with a 50 m HP-1 column). Prior to GC analysis, hydrogen is added to the product stream, which is hydrogenated over a Pt/Al_2O_3 catalyst. A mixture of 15 % i-butane and 85 % 1-butene is introduced by a syringe pump (ISCO model 500 D), temperature is controlled by a Eurotherm 2416, pressure is controlled using a Tescom backpressure regulator.

Prior to weighing, the catalyst was dried at 100 °C for 1 h. The catalyst bed was diluted with SiC and fixed in the isothermal zone of the reactor. After activation for 2 h at 450 °C (rate: 10 °C/min) in air, the system was purged with nitrogen and pressurized to the desired pressure. Subsequently the system was flushed with the feed mixture (5 ml/min) for 2 min. After the desired flow rate is set, temperature program and GC measurements were started.

Standard measurement conditions were at 160 °C and 50 bar with a flow rate of butene mixture of 0.04 and catalyst loading of 200 mg to obtain a WHSV of 6 g g^{-1} h^{-1}. The space velocity was varied by changing the catalyst loading and the feed flow rate.

i-Butane is inert under reaction conditions applied, and was used as internal standard for normalization of GC areas. Conversion, selectivity and yields are calculated according to the following equations:

$$X = \frac{n(butene)_{in} - n(butene)_{out}}{n(butene)_{in}}$$

$$S = \frac{n(product)_{out}}{n(butene)_{in} - n(butene)_{out}} \frac{|\nu_{butene}|}{\nu_{product}}$$

$$Y = \frac{n(product)_{out}}{n(butene)_{in}} \frac{|\nu_{butene}|}{\nu_{product}}$$

REFERENCES

[1] G.C. Bailey, J.A. Reid, SiO2-Al2O3-NiO Catalyst and its Preparation, 1952.
[2] A. Behr, Z. Bayrak, S. Peitz, G. Stochniol, D. Maschmeyer, RSC Advances, 5 (2015) 41372-41376.
[3] S. Albrecht, D. Kießling, G. Wendt, D. Maschmeyer, F. Nierlich, Chem. Ing. Tech., 77 (2005) 695-709.
[4] E.J. Arlman, J. Catal., 3 (1964) 89-98.
[5] P. Beltrame, L. Forni, A. Talamini, G. Zuretti, Appl. Catal. A, 110 (1994) 39-48.
[6] K. Ziegler, E. Holzkamp, H. Breil, H. Martin, Angew. Chem., 67 (1955) 541-547.
[7] A. Brückner, U. Bentrup, H. Zanthoff, D. Maschmeyer, J. Catal., 266 (2009) 120-128.
[8] J. Rabeah, J. Radnik, V. Briois, D. Maschmeyer, G. Stochniol, S. Peitz, H. Reeker, C. La Fontaine, A. Brückner, ACS Catalysis, 6 (2016) 8224-8228.
[9] F. Nadolny, B. Hannebauer, F. Alscher, S. Peitz, W. Reschetilowski, R. Franke, J. Catal., 367 (2018) 81-94.
[10] S. Raseev, Thermal and Catalytic Processes in Petroleum Refining, Marcel Dekker, Inc., New York, 2003.
[11] A. Ehrmaier, Y. Liu, S. Peitz, A. Jentys, Y.-H.C. Chin, M. Sanchez-Sanchez, R. Bermejo-Deval, J. Lercher, ACS Catalysis, 9 (2019) 315-324.
[12] A.N. Mlinar, O.C. Ho, G.G. Bong, A.T. Bell, ChemCatChem, 5 (2013) 3139-3147.
[13] N. Kumar, P. Mäki-Arvela, T. Yläsalmi, J. Villegas, T. Heikkilä, A.R. Leino, K. Kordás, T. Salmi, D. Yu Murzin, Microporous Mesoporous Mater., 147 (2012) 127-134.
[14] M.L. Sarazen, E. Doskocil, E. Iglesia, J. Catal., 344 (2016) 553-569.
[15] H.S. Sherry, H.F. Walton, The Journal of Physical Chemistry, 71 (1967) 1457-1465.
[16] H.S. Sherry, Handbook of Zeolite Science and Technology, Marcel Dekker, New York, (2003) 1007-1061.
[17] D. Amari, J.-L. Ginoux, L. Bonnetain, Zeolites, 14 (1994) 58-64.
[18] A.N. Mlinar, S. Shylesh, O.C. Ho, A.T. Bell, ACS Catalysis, 4 (2013) 337-343.
[19] A. Ehrmaier, R. Bermejo-Deval, M. Sanchez-Sanchez, Y. Liu, J.A. Lercher, S. Peitz, G. Stochniol, Selective Oligomerization of Olefins, in: EPOrg (Ed.), EVONIK Degussa GmbH Technische Universität München, 2018.
[20] A. Ehrmaier, S. Peitz, M. Sanchez-Sanchez, R. Bermejo de Val, J. Lercher, Microporous Mesoporous Mater., (2019).
[21] S.M. Maier, A. Jentys, J.A. Lercher, The Journal of Physical Chemistry C, 115 (2011) 8005-8013.
[22] G. Ertl, H. Knözinger, F. Schueth, J. Weitkamp, Handbook of Heterogeneous Catalysis, Wiley-VCH Verlag GmbH & Co. KGaA, Weinheim, 2008.
[23] C. Morterra, G. Magnacca, Catal. Today, 27 (1996) 497-532.
[24] H. Knözinger, H. Stolz, Fortschrittsberichte über Kolloide und Polymere, 55 (1971) 16-28.
[25] H. Stolz, H. Knözinger, Kolloid-Zeitschrift und Zeitschrift für Polymere, 243 (1971) 71-76.
[26] M. Zaki, M. Hasan, F. Al-Sagheer, L. Pasupulety, In situ FTIR Spectra of Pyridine Adsorbed on SiO2-Al2O3, TiO2, ZrO2 and CeO2: General Considerations for the Identification of Acid Sites on Surfaces of Finely Divided Metal Oxides, 2001.
[27] C.H. Kline, J. Turkevich, The Journal of Chemical Physics, 12 (1944) 300-309.
[28] R.T. Sanderson, J. Chem. Educ., 65 (1988) 112.
[29] M.L. Sarazen, E. Iglesia, Proceedings of the National Academy of Sciences, 114 (2017) E3900-E3908.
[30] P. Cossee, J. Catal., 3 (1964) 80-88.

3. Chapter - Supporting Information:

The Effect of Co-Cations on Amorphous Supported Ni Catalysts in Butene Dimerization

SI-1 Synthesis and characterization of crystallographic and textural properties of amorphous Ni catalysts with different co-cations

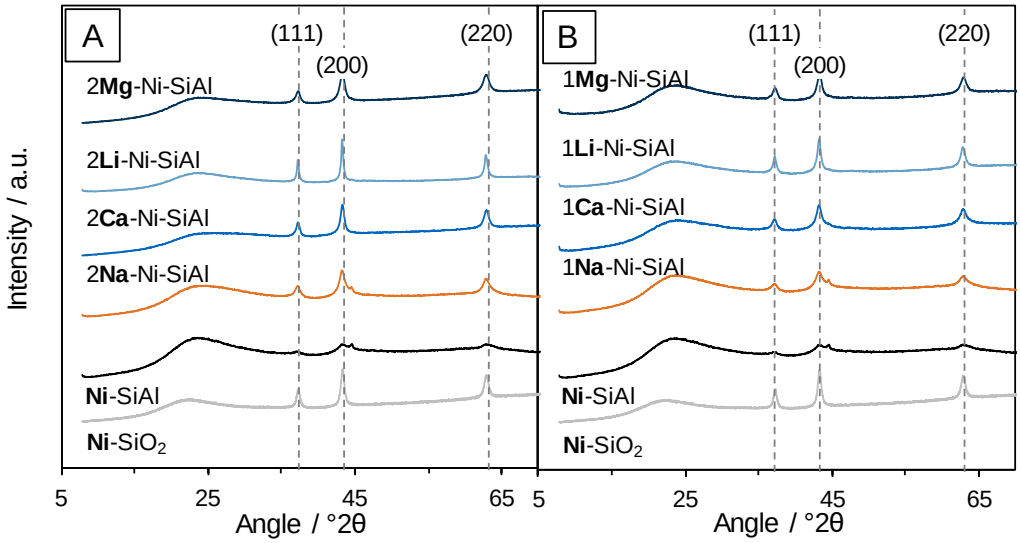

Figure S3-1. X-ray diffraction patterns of Ni silica-alumina supported catalysts with and without different co-cations and Ni supported on SiO_2.

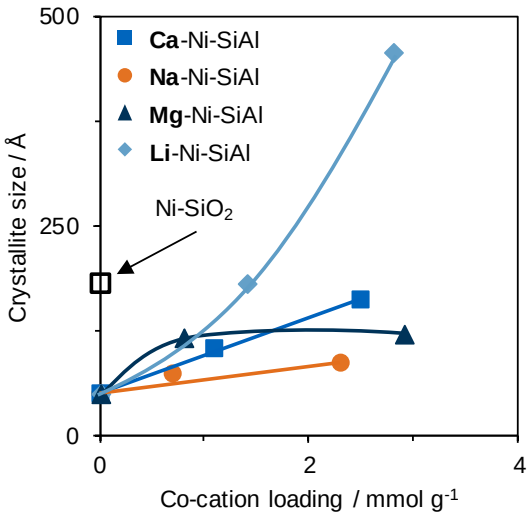

Figure S3-2. Crystallite size of NiO particles in silica-alumina supported catalysts with different co-cations, as well as in 6 % Ni-SiO_2, determined with the Scherrer equation.

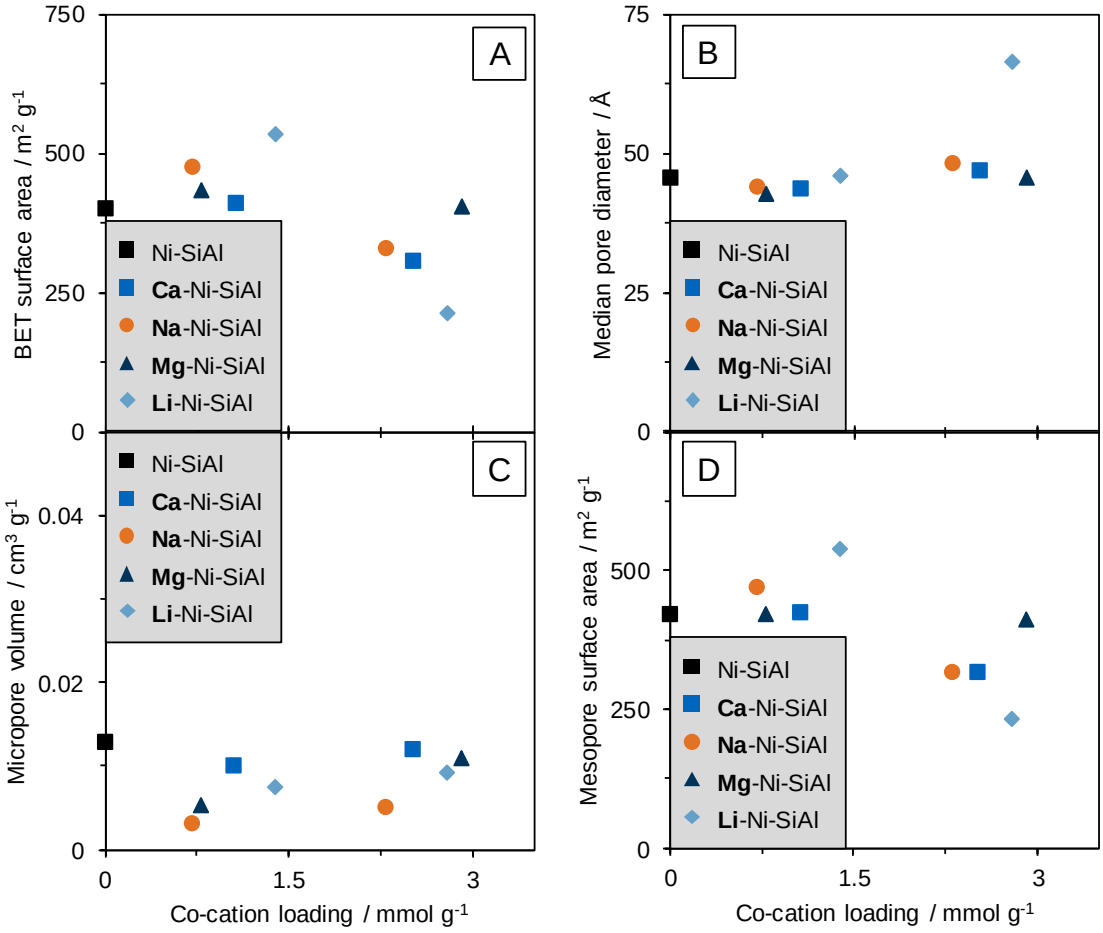

Figure S3-3. Influence of co-cation loading on mesoscopic properties. A) BET surface area, B) Median pore diameter, C) Micropore volume, and D) Mesopore surface area.

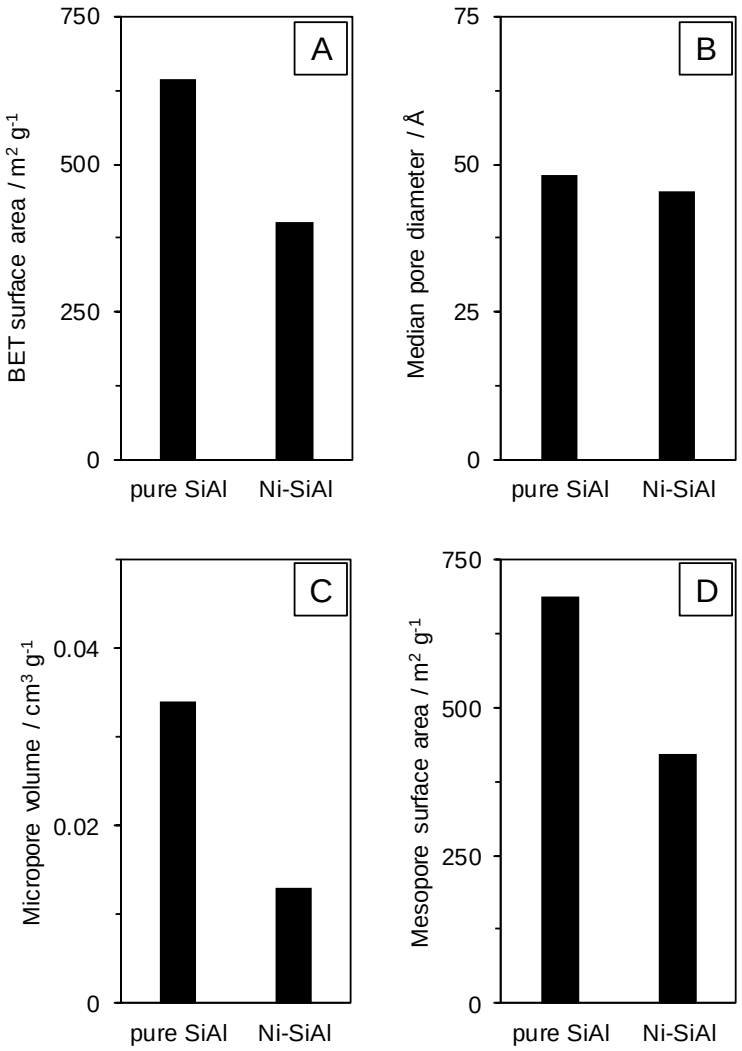

Figure S3-4. Change of mesoscopic properties of amorphous SiO_2-Al_2O_3 support upon impregnation with 6 wt% Ni.

SI-2 Pyridine adsorption on amorphous Ni catalysts with different co-cations

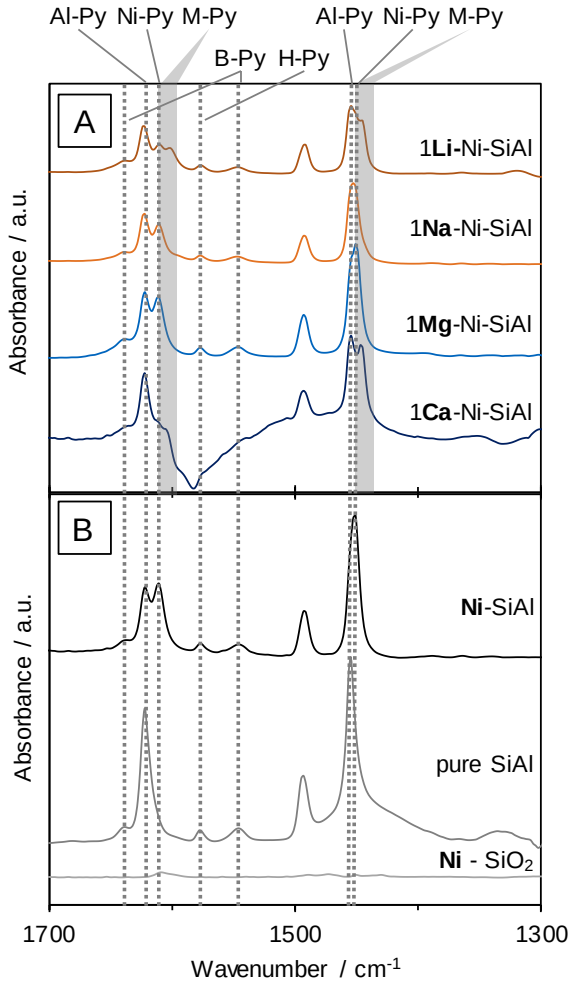

Figure S3-5. IR spectra of 1 mbar pyridine adsorbed at T = 150 °C on Ni catalysts containing ~1.25 mmol/g different co-cations (A) and on co-cation free Ni-SiO_2/Al_2O_3 (B, top) as well as on the pure silica-alumina support (B, middle) and on Ni-SiO_2 (B, bottom). Al-Py: pyridine adsorbed to Al LAS; Ni-Py: pyridine adsorbed to Ni LAS; M-Py: pyridine adsorbed to co-cation LAS, B-Py: pyridine adsorbed to BAS; H-Py: H-bonded pyridine.

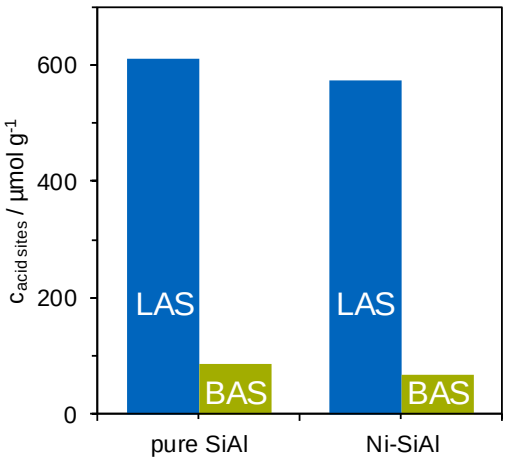

Figure S3-6. Concentration of Lewis and Brønsted acid sites of pure and 6 % Ni (0.97 mmol/g) containing SiO_2-Al_2O_3.

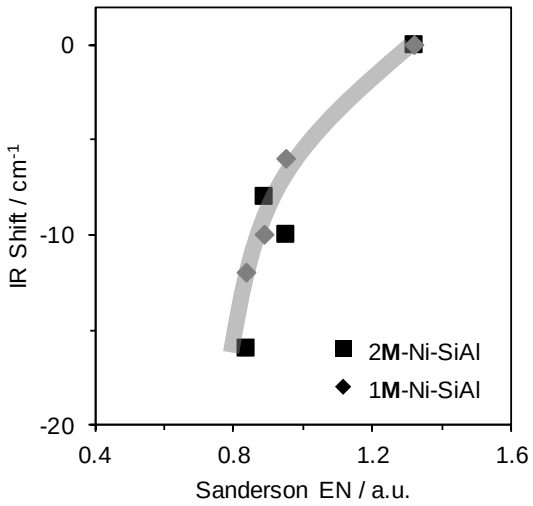

Figure S3-7. The redshift of the M-Py band in comparison to the Ni-Py-band in the 1610 cm^{-1} region as function of the Sanderson electronegativiy of the respective co-cations.

Table S3-1. Integrations areas of deconvoluted 8a vibrational bands (1600 cm^{-1} region) and the resulting concentrations of different LAS.

	c(LAS) 1450 band	area peak 1622 cm^{-1}	area peak 1610 cm^{-1}	area peak co-cation	c(AlPy)	c(NiPy)	c(Mpy)
	µmol/g		a.u.			µmol/g	
6 % Ni-SiO_2/Al_2O_3	574	1.94	3.46	0.00	207	367	0
1Na	358	2.88	2.78	0.29	173	167	18
1Ca	491	5.09	3.49	2.08	234	161	96
1Li	384	2.68	2.04	1.36	169	129	86
1Mg	505	4.41	4.55	1.26	218	225	62
2Na	134	0.48	0.63	1.02	30	39	64
2Ca	239	0.83	0.74	2.47	49	44	146
2Li	170	1.38	0.89	1.49	62	40	67
2Mg	346	0.93	1.21	1.95	79	102	165

SI-3 Catalytic behavior of amorphous supported catalysts in butene dimerization

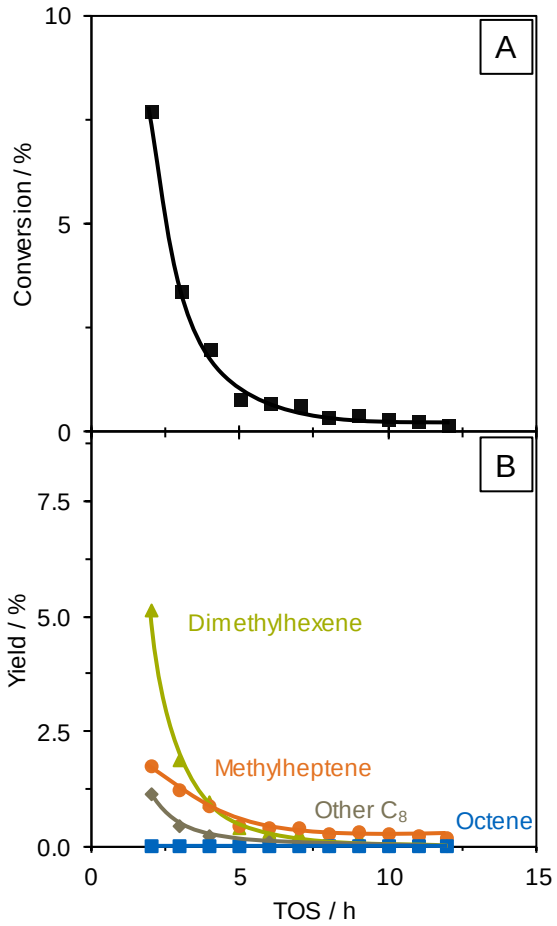

Figure S3-8. Conversion (A) and dimer yield (B) of dimerization of 1-butene over a pure SiO_2/Al_2O_3 support catalyst without any cations (T = 160 °C, p = 50 bar, WHSV = 168 h^{-1}; MHSV = 10 mol_{Butene} mol_{BAS}^{-1} s^{-1}).

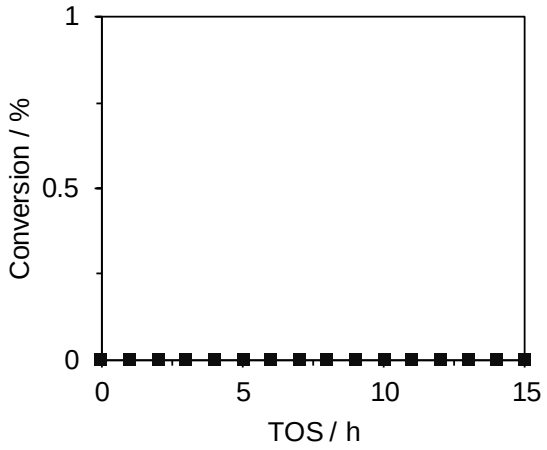

Figure S3-9. Activity of 6 % Ni – SiO_2 in dimerization of 1-butene (T = 160 °C, p = 50 bar, WHSV = 168 h^{-1})

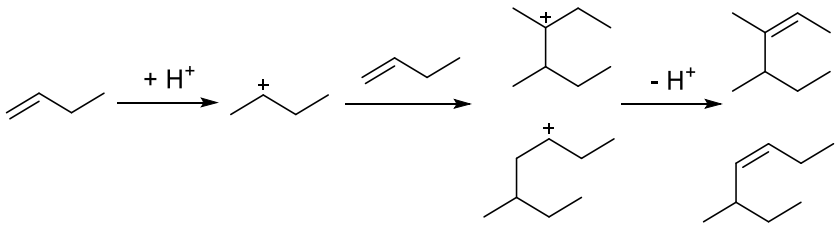

Scheme S3-1. Brønsted acid catalyzed carbenium ion pathway for 1-butene dimerization.

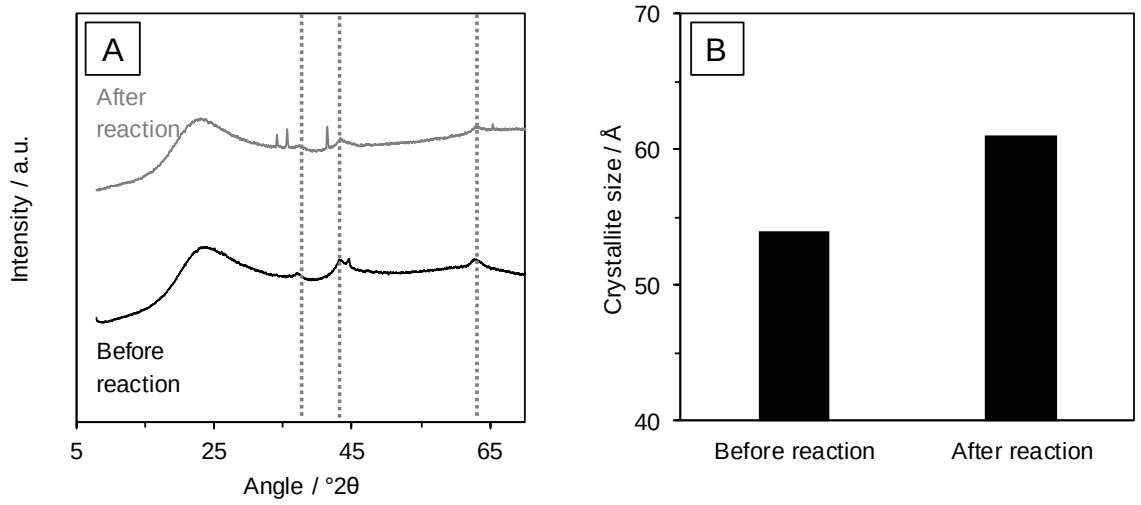

Figure S3-10. A) X-ray diffraction patterns of 6 % Ni - SiO_2-Al_2O_3 catalyst before and after performing the dimerization reaction of 1-butene and B), the respective crystallite sizes determined with the Scherrer equation.

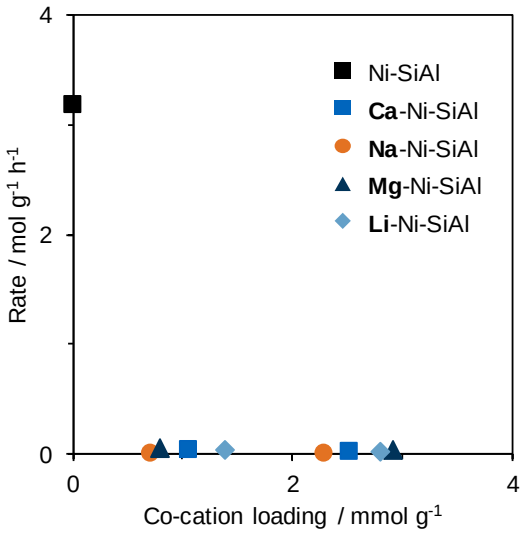

Figure S3-11. Rate of butene dimerization over different co-cation loaded and co-cation free catalysts with 6 % Ni on SiO_2-Al_2O_3 (T = 160 °C, p = 50 bar, $WHSV_{co\text{-}cation\ loaded\ catalysts}$ = 6 h^{-1}; $WHSV_{co\text{-}cation\ free\ catalyst}$ = 1389 h^{-1}).

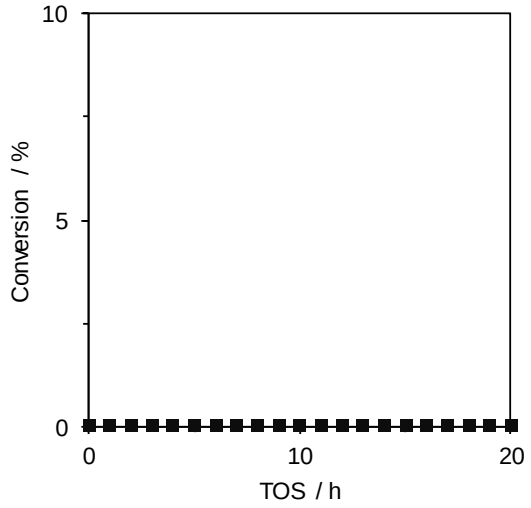

Figure S3-12. Conversion over Ni free Mg / SiO_2-Al_2O_3 catalyst in butene dimerization (T = 160 °C, p = 50 bar, WHSV = 165 h^{-1}).

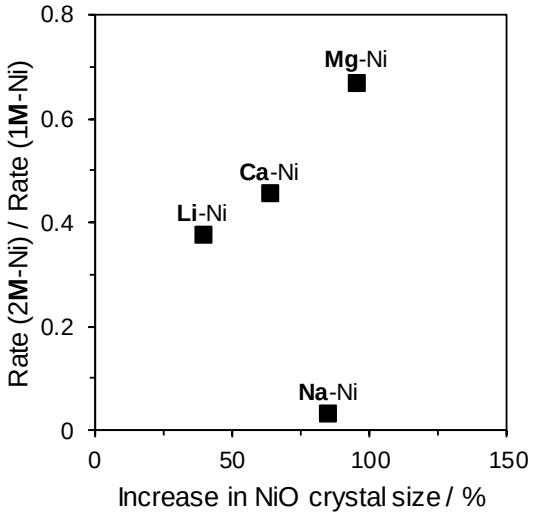

Figure S3-13. Decrease in dimerization rate upon increase of co-cation loading from 1.25 to 2.5 mmol/g as function of increase in NiO crystal size through co-cation addition.

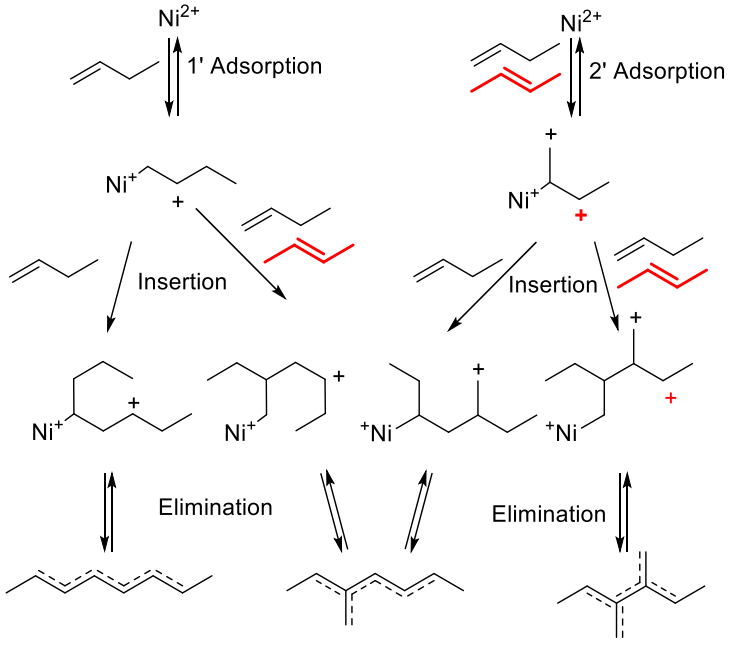

Scheme S3-2. Nickel catalyzed coordinative route for 1-butene dimerization. The possible pathways for 2-butenes are shown in red.

Conclusion

The valorization of the butene fraction to higher hydrocarbons is a challenging process of industrial and academic interest. Besides Brønsted acid catalyzed oligomerization and alkylation, e.g. for fuel additive production, linear dimerization over metal catalysts has gained in interest. These linear dimers are desired and applied as feedstock materials for the synthesis of PVC plasticizers.

The exchange of Ni cations to zeolite LTA resulted in a highly selective catalyst for the linear dimerization of 1-butene. For conversions up to 35 %, linear octenes and 3-methylheptene were formed as predominant products. The ratio of methylheptene/octene varied from 0.7 to 1.4 as function of conversion. Dimethylhexene was formed as secondary product, whereas its selectivity remained below 10 % among the dimers.

The main dimerization pathway is proposed to start with an initial 1'-adsorption of 1-butene to the Ni site. After that, a second butene molecule is coordinated to the Ni site and subsequently inserted into the Ni-C-bond. Thereby, the direction of the adsorbed molecule is crucial for the insertion and determines, whether methylheptene or octene (2'- or 1'- insertion, respectively) is finally formed.

In competition to the dimerization, Ni sites also catalyze the double bond isomerization of 1-butene towards 2-butens. This reaction is suggested to occur through an adsorption-desorption process. Isomerization rate increased with increasing conversion level, reaching the equilibrium at about 35 % conversion to dimers. Higher concentrations of 2-butenes alter the probability for 2'-insertion, increasing the methylheptene to octene ratio. Having 2-butene in the feed, the secondary product, dimethylhexene was observed to be formed. For the formation of dimethylhexene, an initial 2'-adsorption in inevitable, which is the only option for 2-butene to adsorb.

Further, it was shown that the 2-butenes or its oligomers lead to irreversible adsorbates and block the Ni sites, resulting in catalyst deactivation.

Infrared studies were used to follow the adsorption of butene on the Ni catalyst. Thereby, both, Ni-alkyl and Ni-allyl complexes were observed. It is suggested that the isomerization runs via a π-allyl bound complex, while the Ni-alkyl complex is an intermediate in the dimerization cycle.

To study the effect of the co-cations, Ni-LTA catalysts were prepared with different amounts of several alkali (Li^+ and Na^+) and alkali earth (Mg^{2+} and Ca^{2+}) metals as co-cations and tested in the dimerization reaction and their butene adsorption behavior. Although the adsorption capacity varied, the catalysts showed similar rates and dimer selectivities at low conversion. This similar dimerization behavior of pure 1-butene in absence of isomerization points to the conclusion that the Ni-alkyl complex is not affected by the presence of the co-cations.

At higher conversions, the presence of Li and Mg as co-cations led to an increased isomerization rate and hence to a higher selectivity towards branched dimers. Thus, the isomerization equilibrium was reached at ~20 % conversion to dimers, when Mg and Li were present as co-cations, while the isomerization over the Ni-Na-Ca-LTA was equilibrated at ~28 % conversion to dimers. As a consequence of this, the methylheptene to octene ratio of 1 was observed at 10-12 % conversion over Mg and Li promoted LTA and at ~20 % over Ni-Ca-LTA. As the double bond isomerization was observed to be strongly affected by the co-cations, it is proposed that the Ni-allyl complex, which is the intermediate in isomerization, is better stabilized by cations exhibiting higher Sanderson electronegativity (i.e. Mg and Li).

The industrially applied catalysts are mostly amorphous supported Ni catalysts. For this reason, the co-cation effect was tested in this system, as well. Amorphous supported Ni catalysts with different co-cations (Mg, Ca, Li and Na) were prepared by co-impregnation of the respective metal salts. Pyridine adsorption followed by infrared spectroscopy revealed the elimination of the Brønsted acid sites on all impregnated catalysts. The impregnation with Ni led to the formation of Lewis acid sites, same as the presence of the co-cations, whereas the strength of Lewis acid sites varied with the nature of the co-cations. The dimerization activity of the catalyst directly depended on the concentration of the Lewis acid Ni sites. The selectivity depended on the conversion over all catalysts, whereas slight differences were observed regarding the isomerization being affected by the co-cations. In the same way as it was observed on co-cation containing LTA catalysts, Mg and Li stabilize the Ni-allylic intermediate in isomerization mechanism, leading to higher selectivities of branched products.